Positrons in the MOS system

Positrons in the MOS system

PROEFSCHRIFT

ter verkrijging van de graad van doctor
aan de Technische Universiteit Delft,
op gezag van Rector Magnificus prof. ir. K.F. Wakker,
in het openbaar te verdedigen ten overstaan van een
commissie,
door het College voor Promoties aangewezen,
op vrijdag 18 december 1998 om 10.30 uur

door

Maarten CLEMENT

natuurkundig ingenieur
geboren te Voorhout

Dit proefschrift is goedgekeurd door de promotoren:
Prof. dr. A. van Veen
Prof. dr. ir. S. Radelaar

Samenstelling promotiecommissie:

Rector Magnificus	voorzitter
Prof. dr. A. van Veen	Rijks Universiteit Groningen, promotor
Prof. dr. ir. S. Radelaar	Technische Universiteit Delft, promotor
Prof. dr. P. Balk	Technische Universiteit Delft
Prof. dr. ir. H. van Dam	Technische Universiteit Delft
Prof. K.G. Lynn	Washington State University
Prof. dr. P.H. Woerlee	Universiteit Twente
Dr. J.M.M. de Nijs	Technische Universiteit Delft

Printed in the Netherlands

aan Inge

Table of contents

Table of contents

List of publications

7 Relation between defect structure and VUV radiadion hardness

8 Electron momentum distribution at defects in the Si/SiO$_2$ system

List of publications

The following chapters of this thesis have been published as regular contributions in the literature:

chapter 3:

M. Clement, J.M.M. de Nijs, P. Balk, H. Schut, A. van Veen.

Analysis of positron beam data by the combined use of the shape- and wing- parameters.

J. Appl. Phys. **79**, 9029 (1996).

chapter 4:

M. Clement, J.M.M. de Nijs, P. Balk, H. Schut., A. van Veen.

Transport of positrons in the electrically biased metal-oxide-silicon system.

J. Appl. Phys. **81**, 1943 (1997).

chapter 7:

M. Clement, J. M. M. de Nijs, A. van Veen, H. Schut, P. Balk.

Effect of a post oxidation Anneal on VUV radiation hardness of the Si/SiO_2 system studied by positron annihilation spectroscopy.

IEEE Trans. on Nucl. Sc. **NS-42**, 1717 (1995).

Other publications related to this thesis:

M. Clement, J.M.M. de Nijs, H. Schut, A. van Veen, R. Mallee and P. Balk.

Positron beam technique for the study of defects at the Si/SiO_2 interface of a polysilicon gated MOS system.

Mat. Res Soc. Symposium proceedings **442,** 143 (1997).

M. Clement, J. M. M. de Nijs, H. Schut, A. van Veen and P. Balk
Characterization of defects at the Si/SiO$_2$ interface of a polysilicon-gated MOS system by monoenergetic positrons.

Mat. Sc. Forum **255-257**, 718 (1997).

J.M.M. de Nijs, M. Clement, H. Schut, and A. van Veen*Positron annihilation as a tool for the study of defects in the MOS system.*
Micr. Eng. **36**, 35 (1997).

J. M. M. de Nijs and M. Clement.
Characterization of the Si/SiO$_2$ interface using positrons: present status and prospects.
in Fundamental Aspects of Ultrathin Dielectrics on Si-based Devices, edited by E. Garkfunkel et al (Kluwer Academic Publishers, 1998), p. 25.

A. van Veen, H. Schut, M. Clement, J. M. M. de Nijs, A. Kruseman and M. R. IJpma.
VEPFIT applied to depth profiling problems.
Appl. Surf. Sci. **85**, 216 (1995).

A. C. Kruseman, H. Schut, A. van Veen, P. E. Mijnarends, M. Clement and J. M. M. de Nijs.
Positron beam analysis of semiconductor materials using a two-detector Doppler broadening coincidence system.
Appl. Surf. Sci. **116**, 192 (1997).

Chapter 1

Introduction

I GENERAL SCOPE

One of the mainstays of modern microelectronics is the metal-oxide-silicon field-effect-transistor (MOSFET). Integrated circuits based on these devices play a major role in present technology. To date, the MOSFET technology permits an integration density of more than 10^8 devices cm^{-2} which allows a high functionality on a single chip. To further optimize the operation speed of microprocessors and the capacity of electronic memory units these integrated circuits are still the object of intensive research. In many cases, improvement of these parameters implies further miniaturization of devices. Key problems in the mastering of MOSFET technology are controlling the yield of the production process and the device reliability during operation. To realize these goals a continuous effort has to be made to control the defect structure in the metal-oxide-silicon (MOS) system.

The MOS system consists of a silicon dioxide layer positioned between a silicon substrate and an electrode[1]. The electrode is denoted as the gate and consists of a polysilicon or aluminium thin film. The principle of the MOSFET is schematically shown in Fig. 1. The central part of the device is the MOS system situated between two highly doped contact areas in the substrate called source and drain. The bias voltage

applied on the gate electrode determines the density of charge carriers in the underlying silicon substrate. This point is illustrated by the energy band diagram of the MOS system in Fig. 2. By changing the gate bias the carrier density in the region near the Si/SiO_2 interface can be controlled. When applying a proper voltage on the gate one can induce an inversion layer just beneath the oxide that acts as a highly conducting channel between source and drain. In this manner the current through the MOSFET can be switched on and off with the aid of the gate bias.

However, if defects causing localised energy states for electrons are present in the SiO_2 or at the Si/SiO_2 interface the band bending in the silicon is not only affected by the gate bias, but also by the immobile charges at the defects[1]. The immobile charge will thus cause a degradation of the device parameters like transconductance and threshold voltage.
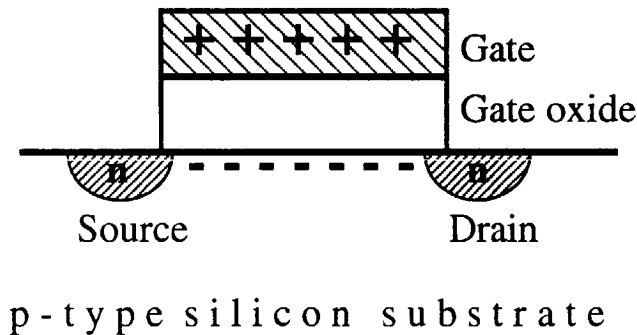
Figure 1. Schematic drawing of a MOSFET. The conducting channel is formed by bringing the p-type substrate in inversion by application of a positive bias voltage on the gate. Through this channel current may flow from the n-type source to the n-type drain upon application of a potential difference between these regions.

When further scaling down the dimensions of the MOS devices the charging of defects will become a more serious problem because of the increased electric field strengts occuring in the smaller devices. When the distance between drain and source decreases, the field in the conduction channel will increase and will be sufficiently strong to heat electrons in the silicon such that a substantial number of electrons will be injected over the barrier into the SiO_2[2,3]. The injected electrons may be trapped at defects which results in a degradation of the SiO_2.

      Furthermore, exposure to energetic radiation will also degrade devices because of the generation of electron-hole pairs in the SiO_2 causing the creation and charging of defects[4]. Energetic irradiation occurs during manufacturing (e.g. vacuum ultraviolet during plasma processing and lithography) and during operation in space or in nuclear applications.
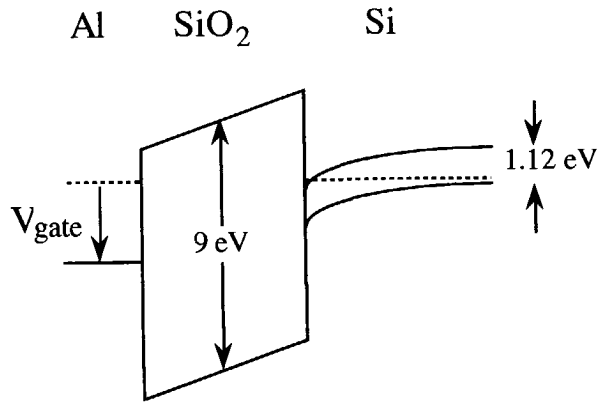
Figure 2. Energy band diagram of an Al-SiO₂-Si structure on a p-type substrate. The wide bandgap material SiO₂ constitutes a barrier for charge carrier transport between the Al gate and the Si substrate. In the figure a positive bias is applied to the gate with leads to the formation of an inversion layer in the Si at the Si-SiO₂ interface.

Reducing the density of defects in the Si/SiO$_2$ system remains an important task for the MOSFET technology[1]. To achieve this goal a good insight in, and control of the defect generation in MOS devices during their fabrication and their operation is of primary importance.

II DEFECTS IN THE MOS SYSTEM

Electrical techniques show the presence of defects that can exchange charge with the silicon substrate[1]. These defects are situated at or very close to the Si/SiO$_2$ interface. Generally they are referred to as interface states. Defects in the bulk of the oxide layer can not be charged from the silicon. Such defects can only change their charge state by trapping of a charge carrier injected into one of the oxide bands. The kind of carrier (electron or hole) being trapped and the capture cross section for trapping depends on the microscopic structure of the trap.
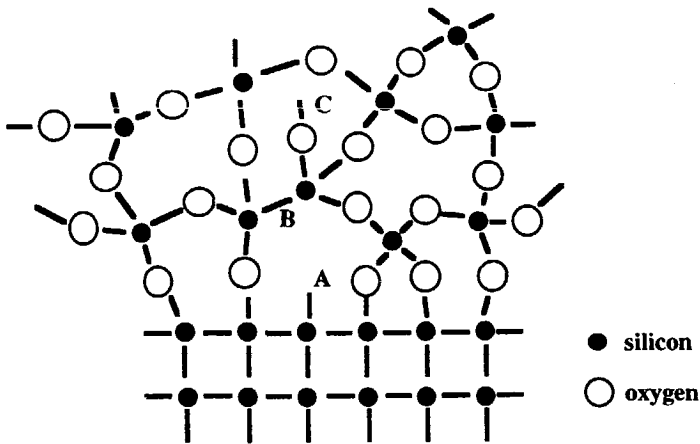
Figure 3. Schematic picture of the Si-SiO2 structure. A Si dangling bond at the Si/SiO$_2$ interface (A), an O-vacancy (B) and O dangling bond in the SiO$_2$ (C) are shown.

The Si/SiO_2 system (see Fig. 3) as used for the gate is generally fabricated by thermal oxidation of the silicon substrate. The resulting SiO_2 layer is amorphous: it is largely chemically saturated and exhibits short range, not long range, order. The Si atoms in the oxide are sp^3 hybridised and bonded to four O atoms; each O atom is bonded to two Si-atoms. This leads to a network consisting of rings formed by SiO_4 tetrahedrons[5]. In the bulk of the oxide the network is fully relaxed and the bond lengths and bond angles are in a low energy configuration.

However, at the Si/SiO_2 interface a transition from crystalline Si to amorphous SiO_2 takes place. To accommodate this transition strained and dangling bonds will be present in the interfacial region[1]. Besides, deviations from the ideal stochiometry near the Si/SiO_2 interface may lead to the presence of O-vacancies in the oxide network. Imperfections, like microvoids and dangling bonds may be present also in the bulk oxide network.

In addition to these intrinsic defects the introduction of hydrogen in the oxide during the oxidation process, which in general practice is unavoidable, will cause extrinsic defects to be present[1]. These include: H_2O and H_2 molecules, and Si-H and Si-OH groups. The Si-OH groups and dissolved H_2O molecules are bulk traps for electrons. O-vacancies are well known as traps for holes and are found in the region near the substrate. Si-H groups are electrically inactive and are present throughout the Si/SiO_2 system; only after removal of the H atom they constitute a trap (dangling bond).

At the present time, the relation between the density of the electrical active defects and the atomic structure of the Si/SiO_2 system is not fully understood yet. The mechanisms for the creation of new defects during processing are still a matter of intensive research. This degradation occurs when charge carriers are introduced in the oxide, by injection from the substrate or gate[2,3] or upon absorption of radiation[4]. As shown by Afanas'ev *et al*[6] and by Druijf et al[7], most of the defects generated upon VUV radiation are related to H atoms that are bonded to strained oxygen atoms. Atomic H is created by dissociation reactions that are induced by free charge carriers or by excitons.

Although the exact mechanisms for the creation and transport of atomic H are not yet fully understood, it is clear that these processes are affected by the detailed structure of the SiO_2 network and by mechanical strain. It is thus attractive to have a method that provides information on these aspects of the Si/SiO_2 system.

III TECHNIQUES FOR THE STUDY OF DEFECTS IN THE Si/SiO_2 SYSTEM

Several types of experimental techniques are used to study defects in the MOS system. Most commonly electrical methods are employed[8]. These electrical characterization methods allow the determination of the densities of electrically active defects down to values as low as 10^{10} cm^{-2}. Neutral defects in the oxide can only be studied after charging them by carrier trapping. This is done through injection of carriers from the gate or substrate into the SiO_2 [9]. A drawback of the electrical measurements is that none of these provides information on the microscopic structure of defects. Furthermore, electrically inactive defects in the Si/SiO_2 system, that may be indirectly involved in degradation processes, are not detected by electrical characterization techniques.

Techniques to study the composition of the Si/SiO_2 system are Nuclear Reaction Analysis (NRA)[10] and Secondary Ion Mass Spectroscopy (SIMS)[11]. These techniques are employed to obtain information on the concentration and spatial distribution of impurities like sodium and hydrogen in the Si/SiO_2 system. The importance of this information stems from the charge trapping properties of such impurities and from their role in the generation of defects.

To investigate the atomic structure of the Si/SiO_2 system several techniques are employed. Electron Spin Resonance (ESR) studies have been applied to obtain information on singly occupied localised electron states[12]. Using this technique, the structure of several electrically active defects such as the O vacancy center was resolved.

The structure of the interfacial region has also been investigated by high resolution transmission electron microscopy[13] and by X-ray photo-emission spectroscopy[14]. Although the results of the latter two studies have contributed to the general understanding of the problem, they have not provided specific insight in the relation between the structural and the electrical properties of the Si/SiO_2 interface region.

An alternative technique that could also provide structural information is positron annihilation spectroscopy. So far the possibilities of this approach were not sufficiently explored to study the Si/SiO_2 system. Positrons probe open spaces and negatively charged centers in the SiO_2 network and yield information on the electron density and chemical surrounding of these sites. The study of the MOS system using the positron beam analysis technique is the subject of the present thesis.

IV POSITRON ANNIHILATION SPECTROSCOPY

During the past few decades positron annihilation spectroscopy has been developed to a useful tool for material analysis[15,16]. In this technique positrons are implanted in solids to use them as a probe for several material properties. After its prediction in 1930 by Dirac[17], the positron was discovered in 1932 by Anderson[18]. The positron (e^+) has the same mass and spin as its anti-particle, the electron (e^-), but it has an opposite charge and magnetic moment. Positrons are stable in vacuum [19], but when thermalized in materials they annihilate with electrons:

$$e^+ + e^- \ -> \ 2\,\gamma. \hspace{3cm} (1)$$

Energy conservation causes the energy of the γ photons to be m_oc^2 with m_o the rest mass of the electron and c the velocity of light, i.e. 2 γ's of 511 keV. When positrons are implanted in materials they will undergo stopping processes related to interaction with electrons and phonons. After thermalization there are three possibilities. Firstly, the

thermalized positron may remain in a delocalized (Bloch) state and diffuse through the material until it annihilates with an electron. In monocrystalline materials with rather low defect concentrations, such as industrially prepared monocrystalline silicon, most positrons annihilate in such bulk states. Secondly, the positron may trap in some defect, its wave function becoming strongly localized, and annihilate in the trapped state. In
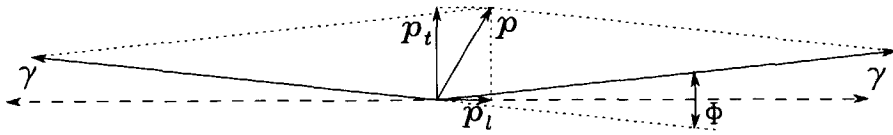
Figure 4. Conservation of momentum for the annihilation of an electron-positron pair with total momentum p. The longitudinal and transverse component of p are p_l and p_t, respectively. The longitudinal component of the momentum causes small energy shifts of the photons whereas the transverse component causes a deviation from collinearity of the two γ's. The magnitude of p is not to scale.

defective, amorphous or polycrystalline materials almost all positrons annihilate after being trapped in defects. Thirdly, the implanted positron may diffuse back to the surface where it is either trapped in a surface state, or is emitted to the vacuum. By means of scattering processes positrons implanted close to the surface may return to the outer surface prior to their thermalization leading to the emission of hot, or epithermal, positrons.

When both the positron and the electron are at rest while annihilating, conservation of energy and momentum causes the two γ photons to be emitted collinearly in opposite directions, each with an exactenergy of $m_0c^2 = 511$ keV. However, when the momentum p of the annihilating particles is non zero, which is generally the case, this will result in a Doppler shift in the energy of the photons, see

Fig 4. Furthermore, a momentum component p_t transversal to the emitted photons results in a small angular deviation ϕ between the emitted photons. For nonrelativistic electrons ($p \ll m_o c$) the photon energies observed in the laboratory system are $m_o c^2 - \Delta E$ and $m_o c^2 + \Delta E$, with

$$\Delta E = \frac{c \, p_l}{2} , \qquad (2)$$

where ΔE is the Doppler shift and p_l the longitudinal momentum component. The angle ϕ is given by

$$\phi = \frac{p_t}{m_o \, c} . \qquad (3)$$

The momenta of thermalized positrons are small compared with those of the electrons. Therefore, the annihilation photons carry information about the local momentum distributions of the electrons in the specimen. When the positrons are trapped at defects, information can be obtained about the electron momentum distribution at these defects. In this manner defect properties as size, and structure can be studied. One can perform such studies by measuring the Doppler shift ΔE of the annihilation photons, thus obtaining information on the longitudinal component of the electron momentum[15,16,20]. Doppler broadening measurements have been employed for the experiments described in this thesis.

Furthermore, one can measure the deviation ϕ from collinearity to obtain information about the transverse components of the electron momentum (see equation 2) which is the basis of the so called ACAR (Angular Correlation of Annihilation Radiation) technique[15,16]. Another category of experiments is based on measurements of the lifetime of the positron between its implantation and the annihilation event[15,16]. The mean positron lifetime, usually of the order of 100 ps, is related to the density of electrons at the annihilation site.

V THE *S*- AND THE *W*-PARAMETER

In Doppler broadening measurements the deviation of the γ photons from 511 keV is recorded to characterize the electron momentum distribution. The Doppler broadening of the peak at 511 keV in the γ-spectrum (the photo peak, see Fig. 5) is typically several hundred electronvolts, whereas the instrumental width of the detector resolution is typically 1.1 keV.
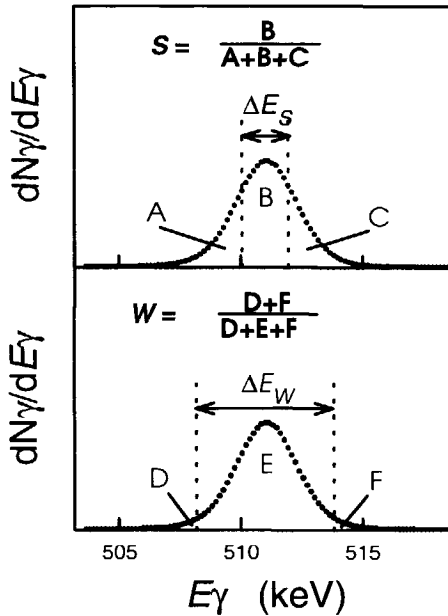
Figure 5. Definition of the shape parameter S and the wing parameter W of the peak at 511 keV. The areas A,B,.. ,F indicate sections defined with the aid of a fixed integration window (ΔE$_S$ and ΔE$_W$). The figure shows a typical experimental spectrum.

In general the peak at 511 keV is for convenience characterized by a so called *S* (shape) parameter, as introduced by MacKenzie *et al* [21]. The *S*-parameter is defined in Fig. 5 as the ratio of the area B, a fixed central part of the peak, and the total area of the total 511 keV peak[15,20,21]. The central energy interval is chosen such that it preferentially contains annihilations with valence electrons. The *W* (wing) parameter,

also defined in figure 5, is used to characterize specifically the contribution of core electrons, that is seen further away from the peak center at 511 keV.

It should be noticed that the absolute values of S and W carry no direct physical information because of their dependence on the resolution of the detection system and the specific choice of the integration intervals. On the other hand, normalized parameters obtained by the ratio of S and W with S and W values of a reference material (e.g. crystalline silicon), respectively appear to be rather independent of the measuring equipment and can be used for absolute quantification[15,20]. For this reason all values for S and W presented in this thesis are normalized to the bulk silicon values.

VI BEHAVIOUR OF POSITRONS IN THE MOS SYSTEM

In the literature, positrons in SiO_2 are often, just as positrons in metals and semiconductors, treated as thermalized particles that are efficiently trapped by defects in the material[20,22]. However, in insulators like SiO_2 the large bandgap excludes a rapid thermalization below 9 eV by interaction with electrons. Based on such considerations, Simpson *et al* [23] predicted that positrons in SiO_2 hardly cool down to zero energy and that non thermalized positrons can easily be transported through SiO_2 by applying an electric field. For the interpretation of the data from the biased MOS system, this issue is of great importance.

Another property, relevant for the understanding of the behaviour of positrons in the MOS system is the potential step for positrons at interfaces caused by the difference between the positron affinities of the adjacent materials. The height of the potential step ΔE experienced by positrons at an interface is of the order of 1 eV, much larger than the thermal kinetic energy ($\sim k_b T$). Therefore, it is highly probable that positrons coming to an interface from a material with a more negative positron affinity are not able to pass the interface[24]. Our results will shed new light on these issues essential for the study of MOS systems.

VII SCALE DIMENSIONS OF INVESTIGATED MOS CAPACITORS

When using MOS capacitors with metal gate, the broad implantation profile of positrons allows only the study of rather thick oxide layers of typical 100 nm. When scaling down the oxide thickness, the signal from the bulk oxide or Si/SiO_2 interface will be disturbed by annihilation of positrons implanted in the substrate and the gate metal. Because of this, most results presented in this thesis concern MOS capacitors with thick oxide layers. However, in chapter 5 a method is presented to overcome this problem by using a polysilicon gate with large grain size. When employing the drift of positrons in the polysilicon gate, one can also characterize the defect structure of thin oxide layers.

Another problem one has to face when investigating MOS capacitors with thin oxides (<10 nm) is related to electrical breakdown. When using a positron beam with diameter of typical 8 mm, one needs large capacitors with an area of about 1 cm^2 which in combination with a thin oxide thickness causes a rather low yield due to electric breakdown when applying a gate bias. Such problems can be avoided when studying small capacitors (<1×10^{-1} cm^2) using a positron beam with a small diameter (<3 mm). The recently developed electrostatic positron beam line with a beam spot of 8×10^{-2} cm^2 e.g. enables the study of industrial MOS capacitors with oxide layers thinner than 10 nm.

VIII SCOPE AND OUTLINE OF THIS THESIS

The topic of this thesis is the analysis of the defects in the MOS system using positron beam Doppler broadening measurements. This work requires understanding of the transport and trapping behaviour of positrons in the MOS system and needs a reliable method to analyze positron beam data for MOS capacitors. The results of this study yield a method to characterize the electron momentum distribution of defects at the Si/SiO_2 interface in MOS capacitors with aluminium or polysilicon gate. We applied this method

to investigate the effect of several annealing treatments and exposure with low energetic electrons and compared these results with those obtained with electrical characterisation techniques.

The structure of this thesis is as follows. In chapter 2 we describe briefly the equipment used for our experiments. In chapter 3 we will treat the analysis of positron beam data. First we describe the conventional positron beam analysis method which uses the dependence of the Doppler broadening shape parameter S on the implantation depth of the positrons. Subsequently we will introduce a novel analysis method based on the use of an extra parameter W which allows characterization of defects with the aid of a so called S-W plot. The two methods will be illustrated by three examples: H implanted Si, a bare SiO_2 layer on Si and an MOS capacitor.

The chapters 4, 5 and 6 deal with the transport and trapping behaviour of positrons in several types of MOS systems and present a method to probe the structure of the Si/SiO_2 interface with positrons. Chapters 7 and 8 will discuss results from the positron beam studies on the defect structure in the MOS system with the aid of positrons.

Chapter 4 gives an extensive description of results on the transport and trapping of positrons in Al and W gated MOS capacitors at different positive and negative bias conditions. We will show that by applying an electric field in the oxide layer, the positrons can be efficiently transported to the Si/SiO_2 interface where they probe its structure. The insights obtained in this chapter will form a basis for the analysis of defects in the MOS system.

In chapter 5 we will discuss results on the transport and trapping behaviour of positrons in the polysilicon gated MOS system. We optimized the doping concentration and the grain size in the gate such that the positrons implanted in the polysilicon gate and the underlying SiO_2 layer could be extracted from both layers by an electric field. Especially for the characterization of the defect structure in thin (<5 nm) oxide layers these results offer interesting perspectives.

Chapter 6 will continue with a study on the vacuum emission of heated positrons from the SiO_2 layer to the vacuum. For this purpose small metal islands were deposited on a SiO_2 layer and were charged to induce electric fields. Although the results indicate that some positron re-emission occurs, the obtained yield is too low for application of MOS capacitors as moderators for positrons.

In chapter 7 we will present results on a comparative study on the defects in Al gated MOS capacitors by both electrical characterization methods and by positron beam analysis. We will show that positrons do provide new insights in the relation between the VUV radiation hardness and the structural properties of the Si/SiO_2 interface region.

Chapter 8 deals with the analysis of the γ-spectrum obtained by coincidence measurements using two Ge detectors. In this manner more detailed information on the defect structure of defects in bulk SiO_2 and at the Si/SiO_2 interface is obtained.

Finally, chapter 9 will give a short overview of the results presented in this thesis. Furthermore, we will discuss in this last chapter the implications and perspectives of the results of this research.

[1] E.H. Nicollian and J.R. Brews, *MOS Physics and Technology* (Wiley-Interscience, New-York, 1982).

[2] D.A. Buchanan, A.D. Marwick, D.J. DiMaria and L. Dori, J. Appl. Phys. **76**, 3595 (1994).

[3] G. van den Bosch, G. Groesenken, H.E. Maes, R.B. Klein and N.S. Saks, J. Appl. Phys. **75**, 2073 (1994).

[4] F.B. McLean, H.E. Boesch and T.R. Oldham in *Ionizing Radiation Effects in MOS Devices and Circuits*, edited by T.P. Ma and P.V. Dressendorfer (Wiley-Interscience, New York, 1989) p. 87.

[5] W.H. Zachariassen, J. Am. Chem. Soc. **54**, 3841 (1932).

[6] V.V. Afanas'ev, J.M.M. de Nijs, P. Balk and A. Stesmans, J. Appl. Phys. **78**, 6481 (1995).

[7] K.G. Druijf, J.M.M. de Nijs, E. v.d Drift, E.H.A. Granneman and P. Balk, J. Appl. Phys. **78**, 306 (1995).

[8] H. Lefèvre and M. Schultz in *The Si-SiO$_2$ system*, edited by P. Balk (Elsevier, Amsterdam, 1988) p. 273.

[9] C. Svensson in *The Si-SiO$_2$ sytem*, edited by P. Balk (Elsevier, Amsterdam, 1988) p. 241.

[10] J. Krauser, F. Wulf, M.A. Briere, J. Steiger and D. Bräunig, Microelectronic Eng. **22**, 65 (1993).

[11] R. Gale, F.J. Feigl, C.W. Magee and D.R. Young, J. Appl. Phys. **54**, 6938 (1983).

[12] P.M. Lenahan, Microelectron. Eng. **22**, 129 (1993).

[13] G. Hollinger, R. Saoudi, P. Ferret and M. Pitaval, in *The Physics and Chemistry of SiO$_2$ and the Si/SiO$_2$ interface*, edited by C.R. Helms and B.E. Deal (Plenum Press, New York, 1988) p. 211-218.

[14] F.J. Himpsel, F.R. McFeely, A. Taleb-Ibrahimi, J.A. Yarmoff and G. Hollinger, Phys. Rev. B **38**, 6084 (1988).

[15] P.J. Schultz and K.G. Lynn, Rev. Mod. Phys. **60**, 701 (1988).

[16] M.J. Puska and R.M. Nieminen, Rev. Mod. Phys. **66**, 814 (1994).

[17] P.A.M. Dirac, Proc. Cambridge Philos. Soc. **26**, 361 (1930).

[18] C.D. Anderson, Phys. Rev. **41**, 405 (1932).

[19] E. Belotti, M. Corti, E. Fiorini, C. Liguori, A. Pullia, A. Sarracino, P. Sverzellati and L. Zanotti, Phys. Lett. B **124**, 435 (1983).

[20] P. Asoka-Kumar, K. G. Lynn and D.O. Welch, J. Appl. Phys. **76**, 4935 (1995).

[21] I.K. MacKenzie, J.A. Eady and R.R. Gingerich, Phys. Lett. A **33**, 279 (1970).

[22] T. C. Leung, P. Asoka-Kumar, B. Nielsen, and K. G. Lynn, J. Appl. Phys. **73**, 168 (1993).

[23] R.I. Simpson, C.D. Beling and M. Charlton, in *The Physics and Technology of Amorphous SiO$_2$*, edited by R.A.B. Devine (Plenum Press, New York, 1987), p. 569.

[24] P.A. Huttunen, J. Mäkinen and A. Vehanen, Phys. Rev. B **41**, 8062 (1990).

Chapter 2

Experimental facilities

I INTRODUCTION

In this chapter the experimental facilities used for the work of this thesis are briefly described. The electrical characterizations and the sample preparations were all performed with the aid of facilities at the Delft Institute of Microelectronics and Submicrontechnology (DIMES). These issues will be treated in sections 2 and 3. In the subsequent section (4) we will describe the Delft Variable Energy Positron Beam (VEP) at the Interfaculty Reactor Institute (IRI) which was used for the positron beam experiments. In the course of the work an *ExB* deflection system for the detection of re-emitted positrons was added to the VEP. This deflection system with its micro channel plate (MCP) detection system will be described in the final section (5).

II SAMPLE PREPARATION

MOS capacitors were fabricated on 4 inch wafers of (100) Si prepared by oxidation in dry O_2 at 1000°C[1]. The gate oxides had a typical thickness of 100 nm. The oxidation process was stopped by changing the gas flow from O_2 to N_2 or Ar, thus subjecting the oxides to a post oxidation anneal (POA). After a certain time, the POA

time, the furnace was ramped down to 800°C, after which the wafers were unloaded. The oxidation furnace is equipped with a special unloading tube to allow the wafers to cool down in a pure (5 ppm impurities) N_2 ambient. With the aid of this tube hydrogen passivation of as grown interface traps is avoided[2]. Transparent (~15 nm) Al and Au gates were deposited by evaporation from a resistively heated W-boat in a vacuum system with a base pressure in the range of 10^{-6} mbar. W-gated capacitors were fabricated by plasma sputter deposition at room temperature. Using a shadow mask we defined 13 mm diameter capacitors for the positron beam measurements and 2 mm ones for the electrical characterizations. In some cases measurements on as grown samples are compared with results obtained after hydrogen passivation of the interface states. Such passivation is performed in a controlled way by a so called post metallization anneal (PMA) in forming gas (10% H_2 and 90% N_2, 1 bar) at 400°C[3]. Capacitors for the positron measurements were first subjected to a quality test; only those that sustained an electric field of 2 $MVcm^{-1}$ were used. Furthermore, during the positron measurements the capacitors were controlled on leakage current.

III ELECTRICAL CHARACTERIZATION

The density of defects in the MOS capacitors was measured using the capacitance voltage (CV) technique. These CV measurements allow the determination of the density of the Si/SiO_2 interface defects as well as of the concentration of charge in trapping centers in the bulk of the oxide. The detection limit of these electrical characterizations depends on the oxide thickness and on the doping concentration of the substrate. For our samples the detection limit typically is 10^{10} cm^{-2}.

Avalanche electron injection was applied to study the electron traps in the bulk oxide layer[5]. With this method, a triangle wave function with a maximum of typical 50V and with a frequency of 30 kHz is applied on the gate of MOS capacitors with a p-
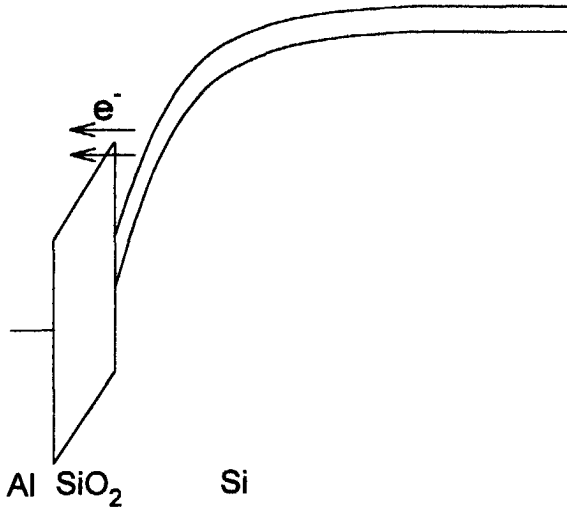
Figure 1. Avalanche injection of electrons in the SiO_2

type substrate. In Si at room temperature the number of minority carriers, in this case the free electrons, is determined by the relation[6].

$$n_e \, n_h \; = \; 1 \times 10^{20} \, \text{cm}^{-6} \qquad\qquad (1)$$

where n_e and n_h are the concentration of free electrons and holes. For an acceptor concentration of 10^{17} cm^{-3} the 0.5 mm thick Si substrate thus contains an equilibrium electron concentration of only $\sim$50 cm^{-2} which is too low to create a negatively charged inversion layer at the Si/SiO_2 interface during the increasing voltage ramp. Such an inversion layer typically requires $\sim 10^{13}$ cm^{-2} free electrons. Because of this absence of electrons, and a too slow thermal generation of electron-hole pairs, the electric field will extend deep into the silicon substrate; only the negatively charged acceptor atoms in a

deep depletion layer of typical 500 nm will shield the field in the silicon. The strong field in the range of 1 MV/cm in this depletion layer will accelerate the few thermally generated free electrons available sufficiently to excite valence electrons to the conduction band, thus creating an avalanche of energetic electrons, see Fig. 1. Some of these electrons reach the oxide with an energy high enough to be injected into the conduction band of SiO_2. In this manner a typical injection current of 10^{-4} Acm^{-2} can be realized. Subsequently, some of the injected electrons are trapped at defects in the SiO_2 network[5]. The cross section of these electron traps is in the range of 10^{-17} cm^{-2} or less so that about 0.1 Ccm^{-2} has to be injected for a charging experiment. The number of the charged centers is determined by periodic CV measurements.
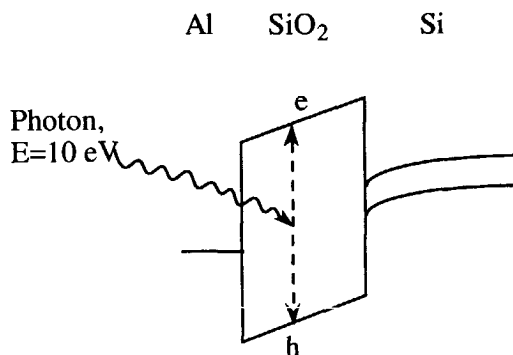
Figure 2. Absorption of a 10 eV photon by generation of electron-hole pairs in the oxide.

For hole trapping experiments we used the technique of VUV hole injection: the capacitor is exposed to the radiation of a Kr source ($h\nu = 10$ eV, 10^{15} photons $cm^{-2}s^{-1}$) while applying a positive gate bias in the range of 10 V, corresponding to an electric field in the oxide layer of 1 MV cm^{-1}, see Fig. 2 [7,8]. The photon energy of 10 eV is just sufficient to create electron-hole pairs. Due to the strong absorption, electrons and

holes are generated in the first 15 nm beneath the gate only[9]. The generated free electrons drift to the gate whereas the holes are transported through the oxide layer towards the substrate, thus filling the hole traps in the oxide. The amount of trapped charge is, again, obtained from CV measurements.

IV POSITRON BEAM FACILITY

The positron-annihilation Doppler-broadening experiments have been performed with the Delft Variable Energy Positron Beam (VEP)[10]. This facility offers a monoenergetic positron beam with a diameter of 8 mm and a typical intensity of 10^5 positrons cm^{-2} s^{-1}. The energy can be varied from 0 to 30 keV with a spread in energy of 1 eV. An extensive description of the VEP has been given by Schut[11], Hakvoort[12] and van Veen[10].

Fig. 3 shows a schematic drawing of the VEP. The system consists of several interconnected parts. The figure shows the source-storage section(A), the source and moderator area (B), the bent section used for positron-energy filtering (C), the section for beam acceleration (D), the section with an ExB deflection system (E) and finally the sample chamber and photon detection area (F).

The positron source consists of a 70 mCi ^{22}NaCl source. The emitted positrons are moderated by a 3 μm thick 99.95 % pure polycrystalline tungsten foil in transmission geometry. After re-emission from the tungsten foil the positrons are pre-accelerated to an energy of 115 eV and subsequently transported from the source area to the sample chamber by a 10 mT static axial magnetic field produced by a set of coils positioned in a Helmholtz configuration. A bent tube with a 1 m radius of curvature provides a filtering of fast moving positrons. After passing the curved section the positrons are accelerated to their final energy (with a maximum of 30 keV) by applying a high voltage to the beam section in front of the acceleration plates. With exception of the positron-source storage vessel all parts meet the requirements set for operation under high

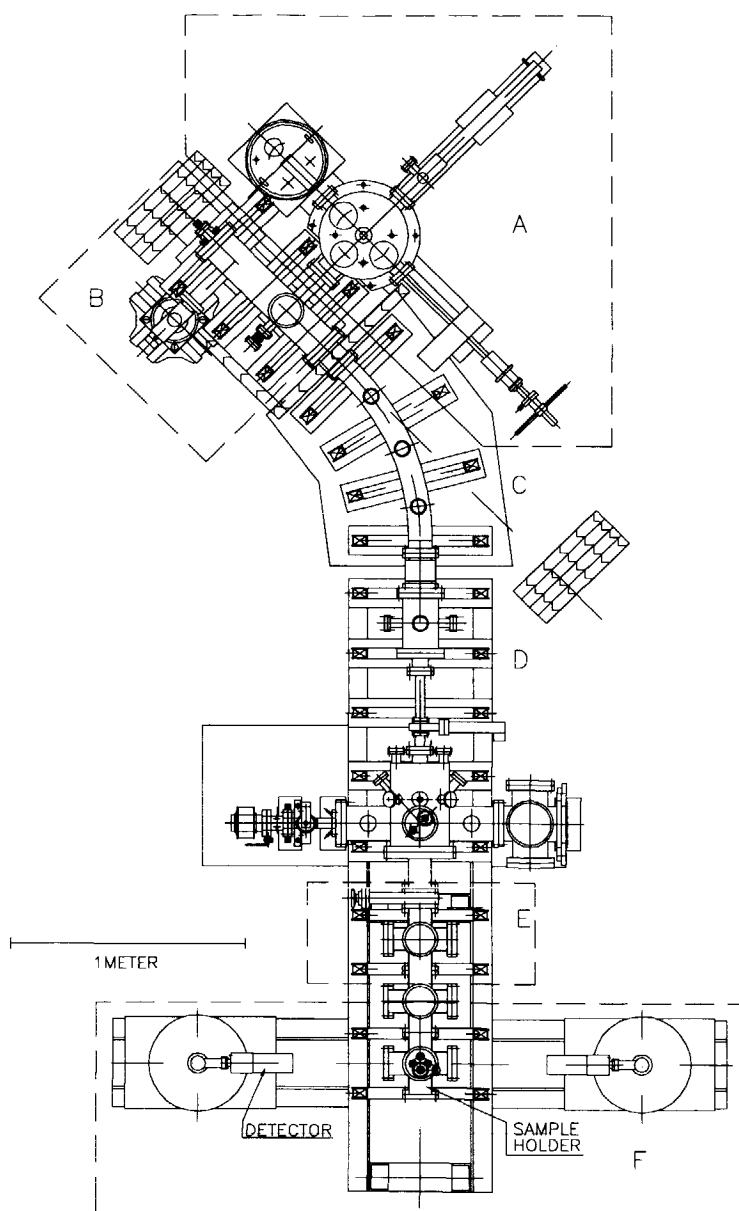*Figure 3. Schematic drawing of the Delft Variable Energy Positron Beam (VEP). The VEP consists of a section for source storage (A), a source and moderator section (B), a bent section used for positron-energy filtering (C), a section used for positron acceleration (D), a section with an ExB deflection system for decoupling of re-emitted positrons from the beam (E), and the sample chamber and gamma detection area (E).*
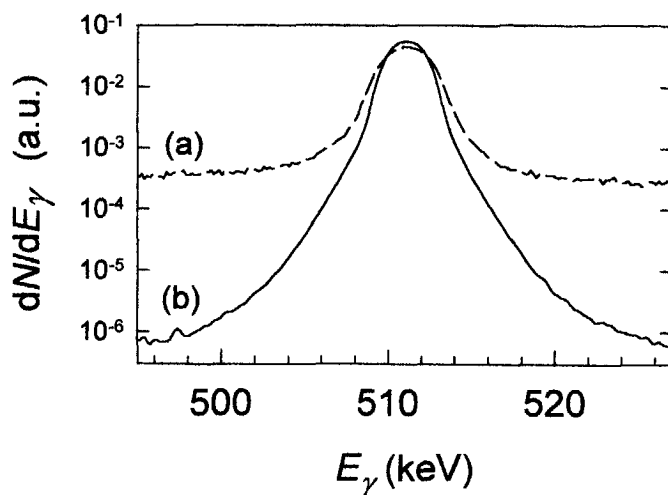
Fig 4. γ spectra for measurements on bulk Si recorded with (a) a single detector and (b) two detectors in coincidence accounting only the events that are simultaneously detected and that are related to photon pairs with a summarised energy of two times 511 keV.

vacuum conditions. During operation the pressure in the sample chamber was typically 10^{-7} mbar, which could be reached without baking the system after changing the samples.

The γ spectrum is measured with an intrinsic germanium solid state detector (EG&G Ortec, GEM-30185-P) with an energy resolution of 1.1 keV at 511 keV and a relative efficiency of 33% at 1.33 MeV. Fig. 4 shows a typical spectrum recorded during an experiment. Besides the annihilation peak at 511 keV there is also a large contribution of photons with a lower energy and a smaller one of photons with a larger energy. The low energy contribution results mainly from energy loss of 511 keV annihilation quanta due to Compton interactions with electrons in the sample, the walls and the detector. The signal above 511 keV is caused by high energetic background radiation. The background in the γ spectrum at 511 keV frustrates the investigation of the side wings of the photo peak which contain valuable information on the interaction with high momentum core electrons. However, the background can be reduced by three orders of magnitude by performing coincidence measurements using a second detector facing the sample from the

opposite direction[13]. Only the events that are simultaneously detected by both detectors and are related to photon pairs with a total energy of two times 511 keV are accounted for. A disadvantage of the two detector coincidence method is the lower detection efficiency which has to be compensated by increasing the time required for a measurement. A simple one detector Doppler broadening measurement requires typically 10 minutes while for a coincidence measurement with the same statistical accuracy 12 hours is required. Because of this, the coincidence measurements technique is applied for obtaining information at one or two well-selected implantation energies only, whereas the single detector set-up is used for depth profiling by measuring the overall Doppler broadening as function of implantation energy.

V *ExB* DEFLECTION SYSTEM

For the study of positrons that are re-emitted from the sample the VEP is equipped with an *ExB* deflection system. Furthermore, this *ExB* system can be used to expose the sample to electrons by guiding electrons emitted from a filament in the *ExB* system to the sample.

The principle of the *ExB* deflection system is demonstrated in Fig. 5 which shows a simulated positron trajectory. As shown in this figure, the incoming positrons follow the magnetic field lines while the electric field is oriented perpendicularly to the moving direction of incoming positrons. When entering the deflection system the positrons are first deflected somewhat in the direction of the electric field defined as the *y* direction. However, because of the magnetic field the *y* component of the velocity is transformed in a velocity component in the *x* direction. Finally the positron will be deflected in a direction perpendicular to the electric field with a velocity component in the *x* direction so that the electrostatic force is compensated by the Lorentz force. The deflection angle α is defined by[14]:
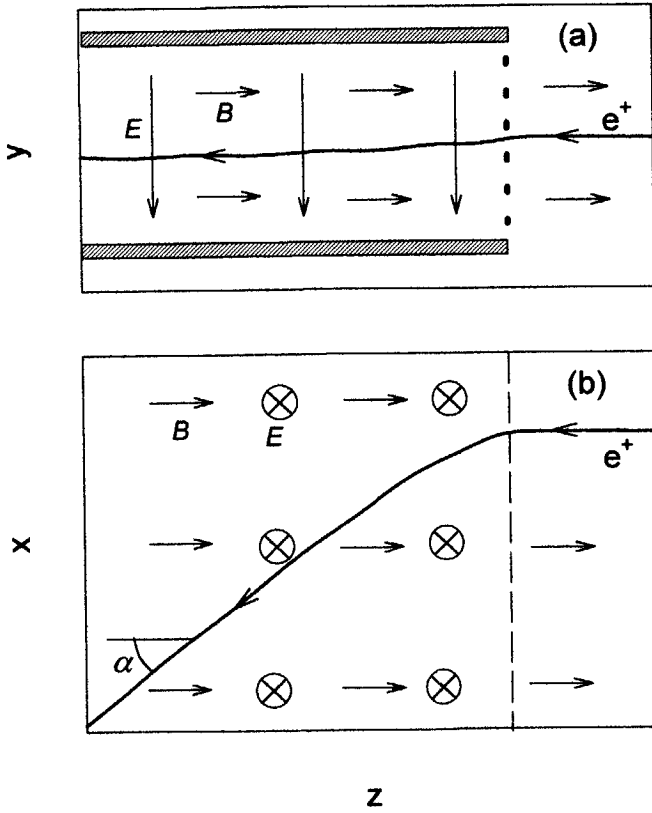
Figure 5. Trajectory of a 1 eV positron in an ExB deflection system as calculated with the computer code SIMION. Part (a) shows a side view of the system with metal field plates and the grid at the edge. Part (b) shows a top view.

$$\tan(\alpha) = \frac{E}{B\,v_O},\qquad\qquad (2)$$

where E and B are the electrostatic and magnetic field intensities and v_O is the initial velocity of the positron. From this formula it follows that the deflection angle is inversely proportional to the initial velocity of the positron; i.e. slow positrons will be strongly deflected whereas fast ones pass unhampered.

A schematic drawing of the ExB deflection system is shown in Fig. 6. As shown in fig. 6 the emitted positrons with energies of typically upto 5 eV are deflected and can be detected by a micro channel plate (MCP) system. The deflection of the high energetic primary beam (0.1 keV - 30 keV) is much smaller and can be corrected by another set of field plates with opposite electric field. At the sample site of the deflection system a grid (Cu, 1×1 mm^2 square meshes, 10% area coverage) is mounted to create a potential barrier for energy selection of the re-emitted positrons.

The used MCP system has a diameter of 27 mm (Hamamatsu F1551) and was used in combination with a metal plate as anode for collecting the charge pulses caused by the positron impacts. The resulting voltage pulses are de-coupled from the high DC potential on the anode by a high frequency pass filter. After pre-amplifying, noise reduction by a pulse height discriminator and translation to TTL pulses, the MCP signal is handled by a personal computer. The front side of the MCP was kept on a negative potential of about -300V to prevent the detection of secondary electrons originating from material surfaces hit by the positron beam. In front of the MCP, a grid (Cu, 1×1 mm^2 square meshes, 10% area coverage) is mounted to shield the electric field caused by the voltage on the MCP system.

A disadvantage of the ExB plates deflection system is the strong dependence of the deflection on the height position of the incoming positron. This problem is illustrated in Fig. 7 by a series of trajectory calculations. Positrons that enter the deflection system exactly between the field plates experience the mean of the two plate
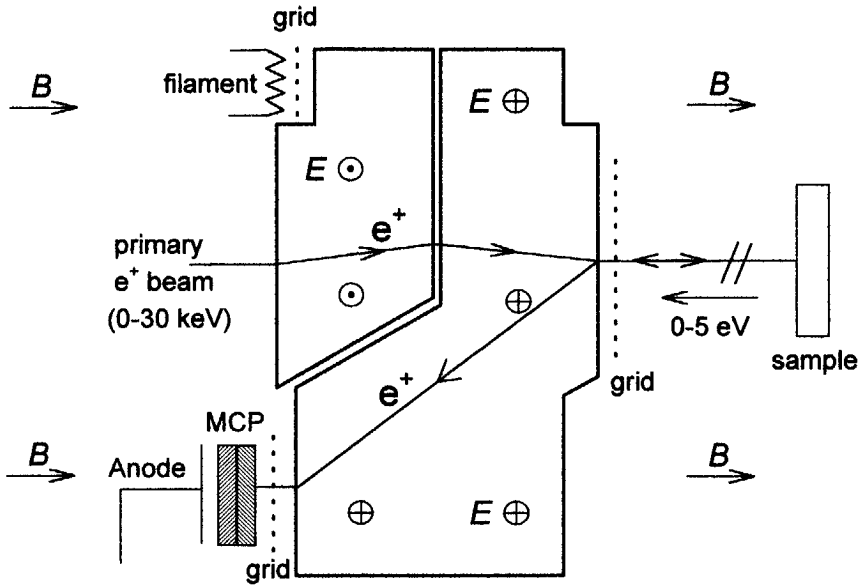
Figure 6. Schematic drawing of the ExB system used for decoupling of low energetic re-emitted positrons (E<10 eV) from the central beam line. The figure shows the metal field plates, the grids, the orientation of the electric and magnetic fields, the MCP system and the trajectories of the primary and re-emitted positrons. The re-emitted positrons are deflected with the aid of the large field plates and are detected with a Micro Channel Plates (MCP) system. The deflection of the primary beam is corrected with the aid of the small field plates.

potentials. However, because of the gradient in electrostatic potential positrons at different height are accelerated or decelerated to different velocities. As a consequence the positrons are deflected over different angles or are reflected at the edge of the deflection system. Note that the positrons are already deflected somewhat before entering the deflection system.
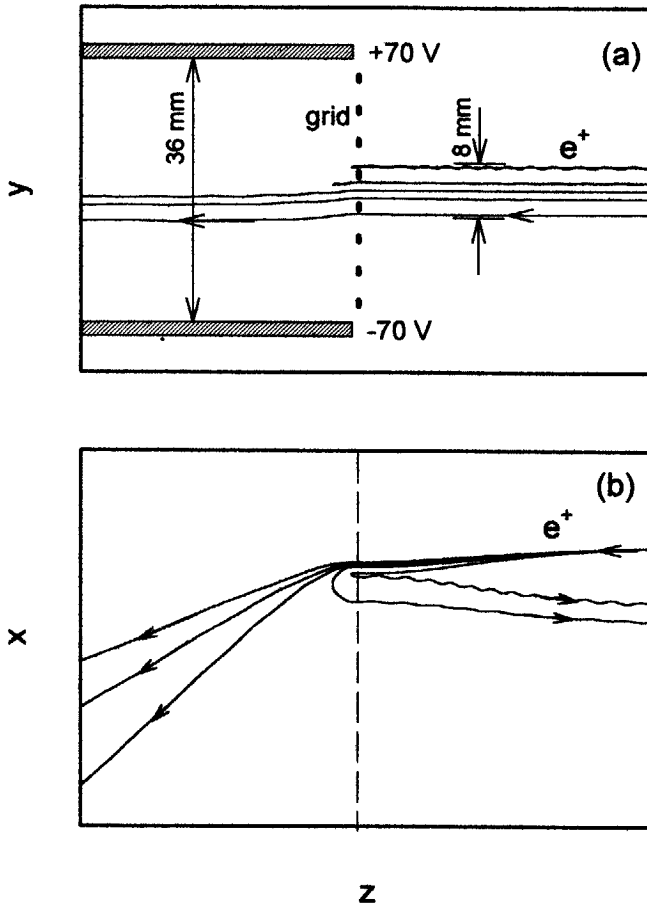
Figure 7. Trajectory of 1 eV positrons entering the EXB deflection sytem at different height positions calculated with the computer code SIMION.

This phenomena is caused by the feature that, in spite of the grid at the edge, the field plates also induce a weak fringing electric field in the region in front of the ExB system. Because of the reflection and varying deflection angle only a small fraction of the incoming positrons reaches the MCP. In chapter 6 we will discuss this issue in more detail. We will show that the ExB deflection system with MCP operates with a typical efficiency of about 1%. Furthermore, a shifting of the centre of the primary beam by

only 1 mm during the energy scan results in significant variations in the MCP count rate. This effect is demonstrated in Fig. 8 which shows the number of positrons from a W foil, as detected with the MCP, versus the implantation energy. The reflection and the spread in deflection angle in the *ExB* system causes clear long range fluctuations in the MCP count rate versus energy signal.
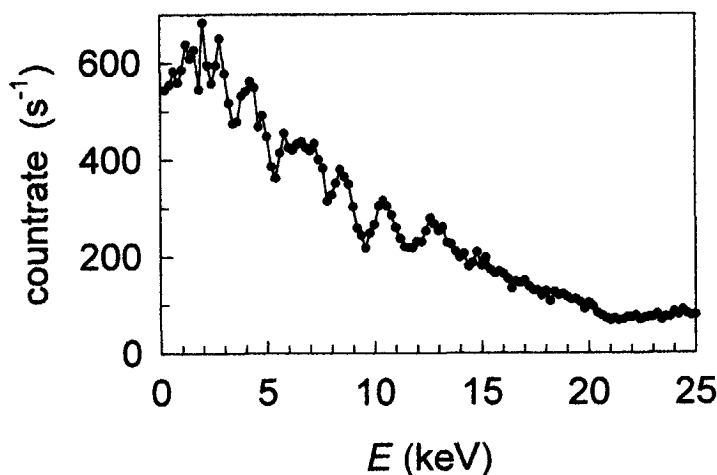
Figure 8. MCP count rate versus the primary positron implantation energy for possitrons re-emited from a W foil.

With the aid of the *ExB* deflection system we can also deflect electrons in order to charge the sample. To this end a W filament is mounted in the *ExB* system behind a grid, see Fig. 9. The electrons emitted by the filament are extracted by applying a negative bias on the filament and a positive potential on the grid after which they are guided to the sample by the electric and magnetic fields. Note that to this purpose the electric field between both sets of field plates points in the same direction. The spread in energy of the emitted electrons is determined by the voltage drop over the filament and amounts typical 2 eV. The emission current from the filament is in the range of 1 mA. For exposure of electrons in the energy range of 1 eV a potential difference of about 50 V over the field plates is needed. Without changing the magnetic field an efficiency of 2%

was realized; i.e. a sample current of 2% of the emission current from the filament was obtained. When switching off the last magnet coil, a more homogeneous distribution of electrons over the sample (~1.5 x 1.5 cm^2) was realized. However, this configuration has an electron efficiency of 0.5% only. For maximum filament power (2V, 2.5A) the exposure on the sample is in the range of 10 μA.
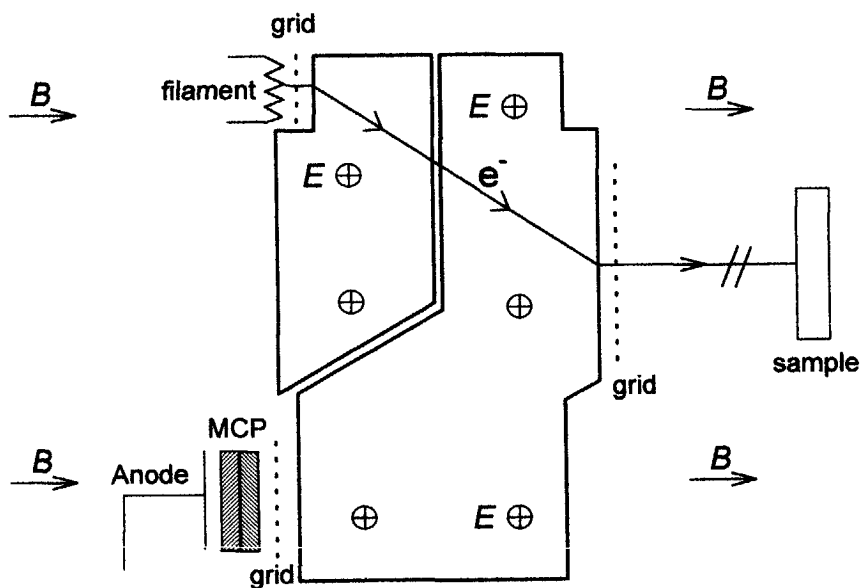
Figure 9. Schematic drawing of the generation of a low energetic electron beam using the ExB deflection system and a W filament. The electrons are extracted from the filament with the aid of a grid and deflected by the ExB system such that they are coupled into the central beam line after which they are guided by the magnetic field to the sample.

1 E.H. Nicollian and J.R. Brews, *MOS Physics and Technology* (Wiley-Interscience, New-York, 1982).

2 K.G. Druijf, J.M.M. de Nijs, E. van der Drift, E.H.A. Granneman and P. Balk, Appl. Phys. Lett. **65**, 347 (1994).

3 E.H. Nicollian and J.R. Brews, *MOS Physics and Technology* (Wiley-Interscience, New-York, 1982), p. 782.

4 H. Lefèvre and M. Schultz in *The Si-SiO2 system*, edited by P. Balk (Elsevier, Amsterdam, 1988) p. 273.

5 E.H. Nicollian and J.R. Brews, *MOS Physics and Technology* (Wiley-Interscience, New-York, 1982), p. 492.

6 E.H. Nicollian and J.R. Brews, *MOS Physics and Technology* (Wiley-Interscience, New-York, 1982), p. 35

7 JV.V. Afanas'ev, J.M.M. de Nijs, P. Balk and A. Stesmans, J. Appl. Phys. **78**, 6481 (1995).

8 K.G. Druijf, J.M.M. de Nijs, E. v.d Drift, E.H.A. Granneman and P. Balk, J. Appl. Phys. **78**, 306 (1995).

9 Z.A. Weinberg, G.W. Rubloff and E. Bassous, , Phys. Rev. B **19**, 3107 (1979).

10 A. van Veen, J. Trace Microprobe Techn. **8**, 1 (1990).

11 H. Schut, *thesis*, Delft University of Technology, Delft (1990).

12 R.A. Hakvoort, *thesis*, Delft University of Technology, Delft (1993).

13 P. Asoka-Kumar, M. Alatalo, V.J. Ghosh, A.C. Kruseman, B. Nielsen and K.G. Lynn, Phys. Rev. Let. **77**, 2097 (1996).

14 J.D. Jackson, Classical Electrodynamics (John Wiley & Sons, New York)

Chapter 3

Data analysis by the combined use of the S- and W- parameters

I INTRODUCTION

Positron annihilation experiments have shown to be a useful tool for the investigation of defects in materials [1,2]. The crux of this technique is that in solid materials positrons are efficiently trapped at defects such as vacancies or voids[3], which makes them a very sensitive probe for studying these defects. After trapping the positron will annihilate with an electron from the immediate surrounding of the defect, thus producing two 511 keV γ-photons. The defect-related information is obtained from properties such as the life time of the positrons, the Doppler broadening of the photo-peak, or the angular correlation between the two photons (two dimensional angular-correlation of annihilation radiation: 2D-ACAR). Furthermore, a mono-energetic positron beam allows for controlled implantation. In this way the depth distribution of the defects can be investigated.

Thus far, the positron beam experiments have been successfully applied to rather simple systems, containing not to many different defects. For more complex systems the investigations are complicated by a lack of sufficiently independent experimental data. It has been proposed to tackle this problem by combination of Doppler broadening measurements with lifetime measurements, by two dimensional angular-correlation of

annihilation radiation measurements, by deconvolution of the photo-peak[4,5] or by coincidence measurements. However, such methods are rather complicated and time consuming or they require large investments in equipment. Therefore, it would be attractive to have a more simple method for the analysis of data from more complicated systems.
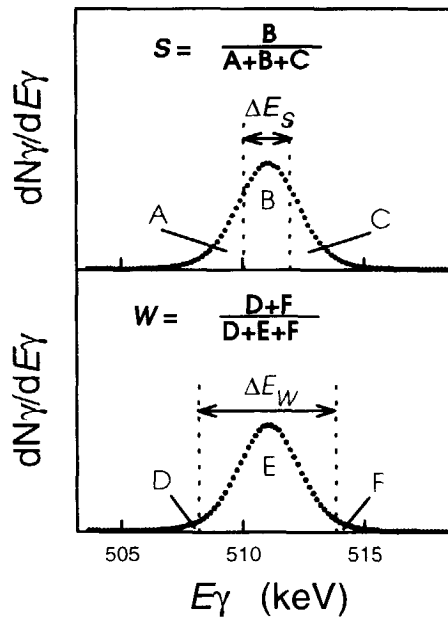
Figure 1. Definition of shape parameter S and wing parameter W of the photopeak. The areas A,B,.. ,F indicate sections defined with the aid of a fixed integration window (ΔE_S and ΔE_W). The figure shows a typical experimental spectrum.

In the case of Doppler broadening measurements commonly only the shape-parameter (*S*-parameter) is used, although, as shown by Liszkay et al.,[6] also the wing-parameter (*W*-parameter) may contain independent and thus valuable information. These authors have studied a series of CdTe samples using 25 keV positrons. The various

defects could be characterized by plotting the shape and the wing data of the different specimens in the *S-W* plane. Conceivably, a similar approach could be attractive for analysis of energy-dependent , and thus depth-dependent, positron beam data.

In the present study we have explored the combined use of the shape and the wing parameter for the positron beam experiments. It was found that plotting the measured *S-* and *W*-data as a trajectory in the *S-W* plane, using the implantation energy as a running parameter, provides a powerful approach for the interpretation of the experimental data. The description of the system in terms of positron trapping layers characterized by a *S*-value and a *W*-value could be directly derived from this plot. In this way, the interpretation problems which can occur for the more complicated systems are simplified or even avoided.

We will discuss three examples of the use of *S-W* plots. The first one is intended to explain the method. It concerns a Si wafer implanted with He which was subsequently annealed in vacuum. For this system the *S-W* plot provides similar results as the conventional method of analysis of $S(E)$ data, which illustrates the correctness of our approach. The second example concerns a metal-oxide-silicon (MOS) system subjected to a positive bias voltage. Analysis of this system employing the conventional approach is complicated by the limited knowledge on the field-induced transport of the positrons in the oxide layer. However, using *S-W* plots one is able to circumvent the positron transport problem and to formulate a model describing the system. The third example, thermally oxidized Si, is added as an illustration of the limitations of the approach.

In the case of three or less positron trapping layers, the combined use of shape and wing data offers another advantage: it is possible to directly calculate the energy-dependent fractions ($f(E)$) of the positrons annihilated in the different trapping layers. Subsequently, one can use each of these $f(E)$ curves as input data for the numerical quantification of the depth distribution of the defects and of the transport of positrons.

II. POSITRON BEAM DOPPLER BROADENING MEASUREMENTS

In positron beam Doppler broadening (DB) measurements the structural properties of materials are investigated by implantation of mono-energetic positrons. After thermalization the positrons diffuse through the material. In defective materials most of them will be trapped at defects. Ultimately, they annihilate with an electron, thus producing two γ-photons with energies of about 511 keV. The information on the defects is obtained from the Doppler broadening of the photo-peak, which is related to the momentum of the annihilated particles. The photo-peak is characterized using two parameters, the shape parameter (S) and the wing parameter (W), defined in Fig. 1 The shape parameter is associated with annihilation with low momentum (valence) electrons.[1,2] In the past decade the shape parameter has been successfully used as a fingerprint of the defects. The wing parameter corresponds to annihilation with high momentum (core) electrons.[1,2] Thus the information about the entire investigated system is provided by the energy-dependent data, $S(E)$ and $W(E)$.

In the conventional approach only the $S(E)$ data are used. These data are analyzed with the aid of a program such as VEPFIT[7]. The program contains an algorithm that simulates the implantation, the diffusion, the trapping and the annihilation of the positrons.[2] The system is described in terms of a stack of different positron trapping layers, each layer being characterized by a thickness (d_i), a characteristic shape parameter (S_i) and a positron diffusion length (L_i). This latter property is related to the defect concentration. The simulation algorithm calculates the energy-dependent distribution of positrons over the layers in the model. The overall S-value of the model system ($S^*(E)$) is then calculated from this distribution of the positrons. In the program, the model parameters are optimized by minimization of the residue function:

$$\chi^2(S_1, S_2, ..., S_n, L_1, L_2, ..., L_n, d_1, d_2, ..., d_n) \quad =$$

$$\frac{1}{N\sigma^2} \sum_{j=1}^{N} (S(E_j) - S^*(E_j))^2 , \tag{1}$$

where N denotes the number of data points and σ^2 their variance.

For our measurements the Delft Variable Energy Positron beam was used.[8] This facility provides positrons with energy ranging from 0 up to 30 keV with a typical flux of 10^4 s^{-1}cm^{-2}. The background pressure in this vacuum system is about 10^{-7} Torr. The spectrum of the γ-photons is measured with a Ge detector with a energy resolution of about 1.1keV at E_γ =511keV. Bulk crystalline silicon was used as a reference; the experimental *S*- and *W*-parameters were all normalized to the *S*- and *W*-parameters independently established on device-quality silicon.

III. HELIUM-IMPLANTED SILICON

In this section we analyze the data from a helium-implanted Si sample. In subsection A we follow the more conventional approach using single $S(E)$- or $W(E)$-data. Subsequently, in subsection B, we demonstrate the use of a S-W plot.

The samples were fabricated by implantation of 0.8 Ωcm^{-1} P-doped (100) silicon with 1×10^{17}cm^{-2}, 30 keV helium ions. This implantation energy corresponds to a projected range of 280 nm and a mean square straggle of about 100 nm.[9] The implantation will produce clusters of two or more vacancies filled with helium. Subsequently, the samples were annealed during 1 minute at a temperature of 800°C in vacuum. During the anneal the helium will desorb from the system and part of the defects will be removed; however, microcavities with diameter larger than 0.9 nm will
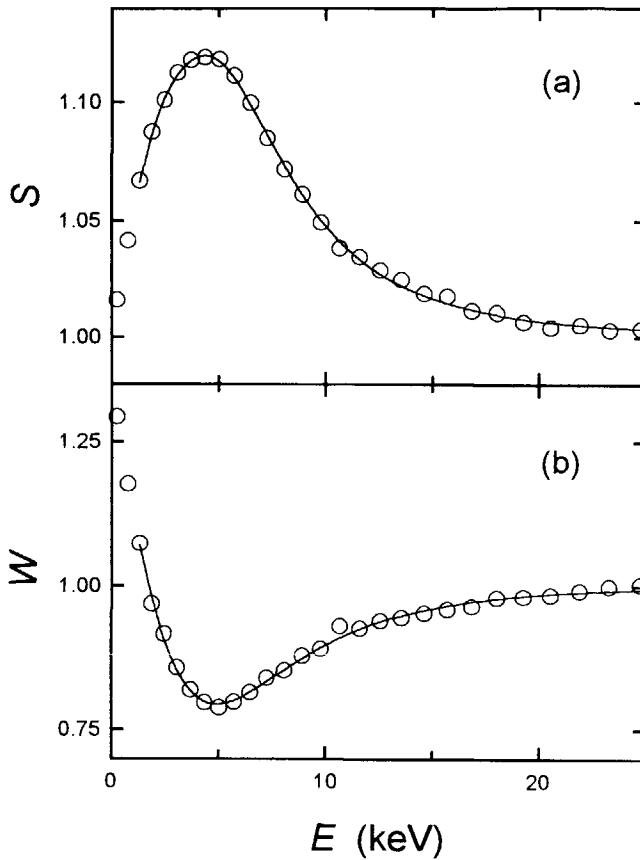
Figure 2. Shape and wing parameters as function of positron implantation energy for a Si sample implanted with 10^{17} cm^{-2} 30 keV He$^+$ and subsequently annealed at 800°C. The data have been normalized to bulk Si values. The curves drawn through the data points are obtained by fitting of the data with VEPFIT using the model of Fig. 3.

remain.[10,11,12] To eliminate the internal electric fields, which would affect the transport of positrons, the measurement was performed at an elevated temperature of 250°C.[13]
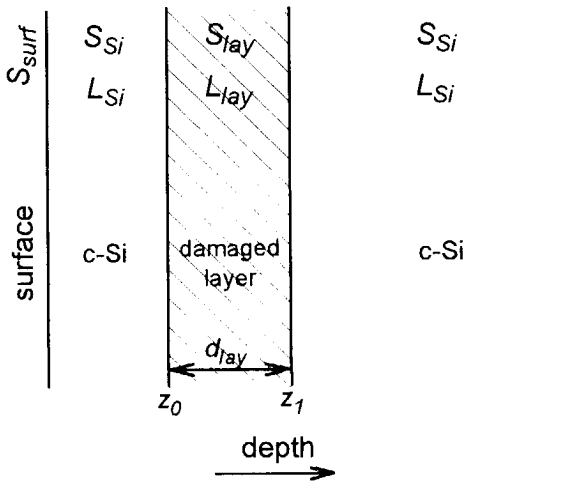
Figure 3 Buried homogenous defect layer model used for the simulation of the data from He-implanted Si.

A. Analysis of the $S(E)$ data

In Fig. 2 we present the normalized shape- and wing- data for the helium-implanted silicon sample. Qualitatively, we make the following interpretation. The low S-value found for the shallow implantation of the positrons is associated with surface annihilation. In the case of deep implantation, the shape parameter monotonically approaches the value ascribed to crystalline silicon. Thus for the deep implantations we have to deal with annihilation in the silicon substrate. For the intermediate energies a high S-value is obtained, which apparently corresponds to positrons trapped at defects in the damaged region.

Based on this qualitative interpretation of the data in terms of annihilation at the surface, in a defective layer and in the substrate, we have performed a quantitative analysis using a model in which the damaged region is approximated by a buried positron trapping

layer with homogeneous defect concentration. This model is schematically shown in Fig. 3. The lower and upper boundaries (z_l, z_u), the positron diffusion length (L_{lay}) and the characteristic S-values (S_{lay}) of the damaged layer, the characteristic S-value of the surface (S_{sur}) and the positron diffusion length of the defect free Si (L_{Si}) are used as free model parameters. The surfacewas considered as a perfect sink from which the positrons cannot escape.[1,3] For energies below 1 keV the measured S-values are also affected by positrons that reach the surface before thermalization.[1,14] Because of this, we only used the data for energies above 1 keV for the analysis. The $S^*(E)$ curve as obtained for the optimized model parameters is shown by the solid line in Fig. 2. As can be seen in this figure, the model satisfactory describes the data. The values of the optimized parameters are listed in Table I. The optimized position of the lower boundary of the damaged layer was located at the surface. Because of this, in Table I only the thickness of the damaged layer (d_{lay}) is given. Actually, this approximately zero lower boundery only indicates that the defect free top-layer is thinner than the positron diffusion length in defect-free silicon.

TABLE I. Positron related parameters derived by different methods for He implanted Si.

used data	S_{lay}	W_{lay}	d_{lay} (nm)	L_{lay} (nm)	L_{Si} (nm)
$S(E)$	1.132±0.006	-	360±35	40±12	175±35
$W(E)$	-	0.73±0.03	310±60	52±10	250±60
S-W plot	1.139±0.008	0.74±0.03	-	-	-
$f_{surf}(E)$	-	-	-	54± 7	-
$f_{lay}(E)$	-	-	315±30	50± 4	225±35
$f_{Si}(E)$	-	-	330±35	49± 6	210±40

The determined parameters are the shape- and the wing-parameter (S_{lay}, W_{lay}) and the thickness (d_{lay}) of the defective layer, and the diffusion length of positrons in this layer (L_{lay}) and in the defect free Si (L_{Si}). These quantities are separately derived from the individual $S(E)$- and $W(E)$-data, from the S-W plot and from the positron fractions $(f_{surf}(E)$, $f_{lay}(E)$ and $f_{sub}(E)$). The shown error values are related to the 95% probability interval which is twice the standard deviation of the fitted parameters.
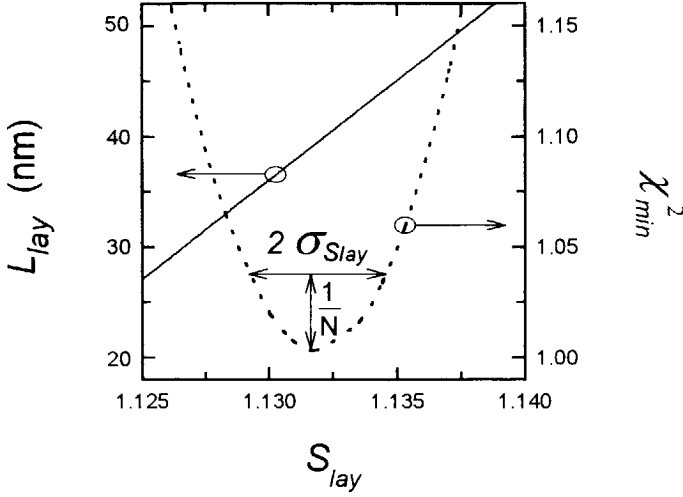
Figure 4. Optimized positron diffusion length L_{lay} of the damaged layer in the model for He-implanted Si as function of the fixed value of Slay (solid line) showing the coupling between these parameters. The dotted line shows the minimized residue χ^2_{min} as function of (fixed) S_{lay}. The model estimation of S_{lay} is given by the position of the absolute minimum of χ^2. The standard deviation related the statistical error, σS_{lay}, is determined by the width at height 1/N above the minimum. The error in L_{lay} is obtained by projecting the error interval of S_{lay} on the $L_{lay}(S_{lay})$ curve.

As remarked by Asoka-Kumar et al. in their review article,[2] the uncertainty in the values of the model parameters can be strongly affected by the coupling between S-values and diffusion lengths in the model used. To determine the actual uncertainty limits of the optimized parameters we have investigated the consequences of the coupling between S_{lay} and L_{lay} of the damaged layer. To this end, S_{lay} was kept at a fixed value and subsequently L_{lay} and the other model parameters were optimized to fit the data. Fig. 4 shows L_{lay} optimized in this way as function of the fixed value of S_{lay}. This curve, which is nearly a straight line in this region, illustrates the numerical coupling between

S_{lay} and L_{lay}. The minimized value of the residue function χ^2 of the fit with fixed S_{lay}, $\chi^2_{min}(S_{lay})$ is also plotted in Fig. 4. The absolute minimum in χ^2 corresponds to the most likely values of S_{lay} and L_{lay}. The accuracy of these values of S_{lay} and L_{lay} is related to the second derivative at the minimum by the equation[15]

$$\sigma_{Slay} = \frac{1}{\sqrt{\frac{1}{2} N \frac{d^2(\chi^2_{min})}{d(S_{lay})^2}}} \qquad (2)$$

where σ_{Slay} denotes the standard deviation related to the statistical error of S_{lay}. This standard deviation indicates the interval in which the real S_{lay} is located with a probability of 95%. From this relation it is deduced that the value of σ_{Slay} can be estimated from Fig. 4 by the width at height 1/N above the absolute minimum. The error in L_{lay} is obtained by projecting the error interval of S_{lay} on the $L_{lay}(S_{lay})$ curve. The uncertainty limits obtained in this manner for the different parameters are shown in Table I. As can be seen in this table, the coupling between model parameters causes a large uncertainty in the optimized value of L_{lay}.

It should be noted that the ability of a model to accurately describe the data does not automatically prove its correctness; conceivably there are other models that fit the data just as accurate. For example, we could have used a model comprizing two different defect layers instead of a single one. The correctness of any particular model can not be deduced from $S(E)$ data exclusively; reliability of the model has to be supported by complementary information obtained from other measuring techniques or from the fabrication procedure of the sample.

In a similar manner we have analyzed the $W(E)$ data using the same model with a buried homogeneous defect layer. The $W^*(E)$ curve, obtained in this manner and shown in Fig. 2, appears to give a good description the $W(E)$ data. The optimized model parameters are again summarized in Table I. This result confirms the conclusions obtained from analysis of the $S(E)$ data. The $W(E)$ data can quantitatively be described by the same model as the $S(E)$ data. However, the use of the $W(E)$ data by themselves does

not substantial improve the accuracy of the optimized parameters, nor does it provide certainty about the correctness of the used model.

B. Application of the S-W plot

In Fig. 5 we have plotted the $S(E)$ and $W(E)$ data of the helium-implanted silicon sample as a trajectory in the S-W plane, using the implantation energy as a running parameter. The arrow denotes the direction of increasing implantation energy. The different trapping layers are characterized by (S, W) coordinates instead of a single S-value. For example, for the high-energy implantation all positrons annihilate in the substrate. In the S-W plane this is seen from the clustering of the experimental data in this case at the point with coordinates $(S_{Si}, W_{Si}) = (1.0, 1.0)$.

The convenience of interpretation of the S-W plot stems from the linearity property of S and W which is a consequence of the particular choice of their definition (Fig.. 1).[1,2] The value of this property for the interpretation of the S-W trajectory can be seen as follows. Suppose that we have a system where the positrons annihilate in two different trapping layers only, which will be designated A and B. These layers are situated at different depth and are characterized by different (S, W) coordinates, (S_A, W_A) and (S_B, W_B). The implanted positrons thus will be distributed over the A and B layer. This distribution can be varied by changing the implantation energy. Because of the linearity property of the shape and wing parameters, such a variation corresponds to a straight line trajectory in the S-W plane running from the coordinates (S_A, W_A) towards (S_B, W_B):

$$S_M \quad = \quad f_A\, S_A \quad + \quad (1\text{-}f_A)\ S_B \qquad\qquad (3a)$$

$$W_M \quad = \quad f_A\, W_A \quad + \quad (1\text{-}f_A)\, W_B\,, \qquad\qquad (3b)$$

where f_A denotes the fraction of positrons trapped in layer A and S_M and W_M are the
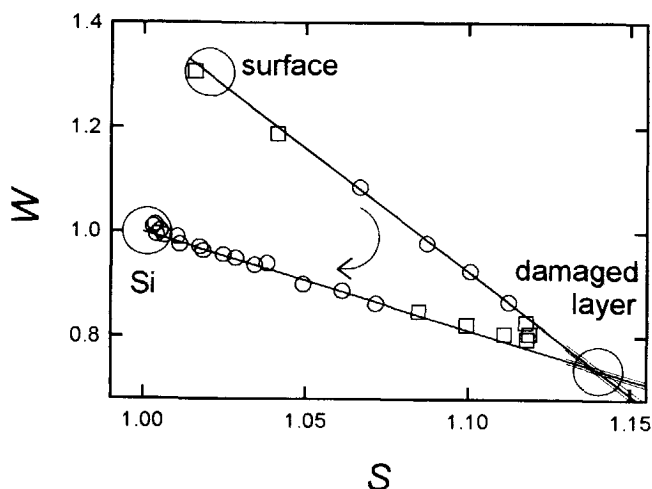
Figure 5. S-W trajectory of He-implanted Si. Arrows indicate the direction of increasing positron implantation energy. The data points denoted by the circles are used for the calculation of the slope of the two straight lines which describe the trajectory for low and high energy. The other data points are plotted as squares.

measured values. The presence of an additional, third, trapping layer with another depth distribution can now be immediately established from the trajectory: it should be curved, unless the characteristic (S, W) coordinates of this third trapping layer is accidentally located on the line (S_A, W_A) - (S_B, W_B).

With the aid of the above interpretations of straight and curved trajectories, we can easily explain our experimental data of the helium-implanted sample. The trajectory exhibits two straight parts, which indicates that for the lower energies and for the higher energies the system can be effectively described by trapping taking place in two distinct layers only. For intermediate energies, the trajectory deviates from the straight lines near their point of intersection. This shows that for these energies three trapping layers are involved and that the S-W coordinates of the third layer is given by the point of intersection.

As stated, the clustering point for high implantation energies corresponds to annihilation in the silicon-substrate. The point of intersection of the straight lines, which is approached for intermediate energies, is associated with positron trapping at defects in the helium-implanted region. For low energies there is no clear cluster point which inhibits the accurate determination of the characteristic (S_{surf}, W_{surf}) coordinates of the surface annihilation sites. Actually, this S-W point is situated somewhere on the straight line, but since epithermal positrons will come into play for energies below 1 keV the exact location could not be established.

The graphical analysis presented above clearly reveals the need of assuming the presence of three positron trapping layers which can be associated with the surface, the defect region, and the substrate; there are no indications of the presence of a fourth layer. This observation thus excludes the precence of two layers with different defects, as mentioned above. The plot also immediately shows that there is no need to consider the presence of an undamaged crystalline silicon layer between the damaged layer and the surface, irrespective of the likeliness of such a layer in view of the process steps of the fabrication of the sample; the positrons are simply not trapped in this layer.

To establish the intersection point we have used a numerical algorithm for linear regression analysis to calculate the best straight lines through the high energy and low energy data points. The data points used for this calculation are indicated in Fig. 5. Note that the first two data points, which are related to energies below 1 keV, are not used in this calculation because they have been affected by epithermal positrons at the surface. The uncertainty limits of the (S_{lay}, W_{lay}) coordinates can now be derived from the variance in the slope of the straight lines. By doing so we obtained comparable uncertainty interval as from the numerical analysis of the $S(E)$ and $W(E)$-data. The actual values are also listed in Table I. As can be seen in this table the values for S_{lay} and W_{lay} which were obtained from the S-W plot does not conflict with the results from the analysis of the individual $S(E)$- and $W(E)$-data.

Having graphically established the characteristic (S, W) coordinates for each of the layers, one can, for three layers or less, calculate the energy-dependent fractions $f(E_i)$
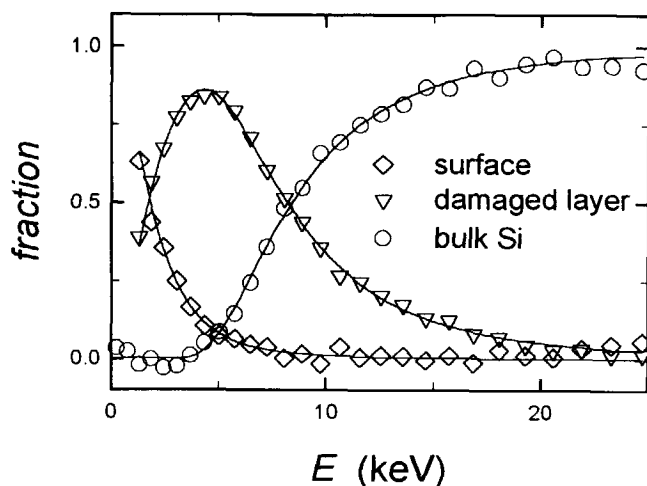
Figure 6. Energy dependent fractions of positrons annihilated at the surface, in the damaged layer and in the substrate for He-implanted Si. Full lines denote the results of fitting these fractions with the aid of VEPFIT.

of positrons that annihilate in the respective trapping layers from the S-W data. This follows from the relations

$$S(E_i) \quad = \quad f_{surf}(E_i)\, S_{surf} \quad + \quad f_{lay}(E_i)\, S_{lay} \quad + \quad f_{Si}(E_i)\, S_{Si} \qquad (4a)$$

$$W(E_i) \quad = \quad f_{surf}(E_i)\, W_{surf} \quad + \quad f_{lay}(E_i)\, W_{lay} \quad + \quad f_{Si}(E_i) W_{Si}, \qquad (4b)$$

in combination with:

$$1 \quad = \quad f_{surf}(E_i) \quad + \quad f_{lay}(E_i) + \quad f_{Si}(E_i). \qquad (4c)$$

In these equations $f(E_i)$ denotes the energy-dependent fraction of positrons that annihilates at the surface, in the damaged or in the bulk Si. In Fig. 6 we have drawn these fractions.

It should be noted that thus far we have proceeded without any detailed knowledge of the implantation and transport of the positrons; however, to obtain quantitative data such as the thickness of the defective layer and the positron diffusion length in this layer, we still depend on a numerical analysis. Table I shows the optimized model parameters as obtained by simulation of the energy-dependent fractions using the model with a homogenous defect layer as described in the previous subsection. As shown by the table, the results obtained from modelling the fractions do agree with those from the $S(E)$ data.

Summarizing, using the S-W plot we have obtained results identical to those derived with the conventional $S(E)$ analysis which supports the correctness of our approach. Apparently, for this system both methods can be applied equally well. Besides, when extending the conventional algorithm for modelling the individual $S(E)$- or $W(E)$-data to a combined analysis of the $S(E)$- and $W(E)$ data we may expect a better accuracy. However, the use of the S-W plot offers the advantage that the graphical presentation provides more direct information on the system. This appears to be of importance for the analysis of the more complicated system discussed in the next section.

IV. THE BIASED MOS SYSTEM

The presence of an internal electric field may considerably complicate the analysis of the positron data. This point is particularly well illustrated by the case of the metal-oxide-silicon (MOS) system which allows applying large and externally controlled electric fields in the oxide during positron implantation. In first approximation such fields affect only the transport of the implanted positrons[16]. However, these field-induced effects are rather dramatic, as shown already by Leung et al.[17].

The variability of the field basically introduces an additional degree of freedom which greatly increases the complexity of the data. In the case of the helium-implanted samples discussed in the previous section, a first qualitative interpretation was directly

obtained from the raw $S(E)$ data. In this approach the numerical simulation and fitting algorithm was used as a tool for verification. In the following we will show that for the MOS system the successful application of this approach is impeded by the complexity of the system. In contrast, the problem of the formulation of a first-order model to start the analytical sequence is in this case resolved with the use of an S-W plot.

For our experiments we used MOS capacitors on (100) 0.05-0.2 Ωcm p-Si with a 105 nm thick gate oxide prepared by oxidation in dry O_2 at 1000°C[18]. Following oxide growth the samples were subjected to a 30 minute post oxidation anneal in N_2 at the same temperature. A thin (10 nm) Al gate was deposited by evaporation from a resistively heated W-boat using a shadow mask.

A. Analysis of the $S(E)$ data

Fig. 7a shows the $S(E)$ data of a MOS capacitor as function of the positron implantation energy and for different bias voltages. In the case of implantation into the Al we obtained a relative S-value of about 1.07. Implantation in the middle of the oxide layer results in a minimum value of the S-parameter. However, this minimum strongly depends on the field strength: for increasing positive voltages it approaches an absolute minimum of about 0.96. This dependence shows that the transport of the implanted positrons is strongly affected by the electric field and that the positrons are not immediately trapped in the oxide layer. Unfortunately, the data are too complex to deduce a clear qualitative picture of the system . The $W(E)$ data, shown in Fig. 7b, exhibit the same behavior but again they do not allow the formulation of a first-order qualitative model.

Irrespective of the availability of a first-order model, one could attempt to continue the quest for the correct interpretation of the $S(E)$ data with the aid of a reliable simulation program. Such a program should correctly predict the transport of the implanted positrons. At this point there are two major questions. First, what is the
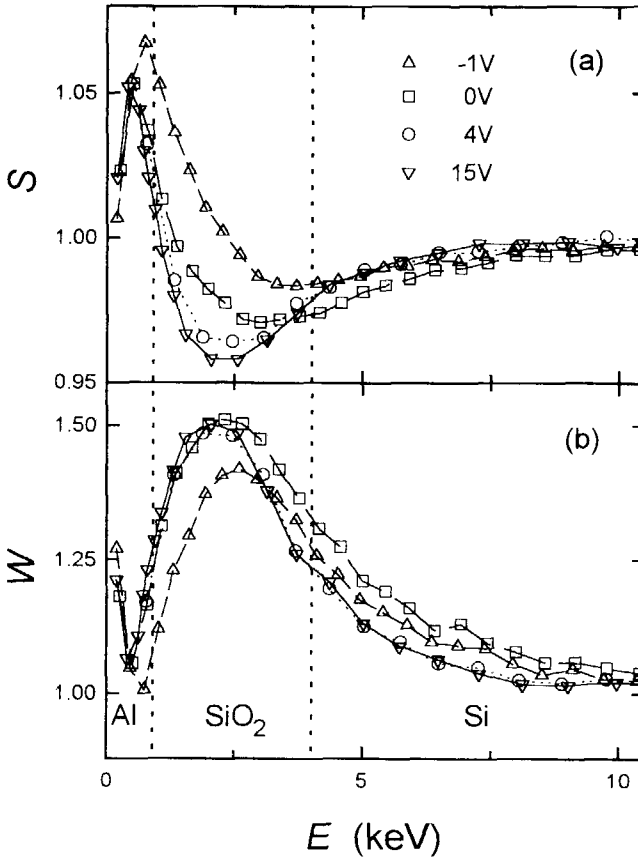
Figure 7. S - en W-parameter versus positron implantation energy for a MOS system subjected to -1, 0, 4 and 15V bias. All data have been normalized to the bulk Si values. The various lines connecting the data points are drawn as a guide to the eye. The vertical dotted lines inicate the positions of the interfaces.

nature of the field-induced transport of the positrons in the oxide? Is the transport simply governed by drift, determined by the product of a positron mobility μ_p and the field strength ξ, or has also the possibility to be considered of accelerating the positrons upto epithermal energies?[4] The second question concerns the Si/SiO_2 interface. Since

positrons will have different chemical potentials for silicon and its oxide, this would result in a potential barrier at their interface.[1] However, there are no accurate data on the chemical potential of positrons in SiO_2 and therefore it is impossible to predict whether the positrons implanted in the oxide will be injected into the silicon or not. To correctly simulate the transport of the positrons, at least the nature of the transport mechanism should be known. For a quantitative simulation, one could then consider the values of the material properties such as the positron mobility and the height of the potential barrier as a part of the problem that has to be resolved by data fitting. As an example, the positron mobility could be included in the simulation and fitting program as a free model parameter.[4] But, such an approach would greatly enhance the problems associated with the coupling of the various model parameters. Leung et al. have explored this formally correct approach to a MOS system subjected to a positive bias, but met only with limited succes.[2,17] In view of the above arguments, we believe that it will be very difficult to reliably interpret the simple $S(E)$ data.

B. Application of the S-W plot

In Fig. 8 we have plotted the positron data for the MOS system at different bias voltages in the S-W plane. For convenience, the data for shallow implantation (E<1keV), which are affected by surface states, are not shown. Annihilation in the Si substrate corresponds to the cluster point $(S_{Si}, W_{Si})=(1.0,1.0)$. Annihilation in the Al gate is presented by a point at about $(S_{Al}, W_{Al}) = (1.10,0.85)$. For large positive bias voltages (Fig. 8a) the S-W trajectory can be quite satisfactorily approximated by two straight lines that intersect at $(S,W)=(0.95,1.55)$. This feature clearly shows that this high-field trajectory is fully determined by trapping and annihilation in only three distinct layers. In the case of the low and intermediate fields (Fig. 8b and 8c), it can be seen that the trajectory runs outside the triangle defined by the straight parts of the high-field trajectory; apparently a fourth trapping layer has come into play when reducing the electric field. The contribution of this low field trapping layer is maximal when the
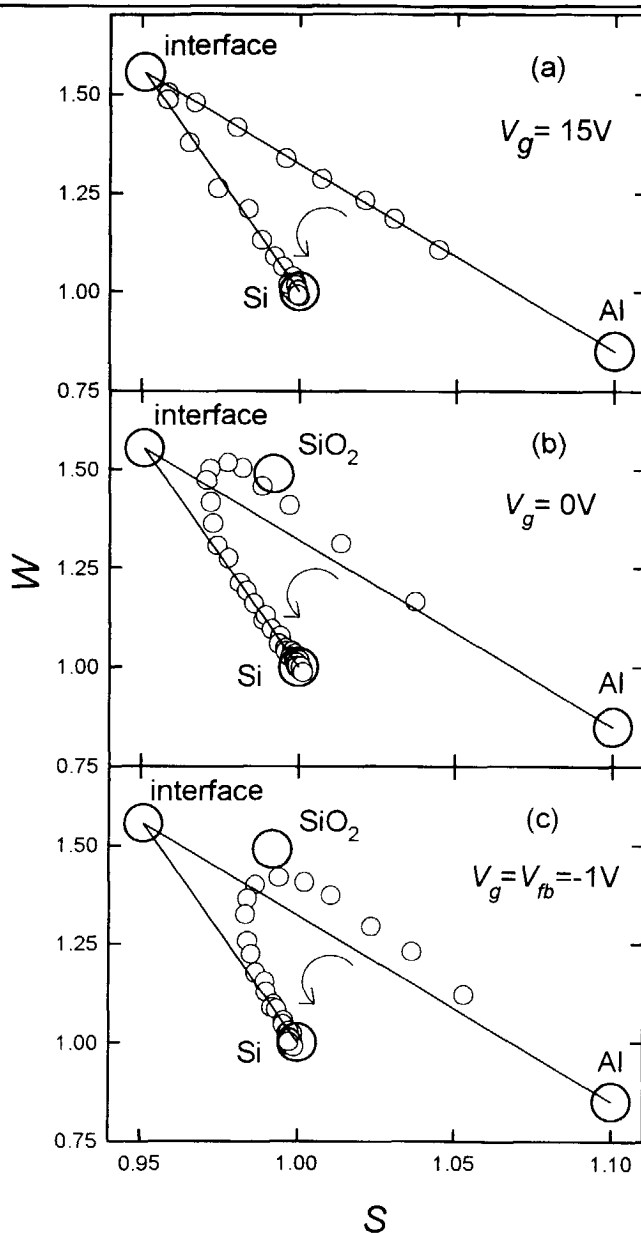
Figure 8. S-W trajectories for positrons implanted in a MOS system for various positive bias voltages and for flatband voltage (-1V). Arrows indicate the direction of increasing implantation energy. Data for shallow implantation (<1keV) in Al, have been omitted (see text).

positrons are implanted into the middle of the oxide layer. From this observation we conclude that the fourth layer may be associated with the bulk of the SiO_2 film. Its characteristic coordinates $(S_{SiO2}, W_{SiO2})=(0.992, 1.48)$ where obtained from an independent measurement on a sample without the aluminium layer (See next section).

The data of Fig. 8a,b and c demonstrate that when applying a large positive electric field, one is able to completely suppress trapping in the oxide layer. Apparently such a field moves the positrons towards the Si substrate. However, the positrons are not injected from the oxide into the silicon; this would have resulted in a straight high-field trajectory running from (S_{Al}, W_{Al}) towards (S_{Si}, W_{Si}). Instead, they annihilate in the earlier mentioned trapping layer associated with the intersection point of the two straight parts of the high-field trajectory. Besides, the experimental trajectory very closely approaches the intersection point, which indicates that almost all positrons annihilate in this layer. Since the Si/SiO_2 interface constitutes the major defect experienced by the positrons on their way from the oxide towards the silicon, we conclude that at high-field condition positrons are trapped at this interface. For convenience we will refer to this point in the S-W plane as the "Si/SiO_2 interface" coordinates.

It should be noted that in the above analysis we have not used detailed knowledge of the transport mechanisms of the implanted positrons; the only basic assumption is that the positrons will move in the direction of the field. The physical nature of the trapping of the positrons at the Si/SiO_2 interface is not resolved. The electrical and structural properties of the near-interfacial oxide deviate from those of the bulk oxide which could explain the efficient trapping of the positrons. However, the trapping could also be explained by the presence of a potential barrier for positrons at the interface.

Summarizing, it appears that the use of S-W plots greatly improves our insight in the trapping of positrons in the MOS system. The ability of the S-W plot to clearly reveal the various trapping layers, each characterized by specific (S, W) coordinates, is the key to success. The potential of this approach is further enhanced by the application of different bias voltages. However, some questions, particularly concerning positron

transport, remain as yet unanswered. We will concentrate on these questions in an forthcoming paper in which the results for the negative gate bias voltages will be discussed. Elsewhere we have already shown that the use of *S-W* plots provides new insights in the relation between structural properties and radiation hardness of MOS capacitors.[19]

V. THERMALLY OXIDIZED SILICON

Although the *S-W* plot may be of great help for the understanding and analysis of positron beam data, its use also encounters limitations. This point is illustrated by the example of thermally oxidized silicon. The sample used for this study was obtained from the same oxidized wafer as the one of the previous section, but it was not provided with an Al gate.

The *S-W* trajectory for this sample is shown in Fig. 9. The data for shallow implantation (E<1keV), which are affected by surface states, are not shown. The low-energy (1keV-2keV) implantation data cluster at a point with coordinates (S_{SiO2}, W_{SiO2})= (0.992,1.48) characteristic for annihilation at sites in the SiO_2 layer. For high-implantation energies again the clustering at the (S, W) point for Si is observed. The trajectory running from the characteristic coordinates of the oxide towards that of the silicon does not follow a straight line, in accordance with the interpretation of the data from the system with gate. As indicated in the Fig. 9, the trajectory could be approximated by two straight lines (solid lines) with a point of intersection corresponding to the coordinates $(S, W) \approx (0.925, 1.55)$. However, one could approximate the trajectory equally well by three straight lines (solid and dashed lines). Thus, using only this plot one is unable to determine the number of defect layers.

Interestingly, within experimental error the point of intersection of the low and middle energy lines agrees with the Si/SiO_2 interface coordinates determined in the previous section. Following this interpretaion we have to assume the presence of an
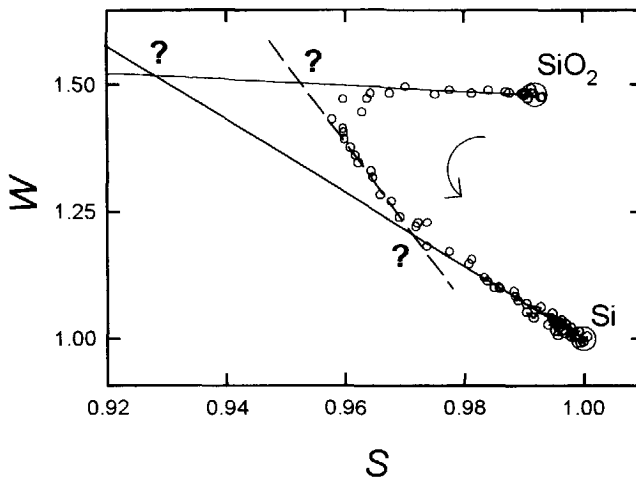
Figure 9. S-W trajectory of a Si sample with a 105 nm SiO₂ layer fabricated by thermal oxidation in O₂ and subsequent N₂ anneal. The arrow indicates the direction of increasing implantation energy. The meaning of the points of intersection denoted by question marks is discussed in the text. The data for shallow implantation (<1keV) are not shown (see text).

additional positron trapping layer between the Si/SiO₂ interface and the bulk of the silicon substrate to explain the intersection point of the medium and high-energy sections. At first sight such an additional trapping layer would be in contradiction with the high-field data from the MOS system of Fig. 8a. However, since this capacitor is in inversion for the positive bias conditions[4,13], the electric field in the silicon just beneath the oxide will remove the positrons from this region. In the case of the bare oxide there will be no electric field moving away the implanted positrons. This difference could explain the absence of trapping at additional sites in the silicon just beneath the oxide layer. Apparently, the interpretation of the data of the oxidized Si requires greatest care. This stands in contrast to the analysis of the more complex MOS-system where the controlled gate bias enlarges the capabilities of the *S-W* plot.

VI. CONCLUSIONS

This work demonstrates the usefulness of $S-W$ plots for the interpretation of positron beam data. The major advantage of this approach is that it provides a more direct insight in the number of the relevant trapping layers and their nature; often the characteristic S- and W-coordinates of the layers can be obtained from this plot without the need of numerical simulation and fitting. Furthermore, at certain conditions the $S-W$ plot allows the calculation of the depth-dependent fractions of positrons trapped in the different defect layers, thus simplifying the numerical analysis. The key to this success is that the linearity property of the shape and wing parameters are clearly visualized when plotting the data in the $S-W$ plane. Thus it is possible to formulate a model in terms of a stack of positron trapping layers without the need to understand the implantation and the transport of the positrons.

1   P.J. Schultz and K. G. Lyn, Rev. Mod. Phys. **60**, 701 (1988).

2   P. Asoka-Kumar, K. G. Lynn and D.O. Welch, J. Appl. Phys. **76**, 4935 (1995).

3   M. J. Puska and R. M. Nieminen, Rev. Mod. Phys. **66**, 814 (1994).

4   A. van Veen , H.Schut, M. Clement, J. M. M. de Nijs, A. Kruseman and M. R. IJpma, Appl. Surf. Sc. **85**, 216 (1995).

5   D. T. Britton and A. van Veen, Nucl. Instrum. Methods A **275**, 387 (1989).

6   L. Liszkay, C. Corbel, L. Baroux, P. Hautojärvi, M. Bayhan, A. W. Brinkman and S. Tararenko, Appl. phys. Lett. **64**, 1380 (1994).

7   A. van Veen, H. Schut, J. de Vries, R. A. Hakvoort and M. R. IJpma, Proceedings of the Fourth International Workshop on Slow-Positron Beam Techniques for Sollids and Surfaces, edited by P. J. Schultz, G. R. Massoumi and P. J. Simpson (AIP, New York, 1990).

8   A. van Veen, J. Trace Microprobe Techn. **8**, 1 (1990).

9 A. F. Burenkov, F. F. Komarov, M. A. Kumakhov, M. M. Temkin, *Tables of mplantation Spatial Distributions,* (OPA, Amsterdam, 1986).

10 A. van Veen, H. Schut, R. A. Hakvoort, A. Fedorov and K. T. Westerduin, Mat. Res. Symp. Proc. **373**, 499 (1995).

11 S. M. Myers, D. M. Follstaedt, H. J. Stein and W. R. Wampler, Phys. Rev. B **45**, 3914 (1992).

12 C. C Griffioen, J. H. Evans, P. C. de Jong, and A. van Veen, Nucl. Instr. and Meth. B **27**, 417 (1987).

13 S. M. Sze, *Physics of Semiconductor Devices* (Wiley, New York, 1981).

14 B. D. Wissmann, D. W. Gidley, and W. E. Frieze, Phys. Rev. B **46**, 16058 (1992).

15 A. van den Bos, in *Handbook of Measurement Science, Vol. 1,* edited by P. H. Sydenham (John Wiley & Sons, 1982), p. 331. This follows from the one dimensional form of the general relation $M=-E(\partial^2 \ln L/\partial\theta^2)$ whereas M is the inverse of the covariance matrix, θ the vector of estimated parameters and E denotes the most likely value of a statistical quantity. L is the so called likelyhood function which is for independent normal distributed measurements equal to $L=(2\pi)^{-N/2} \sigma^{-N} \exp(-1/2\ N\ \chi^2)$.

16 A. Uedono, S. Tanigawa and Y. Ohji, Phys. Lett. A **133**, 82 (1988).

17 T. C. Leung, P. Asoka-Kumar, B. Nielsen, and K. G. Lynn, J. Appl. Phys. **73**, 168 (1993).

18 E.H. Nicollian and J.R. Brews, *MOS Physics and Technology* (Wiley-Interscience, New-York, 1982).

19 M. Clement, J. M. M. de Nijs, A. van Veen, H. Schut and P. Balk, IEEE Trans. on Nucl. Sc. **42**, 1717 (1995).

Chapter 4

Positrons in the metal-gated MOS system

I INTRODUCTION

Positron annihilation constitutes a promising approach for the investigation of defects in solids.[1,2] The merits of this technique originate from the ability of implanted positrons to freely move around in defect-free material, whereas they are efficiently captured by defects. After trapping they annihilate with a nearby electron thereby emitting two photons of approximately 511 keV. Since the energy of the released photons exhibits a spreading which depends on the nature of the defect, the emitted spectra contain valuable structural information on the volume probed by the positrons. For homogeneous materials implantation is conveniently accomplished by direct exposure to the unmoderated positrons as emitted by the source; the analysis of the resulting spectra does not present fundamental difficulties. In inhomogeneous and layered systems monoenergetic positrons of varying energy (i.e. penetration depth) are implanted, thus providing information on the depth distribution of defects.

For structures composed of semiconductors and insulators the motion of the positrons will be affected by the presence of internal electric fields. These fields may result from spatial differences in the work functions of the different materials or from trapped charges. Such uncontrolled internal fields may complicate the interpretation of the data. In contrast, the controlled application of electric fields using electrodes like in MOS

(metal-oxide-semiconductor) structures may be helpful in studying the samples since it could allow guiding the positrons to preselected areas of the samples, like interfaces. A number of studies have clearly demonstrated that an electric field strongly affects the positrons in MOS systems.[3,4,5] Unfortunately, the interpretation of these data contains considerable uncertainties because the fundamental insights on transport and trapping of positrons in electric fields are rather limited. Obtaining a better understanding of these effects requires clarification of three basic issues: The first issue concerns the effect of the electric field on transport and trapping of positrons in insulator films. The second issue is that of the presence of potential barriers at the interfaces between gate electrode, oxide and substrate; such barriers would only allow positron transport in one direction.[1,2] The third question concerns the presence of positron trapping sites at the interface between two layers with different structural and chemical characteristics, like Si and SiO_2; do such interfaces act as perfect sinks for positrons, also when applying an electric field?[1]

To resolve these questions we have made an experimental study of positron annihilation in MOS capacitors with identical Si/SiO_2 systems but with different gate metals. Further parameters were the implantation energy and the magnitude and polarity of the external bias voltage. The annihilation spectra of the structures were not only characterized by means of the shape parameter (S) as commonly done, but in addition we have made a combined use of the shape- and the wing-parameter (W) in so-called S-W plots with the implantation energy (E) as a running parameter. The advantage of this latter approach is that the S-W plot displays information on the number and location of the different positron trapping layers which contribute to the annihilation process.[6]

It will be shown in the following that the study described in this paper leads to results that are of practical interest for the interpretation of positron data. We feel that these insights will provide a surer footing of the positron annihilation method for characterizing the defect structure and in tackling related reliability problems of MOS systems.

II. EXPERIMENTAL

For our positron studies we used the Delft variable energy positron beam.[7] This facility provides a positron beam of 8mm diameter with energy ranging from 0 up to 30 keV and with a typical flux of 10^4 $s^{-1}cm^{-2}$. The energy spectrum of the annihilation photons was measured with a Ge detector with an energy resolution of about 1.1 keV at $E_\gamma = 511$ keV. The 511keV annihilation peak was characterized with the aid of both the S- and W-parameter.[1,6,8] We used bulk crystalline silicon as a reference; the experimental S- and W-parameters were all normalized to the silicon values.

Unless stated differently the experiments were performed using MOS capacitors on 0.05-0.2Ωcm p-type (100) silicon with a 105 nm thick gate oxide prepared by oxidation in dry O_2 at 1000°C.[9] After oxidation, in most cases the samples were subjected to a 30 minute post oxidation anneal in N_2 at the same temperature. Al gates of 12nm, 15nm and 100nm and Au gates of 10nm thickness were deposited by evaporation from a resistively heated W boat using a shadow mask. W-gated capacitors with a $\approx$8nm thick metal layer were fabricated by plasma sputter deposition at room temperature. Using combined high-frequency (1MHz) and quasi-static capacitance-voltage measurements it was established that all capacitors contained $\approx 3 \times 10^{11}$ cm^{-2} interface states and $10^{11}cm^{-2}$ fixed oxide charges.

III. RESULTS

A. Effects of the electric field

To introduce the topic of the effect of the electric field on positron annihilation in MOS systems, we will first discuss the effect of the bias voltage on the S parameter. In Fig. 1 we show the S versus E (implantation energy) data for a capacitor with a thin
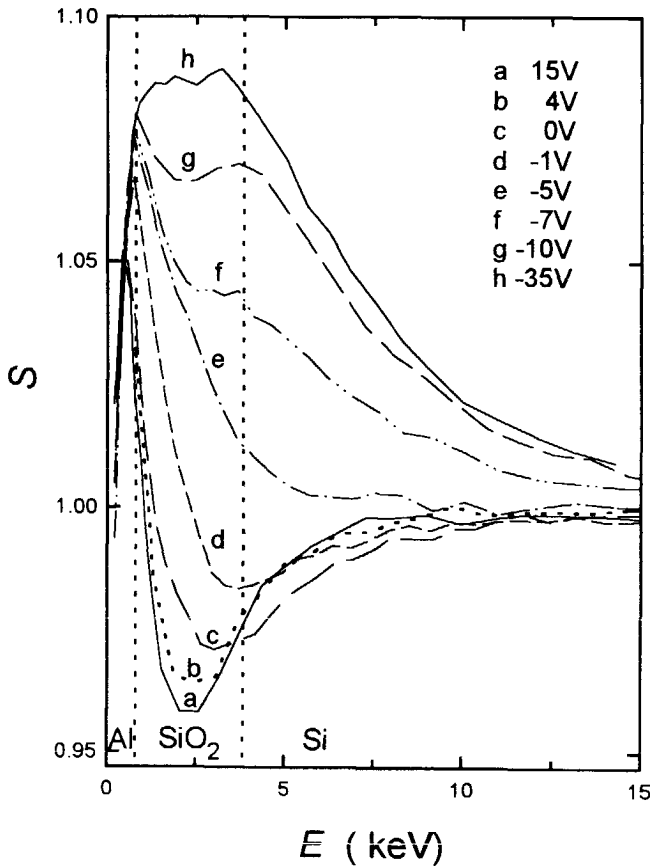
Figure 1. Shape parameter S as function of positron implantation energy for a MOS capacitor with 105nm SiO_2 and a 12nm thick Al gate subjected to different bias voltages. All data have been normalized to the bulk silicon value. The vertical dotted lines indicate energies for which 50% of the positrons are implanted across the SiO_2/Al or Si/SiO_2 interfaces, as calculated with VEPFIT.

Al gate. Similar $S(E)$ curves have been published earlier by Leung et al.[4,5] The data show that variation of the bias causes a substantial change in the shape of the $S(E)$ curves. For deep implantation the curves approach the S value of crystalline silicon, irrespective of the bias voltage. It should be noted that the effect of the field reduces with increasing implantation energy, in agreement with the limited penetration depth of the

electric field into the silicon. For shallow implantation (0.5keV< E <1.0keV) only a moderate effect is observed. For these energies, a major fraction of the positrons is implanted in the Al, where there is no electric field. Only positrons from the tail of the implantation profile extending into the oxide will experience an electric field. A large effect of the field is observed when the majority of the positrons is implanted into the oxide layer (1keV< E <3.5keV) or into the silicon just beneath the Si/SiO$_2$ interface (3.5keV< E <10keV). For implantation into the middle of the oxide layer the effect is most dramatic: simply by changing the gate bias voltage the S-value changes from a minimum to a maximum value; apparently the majority of the positrons implanted into the SiO$_2$ are affected by the electric field.

The effect of an electric field is also demonstrated by the S-W plot Fig. 2, which shows the (S, W) values at a fixed implantation energy, but for different external fields. The particular sample of Fig. 2 had a 350nm thick thermal oxide in combination with a 15nm Al gate. The positrons had an energy of 4keV which warrants that most of them are implanted in the oxide layer. The data unambiguously demonstrates that the electric field strongly affects the annihilation of the positrons implanted in the oxide layer.

In the case of zero field, the positrons are efficiently trapped, which is reflected by a typical diffusion length of 10nm.[4,5,10] Because of this we can safely assume that the majority of the positrons implanted under this field condition, also annihilate in the oxide layer. The characteristic coordinates of thermal SiO$_2$ were also determined from a bare, 105 nm thick oxide, grown under equal conditions.[6] The present zero field data agrees with the bare oxide (S, W) point, which is indicated by the large circle in Fig. 2.

Further appreciation of the data of Fig. 2 requires some understanding of S-W plots. Their advantages follow from the linearity property inherent in the definition of S and W.[6] If annihilation only occurs at two different trapping sites, say A and B, with characteristic coordinates $(S, W)_A$ and $(S, W)_B$, the trajectory associated with the variation of the fractions of positrons annihilating at site A (f_A) and B ($f_B, f_B=1-f_A$) is given by a straight line connecting $(S, W)_A$ and $(S, W)_B$. In the case of three or more positron trapping layers, the trajectory will generally follow a curved course. The trajectory of
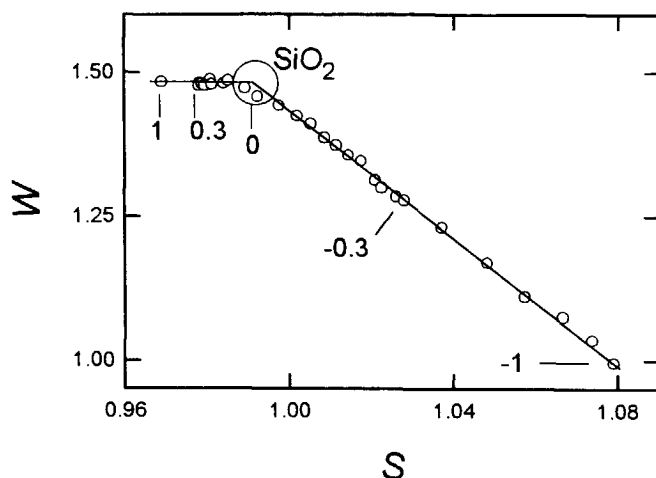
Figure 2. Field dependence of the S- and W-parameter for 4keV positrons implanted into the oxide layer of a MOS system with 350nm oxide layer and 15 nm Al gate. Dimensions of the MOS system and implantation energy were chosen such that 99% of the positrons were implanted into the oxide layer. The numbers denote the electric field strength in MV/cm and the large circle indicate the S and W values measured on a bare SiO$_2$ layer.[6]

Fig. 2 clearly exhibits two straight sections, one for negative fields and one for positive fields, which indicates for both cases the involvement of an additional ambivalent positron annihilation site.

Keeping in mind the unresolved issues regarding trapping and transport of positrons in MOS systems mentioned in the introduction it does not seem feasible to deduce a reliable physical picture of what is happening in the experiments of Figs. 1 and 2. The data of Fig. 1 constitute a too complicated system for such an interpretation, whereas those of Fig. 2 contain no clues on the nature and location of the additional trapping sites. To resolve these problems we will present first (in subsection B) $S(E)$ data from a comparative study of capacitors with an Al, W and Au gate that provides insight

into the basic features of the transport and trapping phenomena. Next, in subsections C and D, we will present the results of additional studies, invoking S-W plots for Al and W-gated capacitors, that will provide a more detailed and complete picture of the effect of the field. Subsection D also provides further confirmation of the concepts deduced in B and C. Finally, we will show in subsection E that the concepts developed in our study also yield very reasonable quantitative results.

B. Effect of the gate material

Comparison of data from capacitors with different gate materials allowed us to make a first inventory of the different aspects of the effect of the field. The crux of this experiment is that the MOS systems are identical apart from the gate, whereas direct implantation of the positrons in the gate is avoided by choosing a sufficiently large implantation energy. For this experiment we used MOS capacitors with Al, Au and W gates of 15nm, 10nm and 8 nm thickness, respectively. Since the deposition of these gate materials was performed at room temperature, we assume that the underlying Si/SiO_2 system remained unaffected.

Fig. 3a shows the experimental $S(E)$ curves for the different capacitors for a positive bias of 15V. Implantation and trapping in the gate ($E < 1$keV) results in the largest differences in S-value between the three gate materials. With increasing energy, the curves are seen to monotonically approach each other. Below 2.5 keV the approach is rapid, above this energy, the rate of approach is reduced and the curves evolve in a nearly similar fashion. The rapid convergence for implantation energies approaching 2.5 keV is caused by the fact that for these energies a substantial part of the positrons is implanted into the gate metal, so that annihilation yields the metal characteristic S value. The remaining fraction is implanted in the oxide where it will annihilate with an S value independent of the metal. For increasing energies the oxide-implanted fraction increases at the expense of that implanted in the metal.
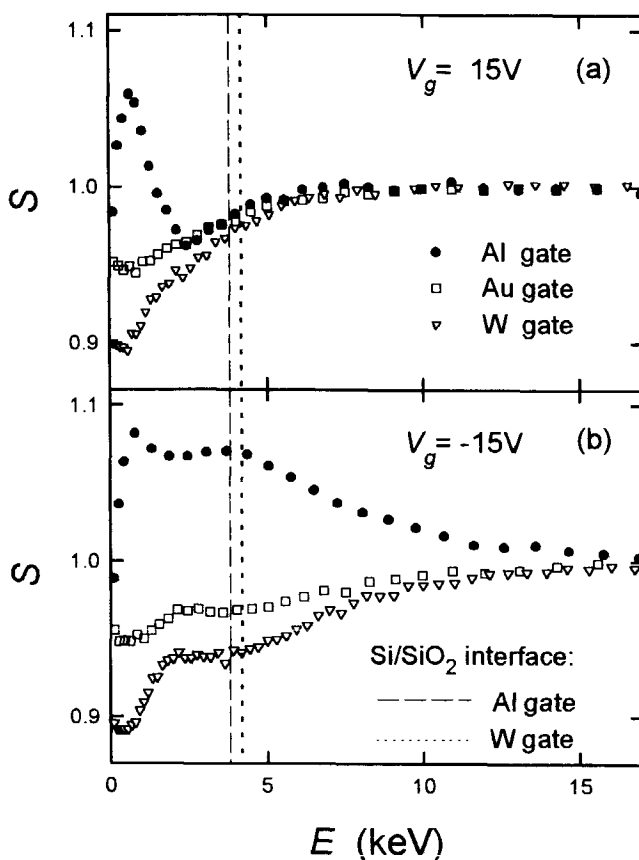
Figure 3. S-parameter versus implantation energy for MOS capacitors with 15nm Al gate, 8nm Au gate and 8nm W gate at 15V positive and negative bias condition. The vertical lines indicate the energy corresponding with 50% implantation into the silicon substrate for a particular sample.

For energies above 2.5 keV, the dependence of the positron implantation profile on the positron stopping power of the gate material shows up. The much larger stopping power of W as compared to Al results for the same implantation energy in a significantly larger fraction of positrons trapped in the W gate than in the Al one. In Fig. 3 we have indicated the implantation energy for which half of the positrons are implanted into the

silicon substrate by vertical lines. A rough correction for this stopping power related difference in implantation profile is obtained by simply shifting the W gate data towards smaller implantation energies such that the implantation energies associated with 50% implantation into the silicon substrate coincide. This causes all curves for energies larger than 2.5 keV to more or less overlap.

The positive bias induces an electric field predominantly in the oxide layer. In the silicon near the Si/SiO_2 interface there will be a smaller field associated with the depletion layer but there will be no field in the gate metal and hardly any deeper in the substrate. The large electric field in the oxide layer (1.5 MV/cm) prevents the implanted positrons from moving towards the gate; a displacement of 0.3 nm against the field already requires the mean thermal energy of the positron. At most, the field plays a role in driving the positrons further away from the gate, deeper into the Si/SiO_2 system, thus suppressing the gate-induced differences.

These positive bias data by themselves do not provide new insights on the transport of the positrons through the oxide layer and across the Si/SiO_2 interface because such information remains hidden due to the equivalence of the Si/SiO_2 systems in combination with the specific direction of the field. However, the situation is clarified by the negative bias experiment when the implanted positrons are pulled back towards the gate.

Fig. 3b shows the negative bias (Vg=-15V) $S(E)$ curves for the same samples. A first look immediately shows that the curves tend to stay apart; only for an implantation energy above 15 keV, which corresponds to implantation deep into the silicon substrate (1μm), the curves approach each other. Apparently, the annihilation of the positrons implanted into the SiO_2 layer and even into the silicon substrate is strongly affected by the gate material, which demonstrates that at negative bias the positrons implanted into these layers are able to return to the gate. This observation excludes the possibility that the transport of positrons through the oxide layer would be impeded by trapping; instead, the positrons are transported across the oxide layer. Furthermore, the observation that positrons implanted into the silicon reach the gate

implies that they are capable of passing the Si/SiO$_2$ interface. From this observation we can conclude that at negative bias the interface does not act as a perfect positron sink.

C. Al-gated system

In the foregoing subsection information on the implantation depth of the positrons played a crucial role: for this reason we discussed $S(E)$ data. In the following the depth information is not the main point of interest. Rather, we focus our attention on the various trapping sites that participate in the annihilation processes. For this reason we will present the data in S-W plots.[6]

Fig. 4 shows the S-W plots for a MOS capacitor with a thin 10 nm Al gate. The arrow in each of the figures denotes the direction of increasing implantation energy. The S-data correspond with those for the $S(E)$ curves shown in Fig. 1. Different trapping layers are characterized by (S, W) coordinates, given by the large circles. By definition, the silicon cluster point is located at the coordinates $(S, W)=(1.0, 1.0)$ in Figs. 4a-e. The characteristic point for SiO$_2$ indicated in Fig. 4 is taken from the data of subsection A.

From the S-W trajectory for +15V gate bias in Fig. 4a it is immediately seen that within experimental accuracy the data points define a perfect triangle. This feature shows that three different positron trapping layers are involved. The cluster point at the high energy end of the trajectory is due to the silicon substrate. For low energies the positrons are implanted into the oxide layer and into the Al gate. With decreasing implantation energy the gate fraction will increase and the low energy trajectory will move towards the characteristic (S, W) point of the Al layer, although a cluster point is not observed.[6,11] The characteristic coordinates of the third trapping layer are given by the point of intersection of the straight low and high energy parts of the trajectory; this point has the coordinates $(S, W)=(0.95, 1.55)$. From the $S(E)$ curve a in Fig. 1, which corresponds to the trajectory of Fig. 4a, it can be seen that the minimum value of S is obtained for implantation in the middle of the oxide layer. This feature makes both the oxide layer and the Si/SiO$_2$ interface a candidate for the trapping layer associated with the

intersection point. Note that the characteristic point of bulk SiO_2 lies outside the triangle. This suggests that in the case of Fig. 4a trapping in the oxide layer itself does not play a significant role. The trajectory for 0V bias voltage (Fig. 4b) runs outside the triangle defined by the +15V data indicating that an additional positron trapping layer has come into play. The deformation of the trajectory towards the bulk SiO_2 point suggests that positrons are now being trapped in the oxide layer. Further reducing the bias voltage down to -1V (flatband voltage, Fig. 4c) shows even stronger deformation of the trajectory towards the bulk SiO_2 point, but it never runs beyond it. This observation indicates that trapping of positrons in the oxide layer only plays a role at low electric fields. The drift of positrons through the oxide was also concluded from the data of Fig. 3b for negative bias voltages. Apparently, already at moderate fields drift reduces trapping in the oxide.

Since for large electric fields positron trapping in the oxide layer is completely suppressed, we conclude that the layer associated with the intersection point $(S, W)=(0.95, 1.55)$ of Fig. 4a for positive bias has to be ascribed to the Si/SiO_2 interface. For completeness we would like to mention that the Si/SiO_2 characteristic coordinates show some scatter related to the details of the oxidation process.[12] To indicate that the coordinates of this intersection point were derived from the data in Fig. 4a, this point is plotted as a fat circle. The thin circles used in the subsequent Figs. 4b-f indicate that the coordinates are not established from the particular figure but obtained from another source. Using the information from the S-W trajectories of Figs. 4b and 4c we are also able to interpret the low field $S(E)$ data in Fig. 1 (curves c and d). The minimum in these curves at $E \approx 3.5$ keV corresponds to positrons implanted across the Si/SiO_2 interface. Apparently, at low fields, a substantial fraction of these positrons is trapped at this interface, as earlier proposed by Nielsen *et. al*.[10] At $E=1$-3 keV the low field data are affected by trapping at defects in the SiO_2 layer, leading to intermediate S values. For negative bias conditions the positrons implanted into the oxide layer are driven in opposite direction, towards the gate. The shape of the trajectory for -5V bias (Fig. 4d), still is similar to that for -1, 0 and +15V bias; however, when the bias voltage
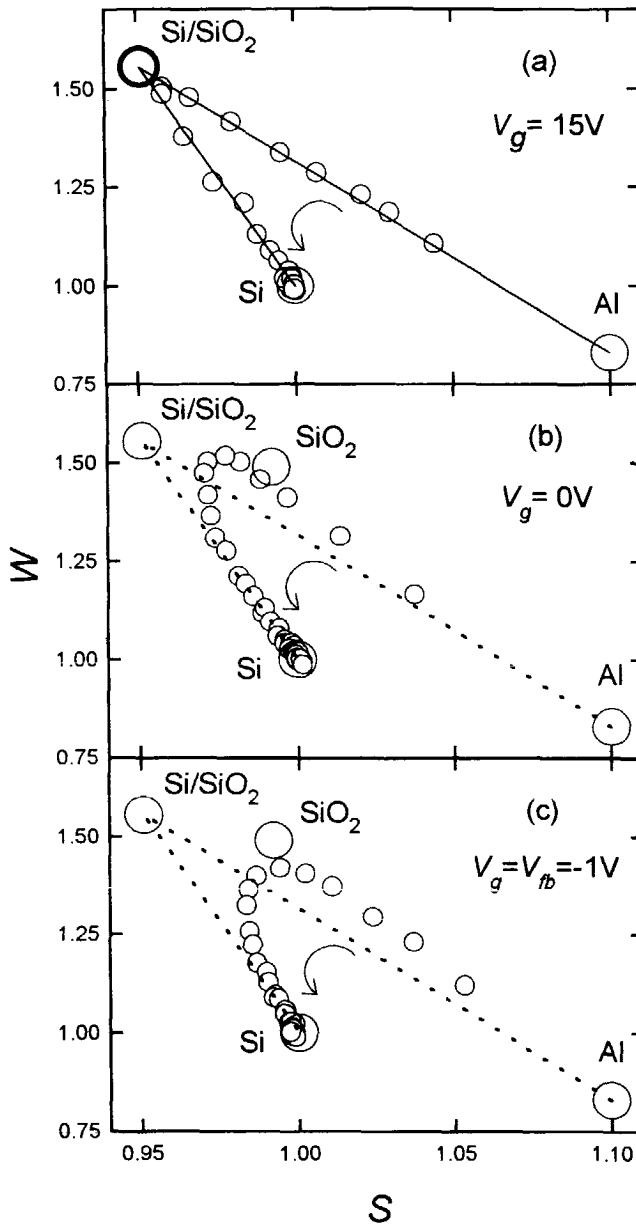
Fig. 4. S-W trajectories for MOS system with 12 nm thin Al gate for various bias voltages. Arrows indicate the direction of increasing implantation energy. The large circles denote the specific (S,W) positions related to the different layers and interfaces. The fat circles indicate that the characteristic coordinates are established from the S-W trajectory of this particular figure, whereas the thin circles indicate that the coordinates -
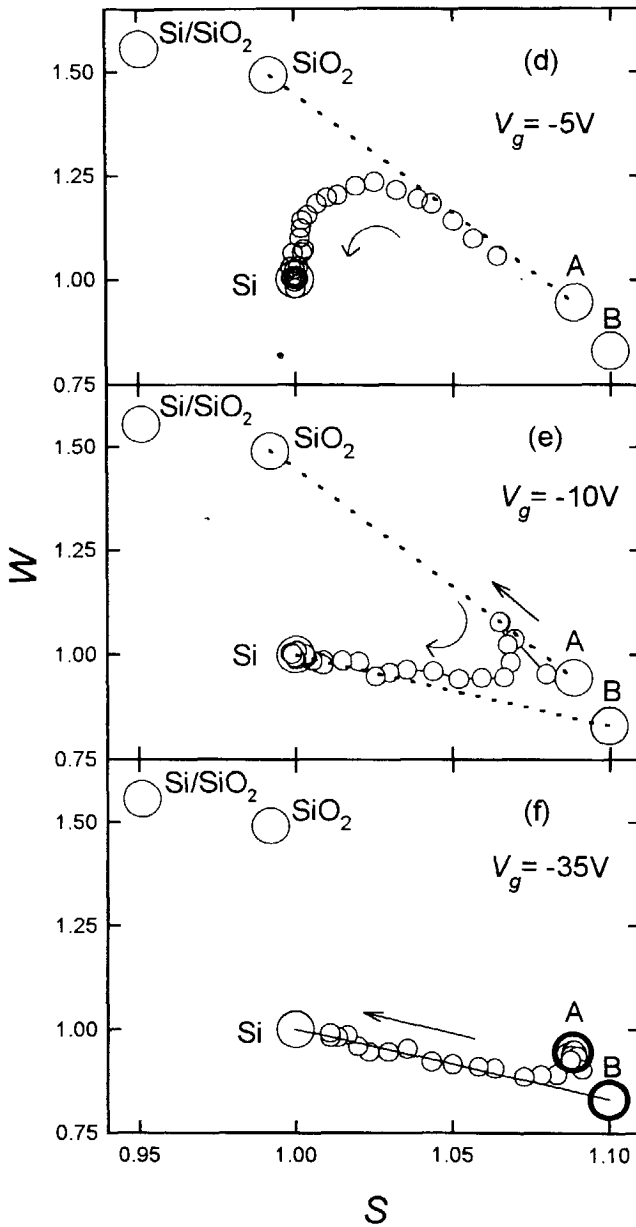
are taken from another plot. In the text it will be argued that point A is related the SiO2/Al interface whereas point B corresponds to the Al gate. The position of this latter point is established from the intersection of the straight lines through the low energy data in (a) and the high energy data in (f).

is further reduced, a strong change is observed (Figs. 4e and 4f), indicating that completely different processes are taking place. Because it is a clear-cut case we will first pay attention to the -35V bias trajectory of Fig. 4f. For the lower implantation energies this trajectory exhibits a distinct cluster point, indicated as A, at (1.09,0.90). In this experiment the characteristic point of silicon was not fully reached because of electrical breakdown of the oxide layer. The low energy cluster point A corresponds to the plateau at S=1.09 in curve h of the $S(E)$ data of Fig. 1. This plateau ranges from 1 up to 3.5 keV implantation energy which roughly corresponds to implantation into the oxide layer. For convenience we will designate these positrons as '*oxide-implanted*'. The large difference between the position of the characteristic coordinates of SiO_2 and that of cluster point A clearly indicates that the oxide-implanted positrons are not trapped in the oxide layer itself, again confirming field-induced positron transport. Because of the direction of the field the positrons are transported towards the Al gate. Whether in cluster point A they are trapped at the SiO_2/Al interface or injected into the Al cannot be concluded from these data.

The overall trajectory of Fig. 4f is slightly curved, but the characteristic point of silicon is being approached along a straight line. Apparently, the high energy side is related to two different trapping layers: the silicon substrate and an as yet unidentified layer with coordinates B. The straight section corresponds to the gradual descent of the $S(E)$ curve f of Fig. 1 from the plateau down to the S value of the silicon substrate, i.e., it is associated with positrons implanted through the oxide layer into the silicon substrate, which will be denoted as '*substrate-implanted*'. Part of the substrate-implanted positrons is unable to escape from the silicon but the remainder is injected into the oxide layer after which it apparently annihilates in the unidentified defect layer B. As can be seen from the high energy part of the trajectory, the injected positrons are not trapped at the Si/SiO_2 interface or in the oxide layer; the positrons are transported to the gate. These substrate-implanted positrons thus appear to annihilate either at the SiO_2/Al interface or in the Al gate, in agreement with the conclusion of subsection A.

The results of the negative bias measurements discussed above can be recapitulated as follows:

- We may distinguish between positrons with different history: substrate-implanted positrons that are subsequently injected into the oxide layer and oxide-implanted positrons.

- The curvature of the trajectories reveals the involvement of two trapping layers apart from the silicon substrate, the oxide-implanted positrons being associated with the cluster point A (1.09, 0.90), and the substrate-implanted positrons that are injected into the oxide layer with the third, not yet identified, point B.

- The oxide-implanted and the substrate-implanted positrons are not trapped in the oxide layer or at the Si/SiO_2 interface; instead, they are transported through the oxide towards the gate. Thus the trapping layer is either the SiO_2/Al interface or the gate metal.

- For both types of positrons it was argued that they annihilate either at the SiO_2/Al interface or in the gate Al; however, in which layer each of them annihilates was not established.

The question thus appears to be whether the oxide-implanted positrons are trapped at the SiO_2/Al interface, in which case the substrate-implanted positrons would be trapped in the Al layer, or vice versa. Unfortunately, the data contain no clues how the association should be made. Since we used a thin Al gate, the data do not show a clear cluster point for Al. Furthermore, the data suggest that the characteristic coordinates of the SiO_2/Al interface and those of the thin Al layer are located close together. Such problems were avoided using capacitors with a thick Al gate and with a thin W gate as discussed further on.

Before proceeding with data from the capacitors with a the thick Al gate, we will shortly comment the -5V and -10V bias voltage data of Figs. 4d and 4e. The -10V trajectory exhibits some differences with respect to the one for -35V. The clustering at (1.09, 0.90) observed at Vg=-35V does not occur at Vg=-10V; instead, the trajectory exhibits an excursion towards the SiO_2 point. This excursion corresponds in Fig. 1

(curve g) to the local minimum seen for implantation in the middle of the oxide layer. Thus at -10V gate bias a fraction of the positrons implanted at this depth is trapped in the bulk SiO_2, i.e., the field is not strong enough to remove all positrons from this layer. Interestingly, the high energy section for the -10V bias condition approaches the same straight line as in the case of -35V bias, indicating that the substrate-implanted positrons, injected into the oxide, exhibit a comparable behavior for -35V and -10V bias. Note that in the $S(E)$ curves the behavior of the latter positrons corresponds to the presence of a second maximum at ≈ 3.5 keV. At -5V bias the high energy trajectory follows quite a different course, directed more towards the SiO_2 point. This can be straightforwardly attributed to an enhanced trapping and annihilation of substrate implanted positrons in the SiO_2 layer and at the Si/SiO_2 interface.

Because only a smaller fraction of the positrons is trapped in the 10 nm thin Al gate, the (S, W) position of this top layer could not be independently determined so that for large negative bias it was not possible to distinguish between trapping in the Al gate and at the SiO_2/Al interface. To obtain a more accurate determination of the (S, W) coordinates of the deposited Al, we performed additional measurements on a capacitor with a 100 nm thick Al gate. For 20V positive bias (Fig. 5a) it can be inferred from the $S(E)$ data in the insert, that the lower energy cluster point (1.035,0.95) can be assigned to implantation into the Al gate. This point thus characterizes trapping in the deposited Al. Unfortunately, measurements on capacitors with a thick Al layer deposited in different process runs resulted in different (S, W) coordinates for the Al gate. In Fig. 6 we have indicated the area in the S-W plane in which the observed $(S, W)_{Al}$ points are situated. The large scatter in the Al points suggests that the structure of the Al top layer strongly depends on the detailed conditions of the preparation process. An additional change (reduction) of the S-value is obtained for a post-metalisation anneal in forming gas (90% N_2 and 10% H_2) at 400°C.

Just as for the system with a thin Al gate the trajectory for positive bias and thick gate in Fig. 5a can be fully explained in terms of the (S, W) points of the Al gate, the Si/SiO_2 interface and the silicon substrate. The data confirms that the low energy part
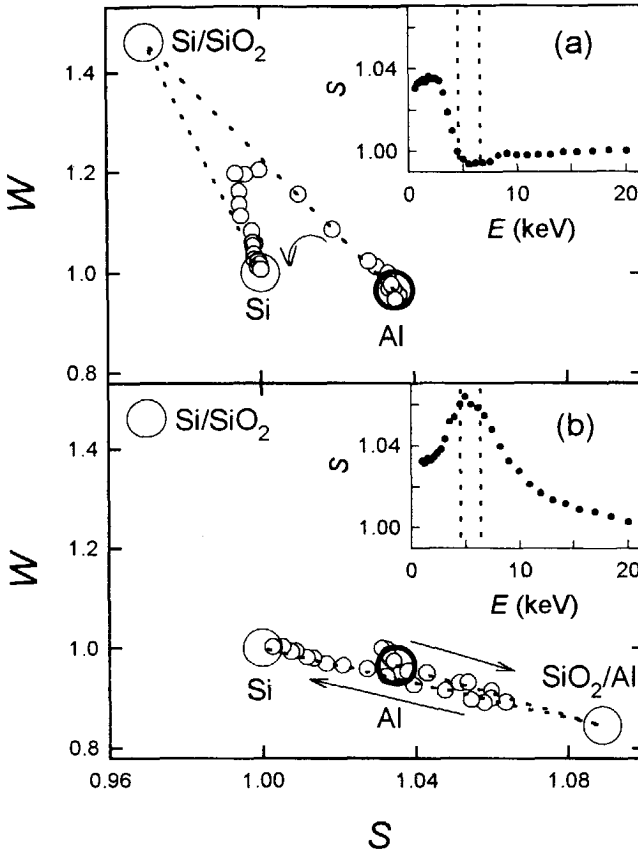
Figure 5. S-W trajectories of a MOS capacitor with a 100 nm thick Al gate for 20V positive (a) and negative (b) bias. The direction of increasing implantation energy is indicated with arrows. The inserts show the corresponding S(E) data whereas the energies for implantation of 50% percent of the positrons across the Al/SiO₂ and the SiO₂/Si interfaces are indicated by vertical dotted lines. Because no 1000°C post oxidation anneal in N₂ was applied, the specific (S,W) position of the Si/SiO₂ interface differs from that of the other samples.[12]

of the trajectory follows the line defined by the characteristic points of the Al layer and of the Si/SiO₂ interface. The high energy trajectory approaches the silicon cluster point, coming from the direction of the Si/SiO₂ point. However, the trajectory does not get

equally close to the Si/SiO$_2$ point as in the case of the thin Al gate capacitor in Fig. 4a. This can be explained from the smearing out of the implantation profile over the Al gate, the SiO$_2$ layer and the silicon substrate caused by the relatively large thickness of the Al gate (100nm).

The trajectory for 20V negative bias in Fig. 5b exhibits the cluster point $(S, W)_{Al}$ for implantation into the thick Al gate, as expected. Increasing the implantation energy results in an excursion in the direction of a point in the surrounding of the cluster point A derived from the thin gate data of Fig. 4f. As shown by the insert, the excursion is associated with implantation into the oxide layer. Evidently, the oxide-implanted positrons do not annihilate in the Al or in the oxide layer but at the SiO$_2$/Al interface. Having associated the oxide-implanted positrons with the SiO$_2$/Al interface, we can correlate, as argued above, the substrate-implanted positrons, that escape from the silicon, with the gate metal. Apparently, these latter positrons are transported across the oxide layer and injected into the gate metal. According to this interpretation the (S, W) point of the thin Al gate has to be localized at the intersection point of the straight lines representing the low energy data of Fig. 4a and the high energy data of Fig. 4f. Furthermore, in Fig. 1 the maximum in S observed for negative bias at ≈ 3.5 keV implantation energy would correspond to the annihilation of substrate implanted positrons in the Al gate. Unfortunately, the S-W plot of Fig. 5b does not provide explicit proof for such an injection because the characteristic points are all located on a single line; these data could be also explained by annihilation of the silicon-implanted positrons at the SiO$_2$/Al interface.

One should note that the positron transport behavior presented above also explains the data of Fig. 2. At zero and low field conditions, and at the implantation energy used in this experiment, all positrons are trapped in the SiO$_2$ layer. When a positive bias is applied the positrons are transported to the Si/SiO$_2$ interface. Because of this the trajectory approaches with increasing bias the characteristic (S, W) point of the Si/SiO$_2$ interface. As stated before, the exact (S, W) coordinates of the latter interface depend on the details of the fabrication process and differ somewhat for the 100nm and
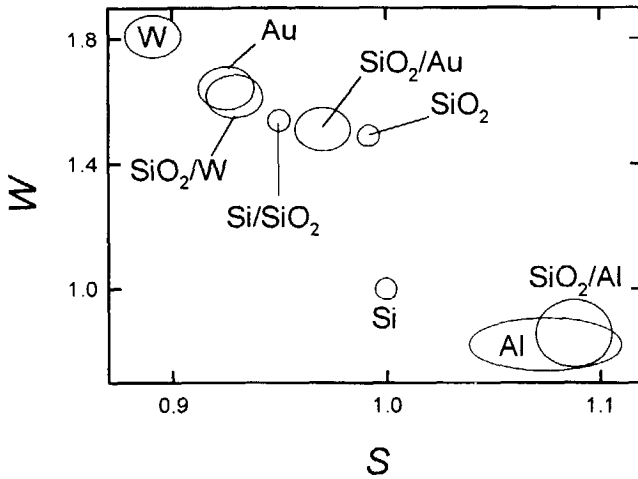
Figure 6. Specific (S,W) values of some layers and interfaces.

350nm SiO_2 layers. For negative bias the positrons are pulled back towards the oxide/Al interface because of which the trajectory approaches the (S,W) point of the SiO_2/Al interface.

D. W-gated system

The picture of the positron transport in Al-gated MOS systems derived in the foregoing has some surprising features. Particularly, the conclusion that for negative bias voltages oxide-implanted positrons are trapped at the SiO_2/Al interface, whereas substrate-implanted ones, after injection into the oxide, are trapped in the Al is rather unexpected. To obtain additional support for this model, some complementary studies were made on W-gated capacitors. One would expect the same qualitative behavior of the trajectories in the S-W plots for the corresponding MOS structures, but since the characteristic points for the two metals are located in opposite corners of the diagram of
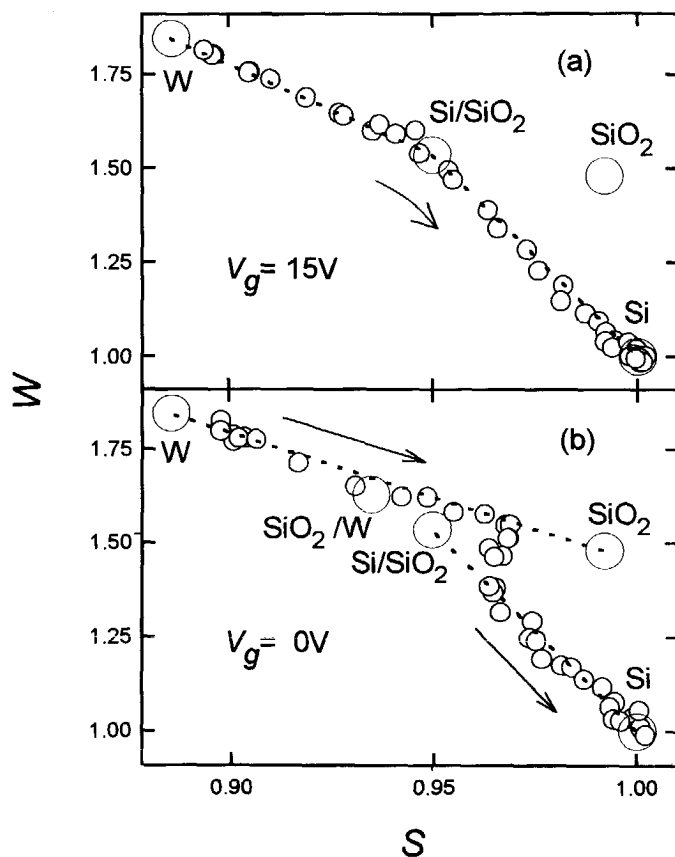
Figure. 7. S-W trajectories of a W-gated MOS system for different bias conditions. The specific (S,W) positions of the W gate and the SiO$_2$/W -

Fig. 6 this will lead to large quantitative differences between the plots. It will be shown that the results obtained on the W-gated capacitors provide further confirmation of the model described in the proceeding part of this paper.

Fig. 7a shows the *S-W* trajectory for the W capacitor for 15V positive bias. As in the case of the positively biased Al system (Figs. 4a and 5a) the trajectory can be approximated by two straight lines, so that the qualitative behavior has been conserved.
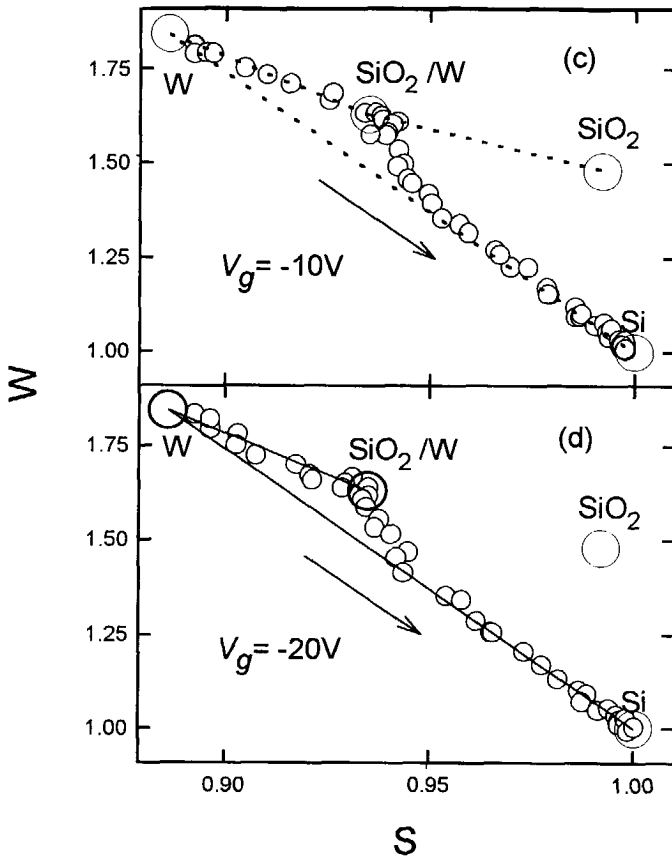
interface were both determined from plot (d) in this figure whereas the other specific points were taken from Fig. 4.

As discussed in connection with the Al data, the trajectory points to annihilation in the silicon substrate, in the gate material and at the Si/SiO₂ interface. Within experimental accuracy the two straight sections intersect at the Si/SiO₂ coordinates taken from the Al data of Fig. 4, which indicates that the positrons are indeed trapped at this interface. Apparently, only the characteristic coordinates of the gate metal are different, in agreement with the exchange of the gate metal. Thus, the explanation proposed for the

behaviour of the Al trajectory for the positive bias condition also fits the W data: positrons implanted in the substrate or the gate are also trapped in these layers, those implanted in the oxide drift through the oxide and are collected at the Si/SiO$_2$ interface.

The trajectory for -20V bias is shown in Fig. 7d. Comparison of this high negative bias trajectory with the corresponding one for the Al capacitor (Fig. 4f) indicates that replacement of the gate material does not change the basic character of the trajectory. The curve shows a cluster point at (0.935, 1.65) which corresponds to implantation into the oxide layer. A similar cluster point was found for the Al capacitor at (1.09, 0.95). In the latter system, the cluster point was ascribed to the gate/SiO$_2$ interface. Thus, we have to associate the coordinate (0.935, 1.65) with the W/SiO$_2$ interface. The coordinates of the W layer then have to be located at the low-energy side of the W/SiO$_2$ point, in agreement with the data of Fig. 7a. From the Al data we derived that the high energy part of the curve should be associated with positron trapping in the gate layer and in the silicon substrate whereas the SiO$_2$/gate interface should not be involved. The picture clearly holds for the trajectory in Fig. 7d; the high energy data distinctly point to trapping of substrate-implanted positrons in the W gate whereas their trapping at the SiO$_2$/gate interface is unambiguously excluded. The (S, W) coordinates of the W layer are given by the point of intersection of the lines through the low and high energy data.

Alternatively, we can also compare the -20V negative bias data for the W capacitor of Fig. 7d with those for the thick Al capacitor of Fig. 5b. For increasing energy the trajectory in Fig. 5b departs from the bulk Al coordinates towards the SiO$_2$/Al point, subsequently returning to the silicon characteristic point. This interpretation of the Al data fully agrees with that of the W capacitor. Moreover, in the thick Al trajectory we could not distinguish between trapping of the substrate-implanted positrons in the gate material and at the SiO$_2$/Al interface. This issue now is resolved by the W data; for increasing implantation energy annihilation at the SiO$_2$/W interface is gradually replaced by annihilation in the W, which again becomes overruled by annihilation in the silicon substrate.

A difficulty presented by the thin Al gate data was that the Al material coordinates could not be clearly established because of the limited thickness of the metal layer and because the $(S, W)_{Al}$ cluster point is located in the proximity of the SiO_2/Al coordinates. Although the W gate data do not show clustering at the W point, the trapping in the W gate is sufficiently enhanced to make its contribution apparent. Moreover, the characteristic points of the W layer and the SiO_2/W interface are clearly separated.

As an additional check on our interpretation we performed measurements on a Au-gated capacitor. This resulted in S-W trajectories comparable with those of the W-gated system. For the Au gate capacitor the high energy data again follows a straight line connecting the (S, W) point for the gate material with that for Si. However, the distinction between the coordinates for the Au gate, and that for the two interfaces was less clear than for the W-gated sample (see Fig. 6). Since the Au gate data do not further contribute to the overall argument we will not discuss them in more detail.

The -10V trajectory for the W-gated capacitors in Fig. 7c clearly resembles the -20V trajectory; only the clustering of the experimental data in the middle of the figure has slightly moved towards the SiO_2 coordinates. The same behavior was shown by the thin Al data (Fig. 4e), indicating that trapping in the oxide layer is not fully suppressed anymore. The substrate-implanted positrons still annihilate either in the silicon or in the gate material. The 0V trajectory is changed drastically; trapping in the oxide layer plays a prominent role again. As expected, the substrate-implanted positrons that escape from the substrate are not trapped in the W layer anymore. Instead, they annihilate at the Si/SiO_2 interface, like observed for the Al-gated capacitors in Figs. 4b and 4c. Apparently, in the absence of an electric field this interface acts as a very efficient positron trap. Furthermore, for the low energy data, a contribution of the SiO_2/W interface can not be excluded because the W, SiO_2/W and the SiO_2 characteristic coordinates lie on a straight line.

E. Annihilated fractions

The results obtained so far from the analysis of the *S-W* plots were particularly concerned with the qualitative aspects of the annihilation process, namely with the presence of trapping layers and with the role of transport mechanisms. The W gate data played an important role in confirming some of the unexpected features of our concepts. Further support was obtained from more quantitative analysis of the experimental data; our concepts also yield quite acceptable quantitative results. We have shown elsewhere that for up to three trapping layers with known (S, W) coordinates the fraction of positrons annihilated in each of the layers can be directly obtained by resolving the *S-W* data using the lever rule.[6] The experimental data for large positive and negative bias satisfies this condition; the results of this analysis are presented below.

Fig. 8 shows for thin Al and W-gated capacitors at 15V positive bias the energy dependence of the fractions of positrons trapped in the metal gate at the Si/SiO_2 interface and in the silicon substrate. These fractions were calculated from the data of Figs. 4a and 7a, using the lever rule. Qualitatively the curves for the two metals are the same, although the W curves are slightly shifted to higher energies compared to those for Al because of the much larger stopping power of W. Comparison of the $S(E)$ data of Fig. 3 with the implantation energy dependent fractions, $f(E)$, of Fig. 8, clearly shows the advantage of the latter approach. The data of Fig. 8b show that the maximum trapping at the Si/SiO_2 interface is achieved for implantation in the middle of the oxide layer, as earlier inferred from Fig. 1 curve a where the minimum S value corresponds to implantation in the middle of the oxide layer. Furthermore, the positive bias induces a field in the substrate just beneath the oxide layer which drives any positron implanted into the silicon further into the substrate, and prevents it from returning to the oxide layer. The silicon annihilated fraction (Fig. 8c) thus actually reflects the part of the positrons implanted into the substrate.

The fractions of Fig. 8 are directly derived from the experimental data. If our concepts are correct, these fractions can also be calculated using a numerical algorithm
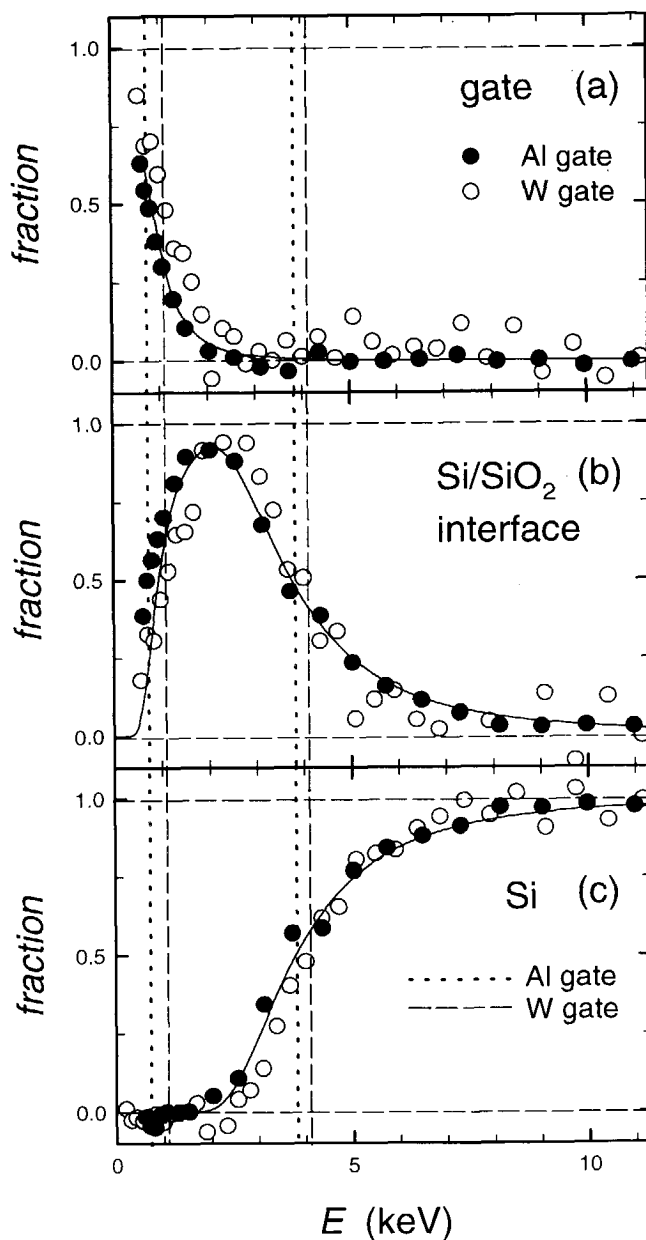
Figure 8. Energy-dependent fractions of positrons annihilating in the gate, at the Si/SiO2 interface and in the silicon for an Al-gated and a W-gated MOS system at 15V positive bias. These fractions were calculated from the data of Figs. 4a and 7a. The vertical lines denote for both samples the energies corresponding to 50% implantation beyond the gate/SiO2 and Si/SiO2 interfaces. The solid curves show the fractions calculated by VEPFIT for the Al-gated sample.
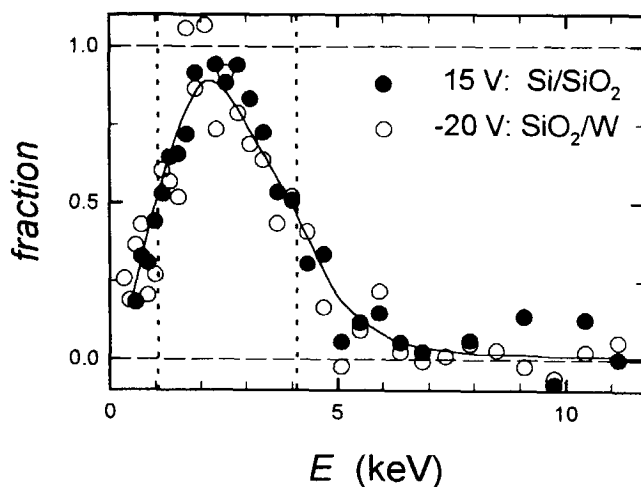
Figure 9. Comparison of energy dependent fraction obtained from the W data of positrons annihilating at positive bias at the Si/SiO$_2$ interface and at negative bias at the W/SiO$_2$ interface. The positive bias fraction is obtained from the data of Fig. 7a, the negative bias data from Fig. 7d. The vertical lines denote for both samples the energies corresponding to 50% implantation beyond the gate/SiO$_2$ and Si/SiO$_2$ interfaces. The solid line is drawn as a guide to the eye.

simulating the implantation profile. For this purpose we have used the VEPFIT programme, assuming a Makovian implantation profile.[1,13]. The sample was modelled as a simple three layer system (Al-SiO$_2$-Si), assuming a short positron diffusion length for Al (4 nm). The positron transport in the oxide and the silicon substrate was assumed to be dominated by field-induced drift. Because of this random diffusion was ignored. Furthermore, trapping of positrons in the bulk SiO$_2$ was assumed to be completely suppressed; instead they are trapped at the Si/SiO$_2$ interface. The Al fraction was obtained by calculating the positron fraction which is thermalized in the Al minus that which escapes into the oxide layer by diffusion.

As shown by the solid line in Fig. 8a, the experimental and simulated data agree satisfactory. The fraction of positrons annihilating at the Si/SiO$_2$ interface should comprize those implanted into the oxide layer plus those that have escaped from the Al by diffusion. Again, these numbers are also easily obtained from the numerical

calculation. The experimental and simulated data again show a perfect match (Fig. 8b). Finally, the positrons implanted in the silicon substrate should account for the silicon fraction of Fig. 8c; injection into the oxide layer should be practically impeded by the inwards pointing field. Also the result of this numerical simulation follows the experimental data points within experimental accuracy. The good overall agreement thus supports our interpretation.
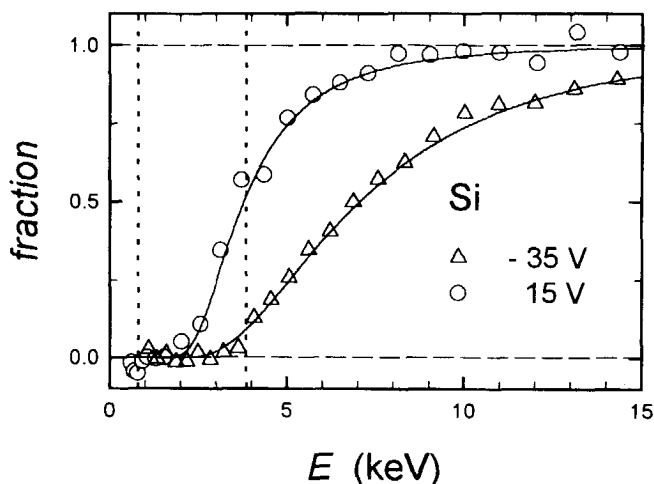
Figure 10. Comparison of energy dependent fractions of positrons annihilating in the silicon substrate of an Al-gated capacitor for positive and negative bias as calculated from the data of Figs. 4a and 4f. The vertical lines denote for both samples the energies corresponding to 50% implantation beyond the gate/SiO2 and Si/SiO2 interfaces. The solid curves show the fractions calculated by VEPFIT for the Al-gated sample.[14] In this model calculation we used for the positron in silicon a lifetime $\tau = 220$ ps, a mobility $\mu = 120$ cm^{2}V^{-1}s^{-1} and a diffusion length $L = 240$ nm.[15-17].

If our concepts are correct, then the positron *positive bias* Si/SiO$_2$ fraction should match the *negative bias* W/SiO$_2$ fraction. This latter fraction can be obtained from the negative bias W data of Fig. 7d, which allow separation in a W gate fraction, a W/SiO$_2$ interface fraction and a bulk silicon fraction. The negative bias W/SiO$_2$ fraction should comprize all positrons implanted in the oxide layer plus those diffusing from the W layer into the oxide; the substrate-implanted positrons that are injected do not contribute to this fraction since they are trapped in the gate metal. Similarly, the positive bias Si/SiO$_2$ fraction should not contain a contribution from the substrate-implanted positrons either; only the oxide implanted positrons plus those diffusing from the W into the oxide layer would contribute. Fig. 9 shows the energy dependent W/SiO$_2$ and Si/SiO$_2$ fractions. Confirming our concepts, these curves match within experimental accuracy.

To demonstrate the effect of the field on the positrons we have plotted in Fig. 10 the substrate-annihilated fraction for positive and negative bias voltage. The data show that the transport of positrons from the substrate to the oxide strongly depends on the applied field. We have modelled this field-enhanced positron transport towards the oxide using VEPFIT in which an model is implemented for the calculation of the local electric field in the silicon substrate.[14] The drift velocity of the positrons then is given by the product of the electric field and the positron mobility, taking the specific parameters for positrons in silicon from the literature.[15,16,17] Without any further optimization, the simulation satisfactorily describes the experimental data of Fig. 10.

IV. DISCUSSION

The results presented in the preceding section show that positrons implanted in an SiO_2 layer in the absence of an electric field behave like they would in any amorphous material. They diffuse around until they are trapped. When applying a field the tendency to be trapped in the oxide is reduced and may even be completely suppressed; in an MOS system the positrons drift through the oxide film until they are trapped at the substrate-oxide interface for positive bias or at the oxide-gate interface in the case of a negative bias. Trapping at the substrate-oxide interface is also significant in the case of small negative bias fields or in the absence of a field; however, for larger negative bias fields this interface becomes transparent for transport from the silicon substrate to the oxide.
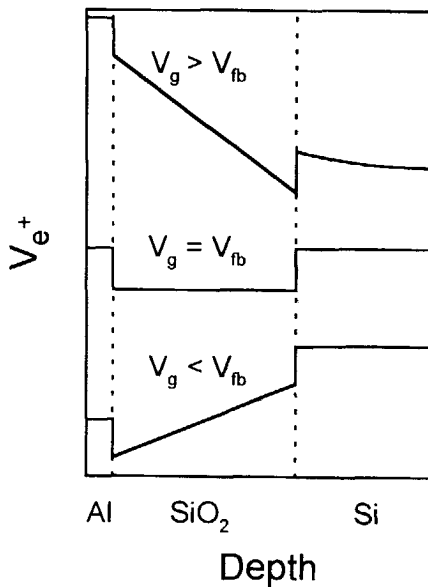

Figure 11. Schematic potential diagram for positrons in the MOS system for positive and negative gate bias voltage and for the flatband condition where the electric field approaches zero. The positron affinity for SiO_2 is higher than that for silicon and the gate metals.

The observations on oxide-implanted positrons indicate that the positron affinity for the oxide is substantially larger than for the silicon and the gate metal and leads to a potential diagram as indicated in Fig. 11. When applying a bias voltage, the positrons are simply collected in one of the potential wells defined by the positron barriers and the external field. They will move around in the well until they are trapped at a defect at the interface.

The observation that for negative bias voltages annihilation of substrate-implanted positrons partially takes place in the gate material is rather remarkable and an unexpected result of our studies. It implies the injection of positrons across the oxide-gate interface. However, such a possibility does not automatically follow from the potential diagram of Fig. 11. Apparently, the substrate-implanted positrons arrive at the oxide-gate interface with sufficient kinetic energy to surpass the barrier, in contrast to the oxide-implanted positrons that do not have sufficient energy for this step. Fig. 12 schematically indicates such transport behavior of positrons for large negative bias. For moderate negative voltages the situation is even more surprising: for these field conditions the oxide-implanted positrons are partially trapped in the SiO_2 whereas the substrate-implanted positrons are still efficiently transported through the oxide layer and injected into the gate. We would like to mention that our study is the first to report field-driven transport of positrons across a dielectric.

To explain the different behavior of the substrate and oxide-implanted positrons at negative bias one may consider among others the following effects:

- When the silicon implanted positrons enter the oxide the potential difference at the Si/SiO_2 interface is released as kinetic energy, giving these positrons an initial velocity in the direction of the gate. The positrons conceivably would conserve their energy during transport through the oxide, or they would be even further accelerated by the field.

- When a positron is implanted into the SiO_2 layer, a spur of free electron-hole pairs will be created in this material. The behavior of positrons implanted into polymers is known to be significantly affected by free charge carriers generated in this

manner.[18] In the SiO_2 film these free charge carriers could screen the externally applied field, thereby inhibiting or reducing the heating of the oxide implanted positrons. For implantation into the substrate most electron hole pairs are generated in the silicon and the transport of the substrate implanted positrons through the oxide layer will be less affected by these carriers.

- The probability of energy loss due to inelastic interactions with the oxide network may well depend on the energy of the positrons, like it is known to happen for the heating of electrons in thermally grown oxides.[19] For electrons the maximum rate of energy loss takes place when they have an overall energy of 0.1 to 0.2 eV; the rate of loss is much less at an energy of 1 eV or more.

Further study will be required to pin down the reason of the observed transport behavior.
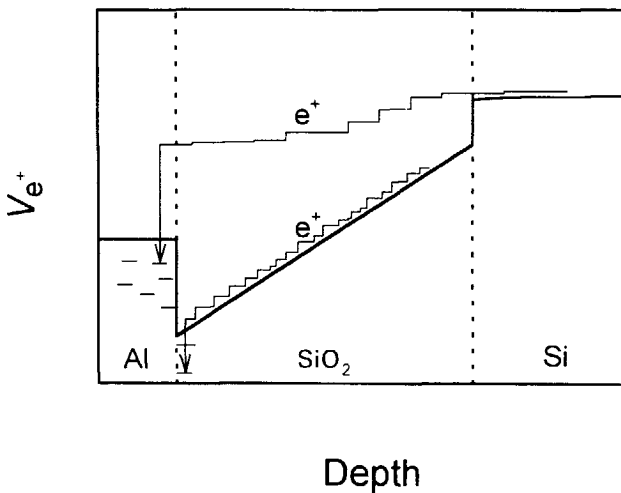

Figure 12. Schematic of transport of oxide- and substrate-implanted positrons for negative bias voltage. Positrons implanted into the oxide are driven by the field to the SiO_2/gate interface but are not injected into the gate material. In contrast, the positrons that drift back from the substrate to the oxide conserve sufficient energy to surpass the SiO_2/gate potential barrier.

Measurements on bare, field free thermal SiO_2 layers on silicon reveal a rather short positron diffusion length (typically 10 nm) which reflects efficient positron trapping.[4,5,10] Our data agree with such an efficient low-field trapping, but they also demonstrate that this trapping is suppressed when applying an electric field. This suppression can be explained straighforwardly by considering that the presence of an electric field results in unfolding of the random walk, leading to a drastic increase in the overall displacement. Also, field-induced heating of the positron up to energies as low as 0.1 eV would inhibit positron trapping at all localized positron states with energy of a few kT below the ground state of the unlocalized positrons, which presumably constitute the majority of defects.[2] For electrons in a thermal oxide, such effects have indeed been observed.[20]

It was mentioned earlier in this paper that $S(E)$ data from positron beam experiments in Al-gated MOS capacitors, published by the Brookhaven group, are in perfect agreement with the results obtained in the present study.[4] However, the interpretation by this group of the negative bias-induced peak at an implantation energy of 3.5 keV (curves g and h in Fig. 1) is rather different. They propose that the substrate-implanted positrons that return to the SiO_2 are at all conditions trapped by defects at the Si/SiO_2 interface. To explain that the 3.5keV negative bias peak in the $S(E)$ curve disappears for positive bias they postulate the involvement of two trapping sites at the interface: an open volume defect with high characteristic S and a silicon dangling bond center with low characteristic S.[4,5,21] The open volume defects are electronically inactive, i.e., these centers are neutral irrespective of bias voltage. In contrast, the silicon dangling bond centers are charged negative, neutral or positive, dependent on the bias voltage. According to the Brookhaven concept, for positive voltages positron trapping is dominated by the (negative or neutral) silicon dangling bond centers with low S, whereas trapping at these centers is prohibited at negative bias because of the Coulomb repulsion between the positron and the field-induced positive charge in the silicon dangling bond center. Instead, the positrons are trapped at the open volume defects with high S.

The Brookhaven group has presented some experimental arguments to support their explanation for the 3.5keV negative bias peak in the $S(E)$ curve. We will show that these arguments are not unique but also fit with our model, where the negative bias-induced peak is associated with substrate-implanted positrons that are transported through the oxide and injected into the gate metal.

A first supporting argument was derived by the Brookhaven group from annealing the sample in a H_2/N_2 ambient at 400°C. Such an anneal has a well documented effect on the silicon dangling bonds: an electrically inactive Si-H bond is formed.[22] Applying such an anneal was found to drastically reduce the negative bias-induced peak, as predicted by the Brookhaven model. However, it should be remembered that this annealing step also affects the Al gate. Since the gate was deposited by evaporation at room temperature, this anneal will change the aluminium structural properties like grain size, which causes a reduction of the value of S for Al, as mentioned earlier. Thus, the observed effect of the anneal also fits our model.

A second argument was obtained by the Brookhaven group from negative bias low temperature (35K) experiments using n-type silicon capacitors. Under these conditions, generation of the holes is strongly suppressed and consequently the silicon dangling bond centers would remain free for occupation by positrons with attendant suppression of the negative bias peak. The peak returned again only after a long waiting period (thermal generation of holes) or by illuminating the sample (optical generation). In our model we also expect such a reduction of the negative bias peak to occur, because at 35K the silicon substrate effectively is an insulator. This leads to an electric field throughout the silicon substrate, in contrast to the room temperature situation where the field in the silicon is limited to a depletion region close to the oxide.[23] Consequently, at 35K the field in the oxide is strongly reduced from the range of 10^6 V/cm down to the range of 10^3 V/cm. The effect of this latter field will be comparable to that of the flatband condition at room temperature; positron transport through the oxide layer and their injection into the gate will be suppressed. Instead, the positrons become trapped in the SiO_2 and at the Si/SiO_2 interface where they annihilate with low S-value. Only upon

building up an inversion layer of holes at the Si/SiO$_2$ interface, by illumination or by waiting, the oxide field will be restored, the positrons will be injected into the aluminium and annihilate with high S value.

To conclude this topic we would like to point out that the Brookhaven model can not explain our observations for the tungsten-gated system. Changing the gate material does not affect the silicon dangling bond states or the open volume defects at the Si/SiO$_2$ interface. Consequently, the negative bias peak should also appear in the negative bias $S(E)$ curve of the tungsten capacitor, which is not the case.

A number of years ago Uedono *et. al.* [3] presented data on lifetime and Doppler broadening from experiments with monoenergetic positrons for an MOS system with thick polysilicon gate. The distinct effect of the electric field was attributed to the transport of positrons through the SiO$_2$, even though conclusive proof could not be given. Our data and analysis provide a confirmation of the correctness of their interpretation.

It is to be expected that the improved positron technique will be helpful in resolving some of the present reliability issues of technologically important MOS systems with thin oxides (10nm) and polysilicon gate layers. The ability to control the transport of positrons with external applied fields may also be utilized for the analysis of other structures with insulating or semiconducting layers. Control of positron drift may be of particular interest for the development of efficient field-assisted moderators, in which positrons are efficiently driven to the surface of the device.

V. CONCLUSIONS

The study presented in this paper provides a comprehensive picture of the effect of an applied electric field on the behavior of positrons in the MOS system. Key to success is the comparison of data from samples with different gate metals and the combined use of S and W parameters, which allows convenient separation of different

positron trapping layers. Additional confirmation was obtained from the energy-dependent fractions of positrons annihilating in each of the various trapping layers.

The basic aspects of the transport process are the following:

- Trapping of positrons in thermally grown SiO_2 is suppressed when applying an electric field.
- The positron affinity of SiO_2 appears to be larger then that of the silicon substrate and the gate metals. This leads to potential barriers at both interfaces of the SiO_2 layer, which prevent positrons implanted into the oxide to escape.
- Positrons implanted into the silicon substrate and driven by a negative bias into the SiO_2 do not lose a substantial amount of energy, so that they are able to pass over the SiO_2/metal barrier and enter the metal gate.

For the latter point a conclusive explanation is still lacking. However, the concepts developed in this paper provide a firm basis for the characterization of defects at the Si/SiO_2 and the SiO_2/gate interface using positrons. They also allow a reinterpretation of earlier published data on the effect of an electric field on positrons in MOS systems.

1   P. J. Schultz and K. G. Lynn, Rev. Mod. Phys. **60**, 701 (1988).

2   M. J. Puska and R. M. Nieminen, Rev. Mod. Phys. **66**, 814 (1994).

3   A. Uedono, S. Tanigawa and Y. Ohji, Phys. Lett. A **133**, 82 (1988).

4   T. C. Leung, P. Asoka-Kumar, B. Nielsen, and K. G. Lynn, J. Appl. Phys. **73**, 168 (1993).

5   P. Asoka-Kumar, K. G. Lynn and D.O. Welch, J. Appl. Phys. **76**, 4935 (1995).

6   M. Clement, J. M. M. de Nijs, P. Balk, H. Schut and A. van Veen, J. Appl. Phys. **79** 9029 (1996).

7   A. van Veen, J. Trace Microprobe Techn. **8**, 1 (1990).

8   L. Liszkay, C. Corbel, L. Baroux, P. Hautojärvi, M. Bayhan, A. W. Brinkman and S. Tararenko, Appl. Phys. Lett. **64**, 1380 (1994).

9   E.H. Nicollian and J.R. Brews, *MOS Physics and Technology* (Wiley-Interscience, New-York, 1982).

10 B. Nielsen, K.G. Lynn, Y.C. Chen, and D.O. Welch, Appl. Phys. Lett. **51**, 1022 (1987).

11 When decreasing implantation energy below 0.5 keV, the trapping of positrons in the thin Al gate becomes overruled by trapping at the surface which acts as a efficient sink for positrons[1].

12 M. Clement, J. M. M. de Nijs, A. van Veen, H. Schut and P. Balk, IEEE Trans. on Nucl. Sc. **NS-42**, 1717 (1995).

13 A. van Veen, H. Schut, J. de Vries, R. A. Hakvoort and M. R. IJpma, in Positron Beams for solids and surfaces, AIP Conference Proceedings 218, edited by P. J. Schultz, G. R. Massoumi and P. J. Simpson (AIP, New York, 1990), p. 171.

14 A. van Veen, H.Schut, M. Clement, J. M. M. de Nijs, A. Kruseman and M. R. IJpma, Appl. Surf. Sc. **85**, 216 (1995).

15 S. Mäkinen, H. Rajainmäki and S. Linderoth, Phys. Rev. B **42**, 11166 (1990).

16 J. Mäkinen, C. Corbel, P. Hautojärvi, A. Vehanen and D. Mathiot, Phys. Rev. B **42**, 1750 (1990).

17 P.J. Schultz, E. Tandberg, K.G. Lynn, B. Nielsen, T.E. Jackman, M.W. Denhoff and G.C. Aers, Phys. Rev. Lett. **61**, 187 (1988).

18 Ken-ichi Okamoto, Kazuhiro Tanaka, Mikio Katsube, Osamu Sueoka and Yasuo Ito, Radiat. Phys. Chem. **41**, 497 (1993).

19 M.V. Fischetti, D.J. DiMaria, S.D. Brorson, T.N. Theis and J.R. Kirtley, Phys. Rev. B **31**, 8124 (1985).

20 T.H. Ning, J. Appl. Phys. **47**, 3203 (1976).

21 E.H. Pointdexter, P.J. Caplan, B.E. Deal and R.R. Razouk, J. Appl Phys. **52**, 879 (1981).

22 P. Balk, Extended abstract of papers, presented at the Electrochemical Society Meeting, Buffalo, NY 10-14 October 1965 (The Electrochemical Society, New York, N.4., 1965), paper 111.

23 S. M. Sze, *Physics of Semiconductor Devices*, 2nd edition (Wiley, New York, 1981).

Chapter 5

Positrons in the polysilicon-gated MOS system

I INTRODUCTION

In the last few decades the positron beam analysis technique has been applied successfully to study defects in materials [1,2]. The use of a monoenergetic positron beam allows for the investigation of the depth distribution of defects. In the specific case of a metal-oxide-silicon (MOS) system it is also possible to control the transport of the positrons in the SiO_2 layer after thermalization by applying an electric field[3,4]. For a positive bias voltage, the positrons implanted in the oxide are pushed towards the Si/SiO_2 interface, but they are not injected into the silicon substrate because of the potential barrier. Instead, they are trapped at the Si/SiO_2 interface. As shown in preceding papers, a sufficiently thick oxide layer can thus be used as an implantation buffer to collect all positrons, from which they are driven to the Si/SiO_2 interface[3,4]. Guiding all positrons effectively to the Si/SiO_2 interface opens new and interesting possibilities to study defects at this interface[5,6,7].

The technologically most relevant MOS systems have an oxide layer of 10 nm or less, which is insufficient to collect the positrons. Moreover, they have a polysilicon gate, that may not be simply replaced by an aluminium one because of the resulting inferior electrical properties of the oxide layer; apparently the structural properties of this
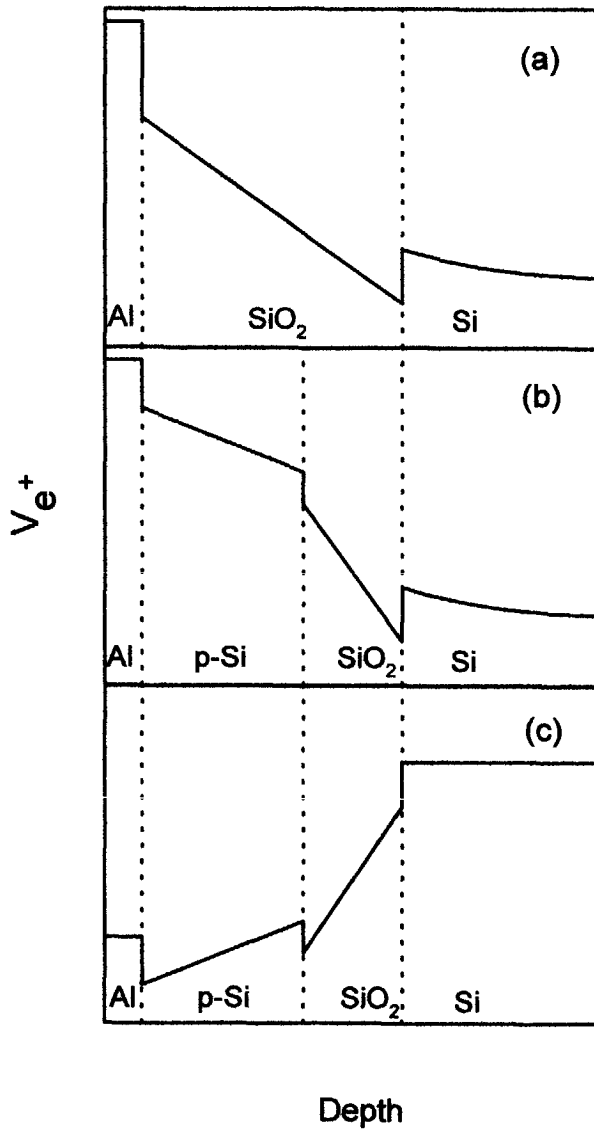
Figure 1. Schematic potential diagram for positrons in MOS system for positive bias voltage: for an Al/SiO₂/Si at positive bias (a) and for an Al/polysilicon/SiO₂/Si at positive and (b) negative bias (c) condition.

interface are affected by the relatively low temperature ($\approx 600°C$) polysilicon chemical vapour deposition process. Conceivably, also the polysilicon layer can be used as an implantation buffer from which the positrons can be injected into the oxide, see Fig. 1b. To this end, the grain size and the doping concentration of the polysilicon layer have to be optimized. Grain boundaries act as efficient positron traps and their number has to be minimized. A stableelectric field in silicon requires the space charge region associated with a depletion zone. To induce a sufficiently strong electric field in this manner, approximately 10^{17} cm^{-3} activated dopant atoms are needed. In this work we will show the feasibility of using a polysilicon layer as an implantation buffer.

II EXPERIMENTAL

For our studies we used MOS capacitors on (100) 2-5 Ωcm n-Si with a 100 nm thick gate oxide prepared by oxidation in dry O_2 at 1000°C. To produce polysilicon with large grains (60 nm or larger) a 60 nm amorphous silicon layer was grown by low temperature (540°C) chemical vapour deposition and subsequently subjected to crystallization anneal at 900°C [8]. Next, the polysilicon was implanted with 10^{13} cm^{-2} phosphorus atoms, followed by an activation anneal. To minimize the number of potential positron traps in the polysilicon (such as unsaturated silicon dangling bonds), we subsequently applied an anneal at 400°C in forming gas ($10\%H_2/90\%N_2$). As a reference, the polysilicon layer of some wafers was removed by wet chemical etching at room temperature. Finally, the polysilicon gated and the bare oxides were covered with a 15 nm Al layer by evaporation from a tungsten boat.

Doppler broadening measurements were carried out using the Delft Variable Energy Positron beam[9]. This facility provides an 8 mm diameter positron beam with energy ranging from 0 up to 30 keV and with a typical flux of 10^5 s^{-1}cm^{-2}. The gamma spectrum was measured using a Ge detector with an energy resolution of about 1.1 keV

at $E_\gamma = 511$ keV. All S- and W-data are normalized to reference S- and W-values of device-quality silicon, see chapter 1.

III RESULTS AND DISCUSSION

To establish whether trapping in the polysilicon layer can be sufficiently suppressed and whether the polysilicon gated system indeed provides accurate information about the substrate/oxide interface, we will make a comparison of data obtained from the Al and polysilicon gated capacitors. First, we will briefly present the results from the Al gated system.

Fig. 2 shows the relative S-parameter (S / S_{Si}) versus implantation energy E, $S(E)$, for an Al gated MOS system subjected to a 15 V positive bias. In the case of implantation into the Al we obtained an S-value of about 1.08. Implantation into the oxide layer results in a minimum S value. As shown in chapter 4, this minimum corresponds to positrons that are transported from the oxide layer towards the silicon where they are trapped at the SiO_2/Si interface[3,4].

In Fig. 3 we show the $S(E)$ and $W(E)$ data as trajectories in the S-W plane, using the energy as a parameter. In this chapter also W is the relative W-parameter. Annihilation at a distinguishable site or layer can now be represented by a characteristic (S, W) point [3,5,10]. The triangular shape of the trajectory reveals that only three distinguishable trapping layers are involved. The cluster point at the high energy end corresponds to the silicon substrate. For low implantation energy the specific (S, W) point of Al is approached. The characteristic coordinates of the third trapping layer are given by the intersection point of the straight high and low energy parts of the trajectory; it is associated with the positrons that are trapped at the SiO_2/Si interface. In the figure we have also indicated the characteristic coordinates of SiO_2, as obtained from an independent measurement on a sample without a gate. The location of this point proves that trapping in the oxide layer is fully suppressed by the electric field
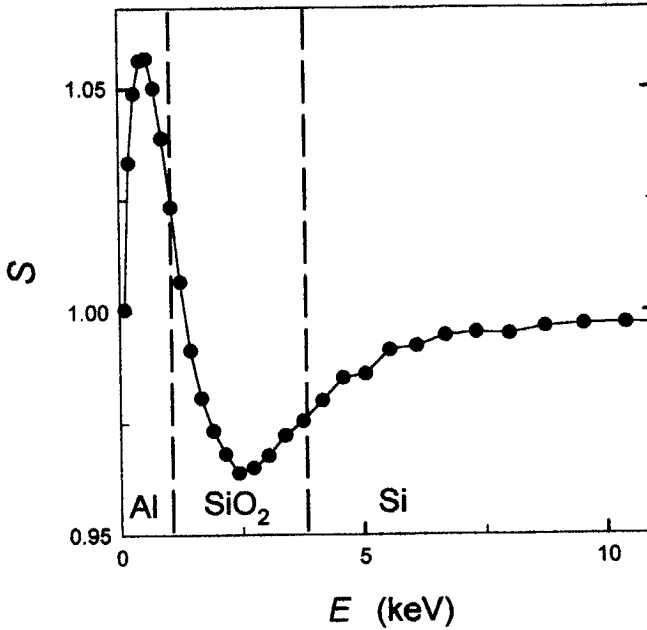
Figure 2. S(E) curve for an Al gated MOS system subjected to +15 V bias.

The trapping of positrons in the polysilicon layer can be investigated by comparison of $S(E)$ data from polysilicon/SiO_2/Si structures without Al, but with different surface treatments. The results of these measurements are presented in Fig. 4. The figure shows the $S(E)$ curves for an as-fabricated specimen with a thin native oxide layer on the polysilicon 'a', the curve after removal of this oxide layer by an HF etch 'b' and the curves after an HF etch followed by chemical oxidation at a temperature of 60°C in HCl/H_2O_2 'c' or NO$_4$/H_2O_2 'd'. The data show that the surface modification strongly affects the S-parameter for implantation in the polysilicon layer whereas the data for deeper implantation are not affected. Apparently, a substantial part of the positrons implanted into the polysilicon migrate to the outer surface. Such a drastic effect of the surface condition would be impossible in the case that the polysilicon layer would

contain large numbers of efficient positron traps. In that case the positrons would be trapped at the defects, unable to diffuse to the (modified) surface. This result thus suggests that positron trapping in the polysilicon layer does not play an important role and that the positrons have a sufficiently long diffusion length.
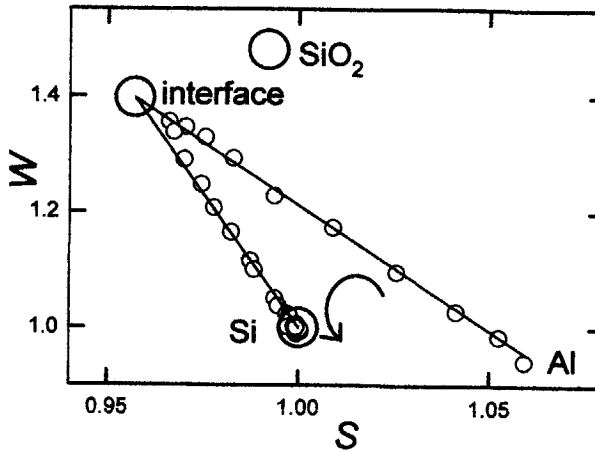
Figure 3. S-W trajectories of an Al gated MOS system subjected to +15 V bias. The arrow indicates the direction of increasing implantation energy. The large circles correspond with the characteristic points of Al, bulk SiO2, the SiO2/Si interface and the silicon substrate.

Next, we performed measurements at different bias conditions on capacitors provided with a thin Al top layer. Fig. 5 shows the resulting $S(E)$ data for -10 V, 0 V and +15 V bias. Implantation into the 15 nm Al top layer results in a high S-value for all bias conditions. For implantation in the polysilicon, in the oxide and in the silicon, the curves reveal a clearfield effect. The 15 V positive bias curve exhibits a broad minimum ($S= 0.955$) for implantation in the polysilicon layer, while for 0 V bias an intermediate S-value is observed. This data clearly demonstrate a field effect in the polysilicon, and thus the feasibility of properly doping this layer. The -10 V negative

bias curve does also show intermediate values for implantation into the polysilicon layer, but exhibits low S values for implantation into the oxide and the underlying substrate region. The minimum (S=0.945) is reached at 6 keV (200 nm) and the curve deviates significantly from the bulk Si value beyond 13 keV (1 μm). The data thus exhibits a field effect extending deep into the silicon, corresponding with the depletion layer that is for the used doping about 1 μm thick.
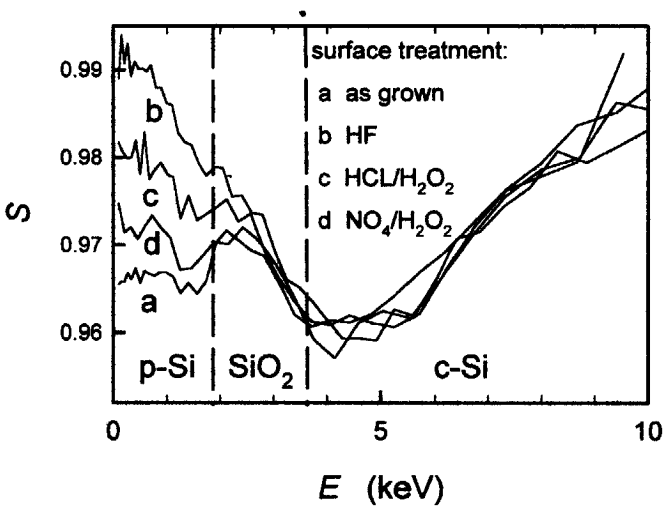
Figure 4. S(E) curves of polysilicon/SiO₂/Si with different surface states. Shown are: as-fabricated specimen with native oxide layer on the polysilicon (a), after removal of this oxide by an HF etch (b), and after an HF etch followed by 60°C chemical oxidation in HCl/H₂O₂ (c) or NO₄/H₂O₂ (d).

For the interpretation of the $S(E)$ curves it is convenient to consider the corresponding S-W plots of Fig. 6 [11,12]. The data for +15 V bias are all located on two straight lines that intersect at $(S, W) = (0.955, 1.38)$. The intersection point also coincides with a clustering point. Comparison with the trajectory of Fig. 3 shows that the intersection point is identical to the (S, W) point of the SiO₂/Si interface of the specimen without polysilicon gate. The intersection point of Fig. 6 is associated with the broad

minimumof the +15 V bias *S(E)* curve for polysilicon and oxide-implanted positrons. Apparently, the positrons implanted in the polysilicon and in the oxide are efficiently transported by the field to the SiO2/Si interface where they are trapped. Most remarkable is that the +15 V *S-W* trajectories of the specimen with (Fig. 6) and without (Fig. 3) polysilicon layer are identical within experimental error; it looks as if there is no polysilicon layer at all.

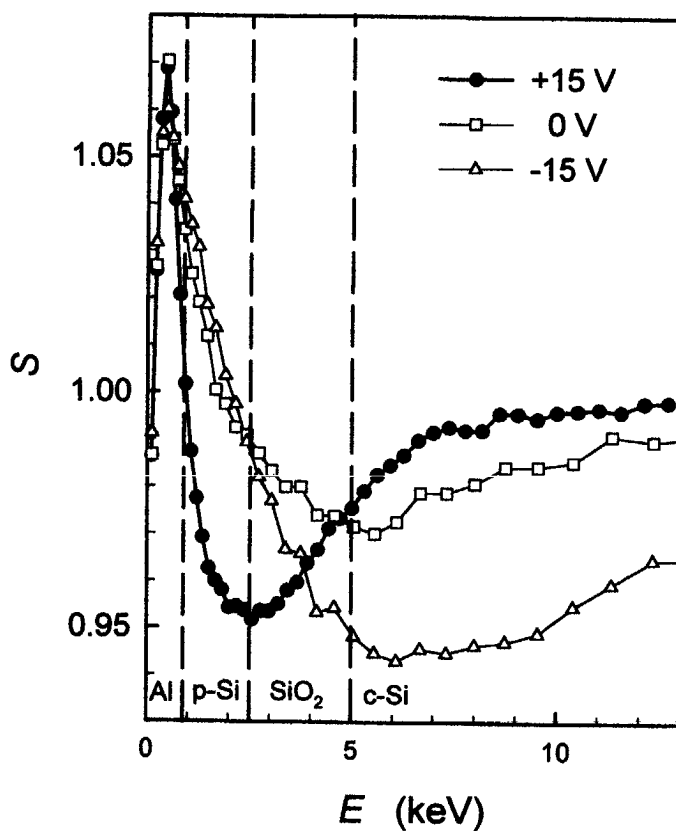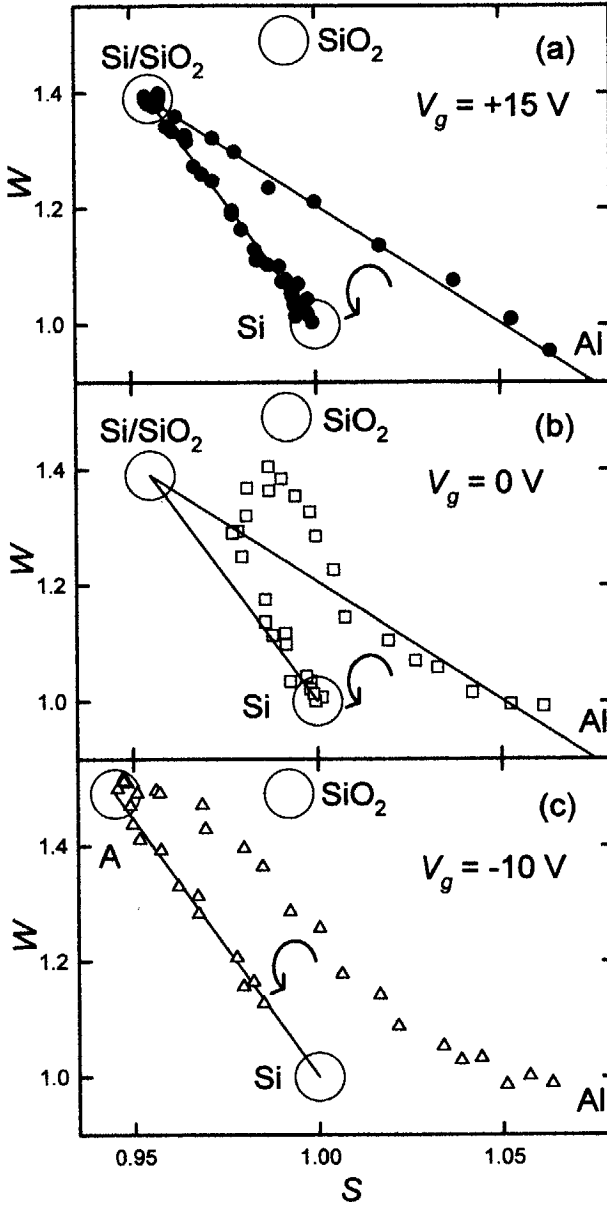*Figure 5. S(E) curves for an MOS system with polysilicon layer subjected to +15 V, 0 V and -10 V bias.*

Figure 6. S-W trajectories for an MOS system with polysilicon gate subjected to + 15 V (a), 0 V (b) and -10 V (c) bias. The large circles correspond with the points of Al, bulk SiO$_2$, the SiO$_2$/Si- and the polysilicon/Si-interface and the silicon substrate.

One should note that the SiO$_2$/Si characteristic (S, W) coordinates, $(0.955, 1.38)$ of Figs. 3 and 7, differs substantially from the earlier reported values of $(0.95, 1.55)$ for specimens that were not provided with a polysilicon gate[4,5]. Apparently, structural changes are clearly sensed by the positrons. Unfortunately, we can not interpret this information yet.

In Fig. 6b we have drawn the 0 V bias trajectory, which reveals some additional features of the transport and the trapping of the positrons. For low energies, which correspond with implantation in the polysilicon, the trajectory is almost straight, possibly with a small deviation towards the silicon point. This deviation could point towards some trapping in the polysilicon layer; however, such a contribution may be well neglected for the present discussion. The majority of the positrons are trapped either in the Al top layer or in a trapping layer with a characteristic point situated on the line defined by the Al and the SiO$_2$/Si characteristic coordinates. This suggests that the polysilicon implanted positrons probes the Al/polysilicon- and the polysilicon/SiO$_2$-interface. For moderate implantation energies, the trajectory runs outside the triangle Al-SiO$_2$/Si-Si, towards the bulk oxide characteristic point. Apparently, without the applied field a substantial fraction of the positrons is trapped in the bulk oxide layer. For increasing energy the trajectory returns to the bulk silicon coordinates, with however a clear deviation towards the SiO$_2$/Si interface point, and approaching the substrate point according to the line defined by the characteristic points of the SiO$_2$/Si interface and of the silicon substrate. This 0 V trajectory shows that trapping at the SiO$_2$/Si interface still is important, but not as dominant as in the case of positive bias. Likely, a major fraction of the positrons trapped at the interface can be ascribed to substrate-implanted positrons that diffuse back to the oxide.

The S-W trajectory for -10 V negative bias, shown in Fig. 6c, exhibits a different behaviour. For shallow implantation, the data again approach the characteristic point for the Al top-layer. For increasing implantation depth, the data are not situated on a straight line but the trajectory exhibits a kink at $(S, W) \approx (1.02, 1.1)$. This part of the trajectory can not be explained by trapping in two different material layers only. From

Fig. 5 it can be seen that the kink corresponds with implantation into the polysilicon. The complex low energy trajectory points to a mixture of annihilation in the Al, at the Al/polysilicon interface, in the polysilicon, at the polysilicon/SiO$_2$ interface and in the SiO$_2$. Positrons implanted in the polysilicon experience at negative bias only a weak electric field due to the n-type doping (see fig 1c). They are trapped at grain boundaries or diffuse to the Al/polysilicon interface. Most positrons implanted in the SiO$_2$ are collected at the potential well at the polysilicon/SiO$_2$ interface due to the field.

For deeper implantation, the data exhibit clustering at $(S, W) = (0.945, 1.55)$. This clustering corresponds with the broad plateau seen in Fig. 5 for implantation in the SiO$_2$ and in the substrate region beneath the oxide. This cluster point can be ascribed to positrons implanted in the SiO$_2$ and into the 1 μm deep depletion layer in the substrate that are transported by the electric field to the polysilicon/SiO$_2$ interface (see Fig. 1c). Positrons at this interface are confined to the potential well and probe the defect structure. Only for implantation deep into the substrate $(E_{imp} > 25$ keV) the data approach the bulk Si point.

IV CONCLUSIONS

Our results clearly demonstrate the possibility to use a polysilicon layer as an implantation buffer for positrons; trapping can be sufficiently suppressed and the layer can be doped to induce a sufficiently strong field. We have shown that indeed all positrons implanted in the polysilicon and oxide layer can be collected at the SiO$_2$/Si interface. This technique offers new and very promising opportunities to study defects at the SiO$_2$/Si interface of technological important MOS systems.

1   P. J. Schultz and K. G. Lynn, Rev. Mod. Phys. **60**, 701 (1988).

2   M. J. Puska and R. M. Nieminen, Rev. Mod. Phys. **66**, 814 (1994).

3   M. Clement, J. M. M. de Nijs, P. Balk, H. Schut and A. van Veen, J. Appl. Phys. **79**, 9029 (1996).

4   M. Clement, J. M. M. de Nijs, P. Balk, H. Schut and A. van Veen, J. Appl. Phys. **81**, 1943 (1997).

5   M. Clement, J. M. M. de Nijs, A. van Veen, H. Schut and P. Balk, IEEE Trans. on Nucl. Sc. **NS-42**, 1717 (1995).

6   J.M.M. de Nijs, M. Clement, H. Schut, and A. van Veen, Microelectronic Eng. **36**, 35 (1997).

7   J.M.M. de Nijs and M. Clement, in Fundamental Aspects of Ultrathin Dielectrics on Si-based Devices, edited by E. Garkfunkel et al (Kluwer Academic Publishers, 1998), p. 25.

8   P.J. French, B.P. Drieënhuizen, D. Poenar, J.F.L. Goosen, R. Mallee, P.M. Sarro and R. Wolffenbuttel, J. Microelectromechanical Systems, **5**, 187 (1996).

9   A. van Veen, J. Trace Microprobe Techn. **8**, 1 (1990).

10 L. Liszkay, C. Corbel, L. Baroux, P. Hautojärvi, M. Bayhan, A. W. Brinkman and S. Tararenko, Appl. Phys. Lett. **64**, 1380 (1994).

11 M. Clement, J. M. M. de Nijs, H. Schut, A. van Veen, R. Mallee and P. Balk, MRS Symposium Proceedings **442** , 143 (1996).

12 M. Clement, J. M. M. de Nijs, H. Schut, A. van Veen and P. Balk, Mat. Sc. Forum **255-257**, 718 (1997).

Chapter 6

Re-emission of positrons from the Si/SiO_2 system

I INTRODUCTION

For the generation of a monoenergetic positron beam, positrons have to be moderated to low energy[1,2]. Mostly, this is performed using ultra pure tungsten or copper as a moderator material. The energetic positrons from the source (e.g. ^{22}Na) are implanted in the moderator material where they thermalize. A minor fraction of the thermalized positrons diffuses back to the surface from which they are emitted because of the positive positron affinity of the moderator. The presently used moderators have a typical emission efficiency of 0.1%. Evidently, increase of this efficiency is very desired for many applications.

To realize a higher emission efficiency, it has been suggested to fabricate a so-called field-assisted positron moderator. Such a system is based on a layered structure in which an electric field can be applied to push the implanted positrons to the surface. In the literature results have been reported for moderators made of SiC and diamond that demonstrate the influence of an internal electric field on the transport of thermalized positrons[3,4]. However, because of a too large trapping rate at defects, the positron yield of these structures was not much better than that of conventional moderators.

Recently, we have demonstrated for the metal-oxide-silicon (MOS) system that positrons in the SiO_2 layer can be efficiently transported over distances of 300 nm or longer when applying an electric field ≥ 1 MV/cm[5]. For negative gate voltages a substantial fraction (up to 40%) of the positrons implanted in the Si diffuses back to the oxide layer and are subsequently transported towards the gate. Interestingly, at this field condition the positrons are injected into the gate material, although there is a potential barrier. Apparently, the positrons are sufficiently accelerated by the electric field to overcome this barrier[6]. Similar 'heating' effects have been reported for electrons in SiO_2 [7].

Conceivably, an MOS system with a negative gate bias may provide an improved moderator. The positrons from the source thermalize in the silicon substrate. Due to the negative bias, they are transported towards the gate where they are injected into the gate metal. Next, they traverse the gate layer to be finally emitted at the vacuum side. To verify the feasibility of this concept we had made some moderators with ≈ 10 nm W, Ni and Co gate layers. Unfortunately, we did not observe an increased positron emission when applying an electric field. This negative result can likely be ascribed to defects in the metal contacts. To circumvent this trapping problem, we have fabricated samples with small metal islands instead of a blanket gate layer. The islands can be charged using an electron spraying technique, so creating the electric field. The question now, is whether a substantial fraction of the positrons will be injected from the oxide immediately into the vacuum or not.

In this chapter we present the results of an exploratory study of positron re-emission from a MOS system with small, charged Au islands. We will show that it is possible to charge the islands sufficiently to induce an electric field of 5 MVcm^{-1} in the SiO_2 layer. Next we discuss positron re-emission from such a moderator. We used two approaches to assess the re-emission. With the aid of three additional grids, the slow re-emitted positrons are accelerated and injected backwards into the beam system. Next they are selected by the ExB deflection system (see §2.5) and guided towards the multiple channel plate (MCP) detector. In the other approach, re-emission data were obtained from

the rate of annihilation events in the MOS moderator using the Ge detector. Re-emission should result in a reduction of the count rate. Our results indicate that field-assisted positron re-emission from the MOS moderator indeed occurs; however, for an efficient moderator, the yield is too low and has to be improved by an order of magnitude at least.

II EXPERIMENTAL

For the MOS moderator we used B-doped 0.2-0.05 Ωcm (100) Si samples with a 105 nm thick SiO_2 layer. The oxide was grown by a 180 minute dry oxidation at 1000°C which was immediately followed by an anneal of 20 minutes in dry N_2 at the same temperature.

The islands were obtained by deposition of $\approx$10Å of Au on the oxide surface. The Au was evaporated using a resistively heated W boat. In Fig. 1 we show a picture of the islands made by secondary electron microscopy. Clearly, we have obtained well-defined and isolated islands, as intended. The islands have a typical size of 10 nm and a mutual distance of about 10 nm. They cover the surface for approximately 40%.

The structure was placed in the positron beam system. For the measurements, three additional grids were mounted in front of the sample. These grids allow an energy selection of the re-emitted positrons and suppression of electric stray fields that would distort the particle trajectories.

Figure 1: SEM micrograph of the SiO_2 surface covered with Au islands of about 10 nm diameter.

III CHARGING THE ISLANDS

Fig. 2a gives a schematic picture of the experimental set-up that we used for charging the islands. The electrons are obtained from a W filament situated behind the ExB deflector (see chapter 2) which is used to inject the electrons into the beam system. To distribute the electrons homogeneously over the sample surface, the last solenoid is switched off thus creating a locally divergent magnetic field near the sample.

To charge the Au islands, the potentials on the filament leads are set to -2 V and 0 V respectively. After passing the extraction grid and the ExB system, the electrons arrive at the sample with an energy of 3 eV at most. The electrons that are injected into the Au islands are all trapped at these sites while those reaching the SiO_2 surface are, because of the electric field, transported through the oxide layer to the substrate. In the beginning, the islands are neutral so that they can be reached by the electrons; however, charging the islands raises their potential such that the electrostatic repulsion prevents further electron injection in the metal., i.e., the charging is a self limiting process. To enable further charging we applied a positive potential on the substrate (V_{sub}) which lowers the surface potential again. The potential diagram of Fig. 2b illustrates this point.

When charging the moderator we noticed that one should not use a too large positive bias. For example, for an electron energy of 15 eV at the surface we observed a rapid decrease of the negative charge on the islands. For such energies, the electron energy is dissipated by generation of electron-hole pairs in the oxide layer. The holes drift to the Au islands where they neutralize the trapped electrons. Apparently one has to limit the positive substrate potential so that the energy of the arriving electrons remains below 9 eV, the excitation energy for electron-hole pairs. Because of this, the moderator was charged in subsequent steps in which V_{sub} was increased with 1 V. During each step the sample was exposed with $3 \ 10^{11}$ cm^{-2} electrons.

To measure the charging of Au islands we analyzed the reflection of a low energy positron beam as a function of the external applied substrate potential V_{sub}. The

reflection can be deduced from the rate of annihilation events in the MOS system. Fig. 3 curve A shows the emission rate of γ photons versus V_{sub} for the case of uncharged islands. The implanted positrons have an energy of about 12 eV (10.0 V on the acceleration
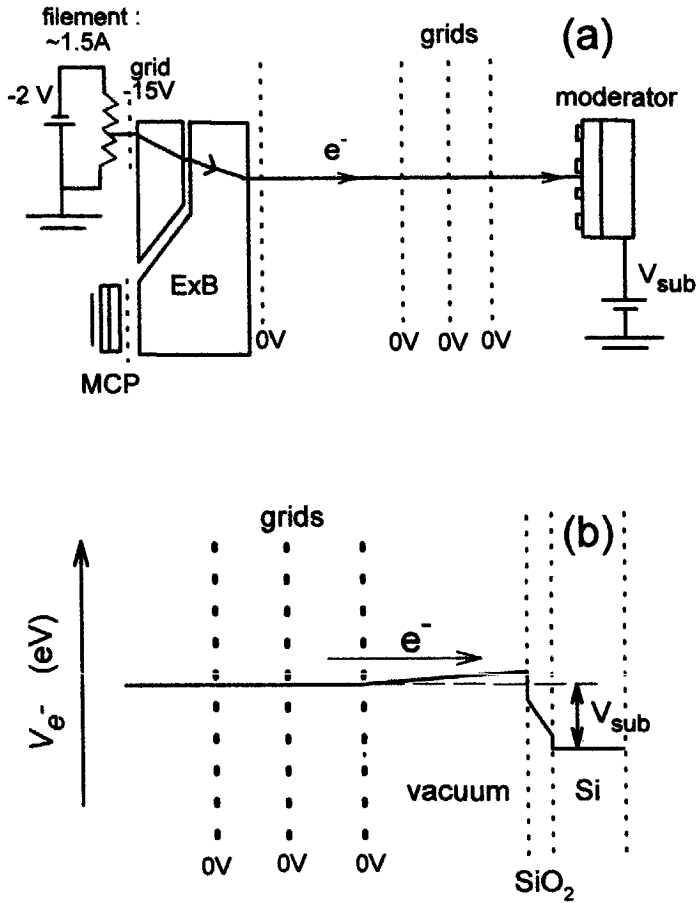

Figure 2: Experimental set-up (a) and electron potential diagram (b) during charging the SiO₂/Au surface.
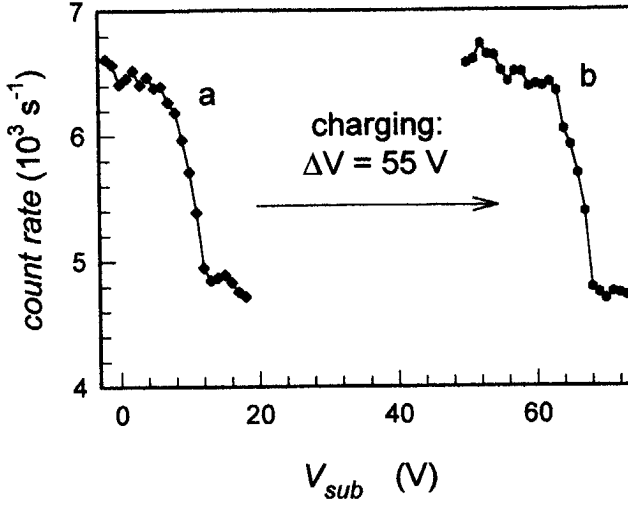
Figure 3: Count rate in Ge detector as function of the potential V_{sub} on the substrate (a) for a uncharged and (b) for a charged MOS moderator for the experimental set-up shown in fig. 2.

plates). For low bias voltages the positrons are implanted in the moderator. When raising the bias above a certain value, the positrons are reflected at the surface. The positrons escape from the sample and their annihilation does no longer contribute to the detector signal. This effect is clearly seen as a decrease in the count rate in curve A of Fig. 3.

Charging the islands changes the surface potential of the sample according to

$$\Delta V_{surf} = \frac{Q_{surf}}{C_{ox}}, \qquad (1)$$

where C_{ox} is the capacity of the Au/SiO$_2$/Si system per unit area, ΔV_{surf} the change in surface potential and Q_{surf} the area density of trapped charge. The effect of charging is shown by curve B of Fig. 3, which was recorded after an exposure of 1×10^{14} electrons cm^{-2}. As argued, during charging the substrate bias voltage was increased gradually, in this particular case up to 50 V. The charging has shifted the curve of Fig. 3 by 55 V.

Furthermore, it can be seen that the shape of the curve is conserved, which indicates that charging the islands only affects the surface potential, as expected. Because of this we can use the shift as a measure for the trapped charge. In this case the shift of 55 V corresponds with a density of 1×10^{13} cm^{-2} or ~10 electrons per island. The shift also corresponds with a static electric field of 5 MV cm^{-1} in the oxide layer, which is rather large as compared to the fields needed for positron injection into the gate material.

The observation that the shape of the curve is conserved shows that the charge is homogeneously distributed over the surface. This homogeneous distribution is due to the self-limiting property of the charging process of islands in conjunction with the divergence of the magnetic field near the sample surface.
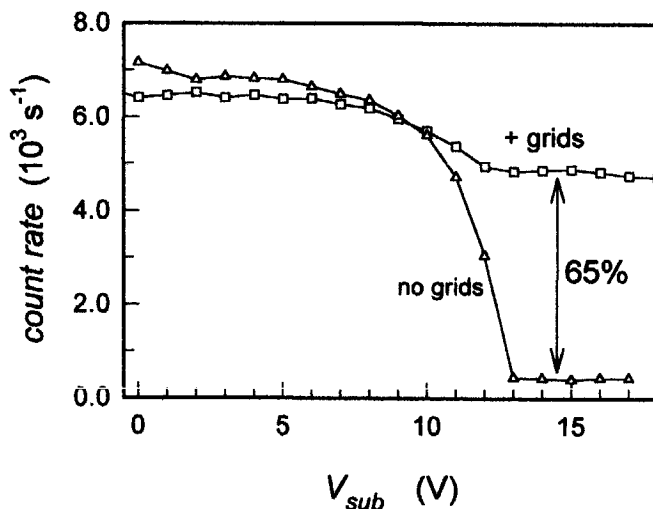
Figure 4: Count rate in Ge detector versus the potential V $_{sub}$ on the substrate of a uncharged MOS moderator with and without the presence of three grids in front of the MOS moderator.

Although the curves of Fig. 3 reveal a clear reduction in count rate, one could wonder why the count rate does not drop to zero. After all, if the positrons are reflected, none of them should annihilate in the sample. We expected that most of them would be

trapped in the three additional grids. To verify this explanation we have repeated the experiment after removal of the grids. Fig. 4 shows the count rate versus the substrate bias for this situation. As expected, the count rate now drops to zero. From this result we conclude that about 65% of the reflected low-energy positrons is implanted in the grid material, either on its way to the sample or upon its return. Apparently, the grid system is a large scavenger for low-energy positrons.

During the re-emission experiments, the incident positrons are implanted with an energy of several hundreds of electron volts. This energy is dissipated in the oxide by generation of electron-hole pairs. Because of the strong electric field, the electron-hole pairs are separated; the holes are transported to the Au islands and the electrons to the substrate. This mechanism results in a continuous loss of negative charge on the islands. Typically for SiO_2, every 20 eV energy loss corresponds with the generation of one electron-hole pair. For implantation of 2 keV positrons in the oxide layer, about 100 electrons and holes are generated. With the used implantation rate of 10^5 $cm^{-2}s^{-1}$ and with a typical exposure time of 48 h, one thus expects the neutralization of $1.5 \ 10^{12}$ cm^{-2} trapped electrons. Such a loss is acceptable when considering the total charge on the islands. We have checked this point by implanting a charged sample during two days with positrons with energies of 0.2 keV up to 20 keV. This exposure resulted in a charge loss of $\sim 1 \times 10^{12}$ cm^{-2}, in agreement with our estimation.

IV POSITRON RE-EMISSION

Apart from field-assisted positron moderation, there is an incomplete moderation mechanism based on scattering: some of the positrons return to the material surface after one or more scattering events without complete thermalization, having enough energy to escape into the vacuum. To avoid the use of lengthy descriptions to indicate the history of the positrons, we will refer to these latter positrons as 'backscattered' positrons

whereas the ones moderated according to the field-assisted mechanism will be called 'field-moderated' positrons.

To start, we had to find an experimental approach to distinguish the backscattered and the field-moderated positrons. The probability for backscattering of positrons decreases monotonously with the implantation energy. In contrast, field-assisted moderation requires the implantation of the positrons deep into the 105 nm oxide layer or into the silicon just beneath this layer. An implantation energy of at least 2 keV is needed to reach such depths. Therefore, the dependence of the re-emission rate on the implantation energy is a key parameter to establish the history of the positrons. In addition, one can use the controllability of field-assisted moderation; it can be switched on and off by charging and neutralizing the moderator, in contrast to the backscattering which doesn't dependent on the electric field.

For the measurements, use was made of the three-grid system in combination with the substrate bias. In Fig. 5 we illustrate the configuration of the system and the spatial potential. First, the surface potential was kept approximately at 0V by adjustment of the substrate bias; for uncharged islands the substrate bias was 0V whereas for charged islands +50V bias was applied. Re-emission was stimulated by applying a negative potential of -2.5 kV on the first grid situated 1 cm in front of the sample. The third grid was always connected to ground so that after passing the positrons have their initial escape energy again. The middle grid now can be used to make an energy selection. This capability was applied for a differential measurement to improve the accuracy. Only positrons with an initial escape energy larger than the second grid potential can pass. For 0V bias, all positrons are let through whereas for 20V bias only those with an escape energy of 20 eV or more. Hence, the difference of the 20V and 0V re-emission rates is associated with the re-emitted positrons with energy between 0 and 20V.

As mentioned in the introduction, positron re-emission was assessed by two different methods. Using the three grid system, the re-emitted positrons are injected into the beam system in opposite direction. At the ExB deflection system, they are selected from the beam and guided towards the MCP detector, see Fig 5a. The second approach is
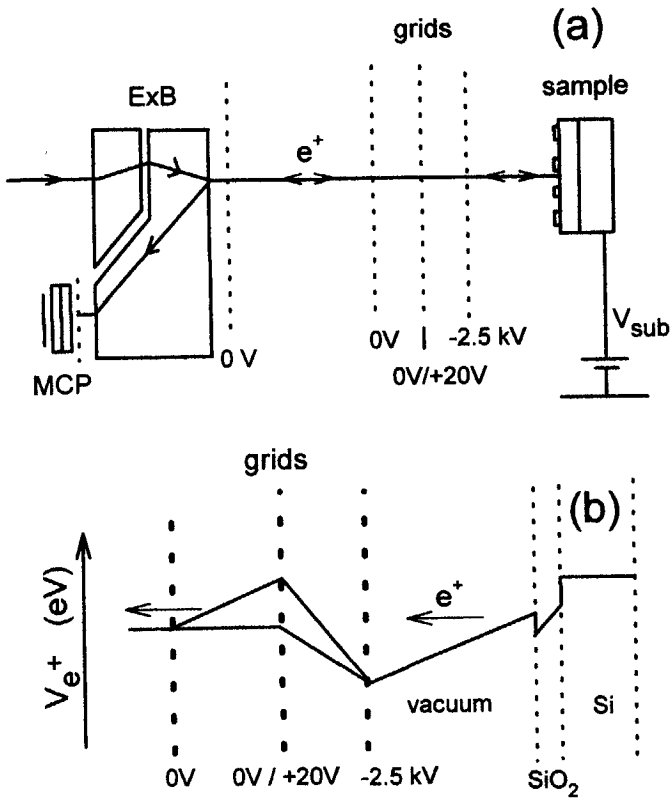
Figure 5: Experimental set-up (a) and positron potential diagram (b) during the re-emission experiments.

based on the reduction of the number of annihilation events in the moderator region that includes the moderator and the system of three grids just in front of it. When a substantial number of positrons escape from this moderator region as result of their re-emission this can be monitored by changes in the count rate in the Ge detector. In the following, we will first present the results of the measurements using the extraction technique and the MCP followed by those obtained from the Ge detector.
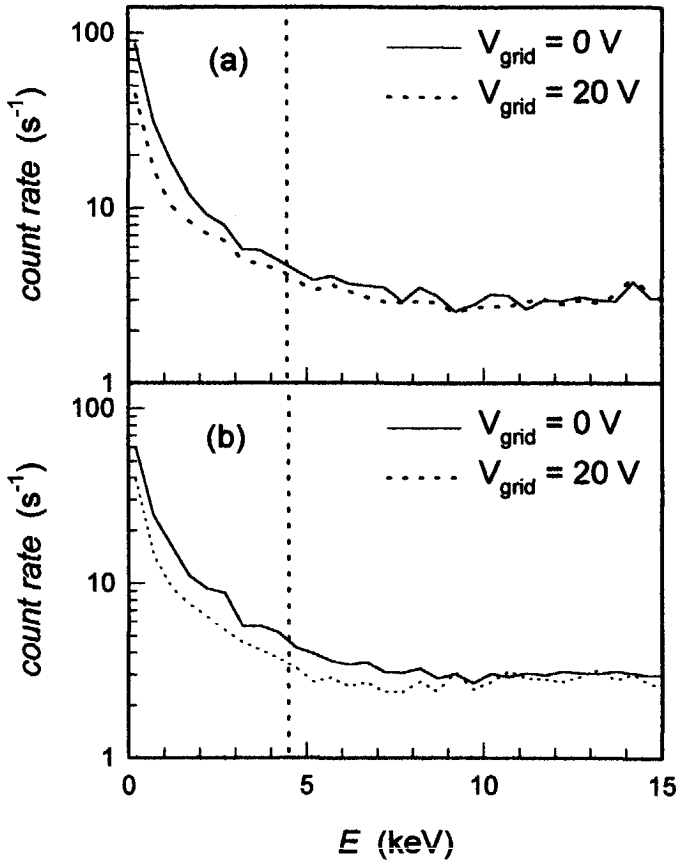
Figure 6: Count rate in micro channel plate (MCP) detector for zero potential and positive potential on the second grid in front of the neutral (a) and the charged (b) MOS moderator. The vertical dotted line indicates the position of the Si/SiO$_2$ interface.

First we have explored the case of neutral islands. In this state the field-assisted moderator is switched off. In Fig. 6a we show the MCP count rate as a function of the implantation energy for 0 V and 20V bias on the middle grid. As can be seen, the number of positrons detected by the MCP decreases with increasing implantation energy, irrespective of the grid voltage. This effect can be ascribed to positrons backscattered from

the grids and from the moderator surface. The figure also clearly shows that only a minor contribution of the signal comes from the positrons re-emitted from the moderator surface with an energy below 20 eV, thus illustrating the necessity of a differential measurement.

Figure 7: Detection rate of positrons in the range of 0 to 20 eV by the MCP versus the implantation energy for the charged and uncharged MOS moderator. The curves were obtained by taking the difference between the curves for zero and positive potential in the figs 6a and 6b. The vertical dotted line indicates the position of the Si/SiO$_2$ interface.

Next we have repeated the measurements for the charged Au islands, i.e., with the field-assisted emission switched on. The MCP count rate versus implantation energy for 0 and 20 V grid voltage is shown in Fig. 6b. Again it shows that the signal is dominated by backscattering.

In Fig. 7 we show the emission rate of positrons with an energy in the range of 0 up to 20 eV for the charged and the uncharged moderator as calculated from the data of Fig. 6. For implantation energies smaller than 2 keV there is hardly a difference which confirms that in the case of shallow implantation, the signal is dominated by backscattering. This process is not affected by the electric field in the oxide layer. For

implantation energies larger than 7 keV, the positrons are implanted deep in the silicon beyond the field charge region. As expected, such positrons cannot return to the moderator surface. For energies ranging from 2 up to 7 keV the positrons are implanted in the oxide layer and in the silicon just beneath. In this energy range also, the data reveal a small but systematic increase of the positron detection rate due to the charging of the Au islands. Apparently, we observe a field effect although not a large one.

The data of Fig. 7 show that the field-moderated positrons account for an increase of the MCP count rate of typically 1 s^{-1}. Fortunately, the total number of field-moderated positrons is much larger because only a small fraction of them reaches the MCP detector. Scattering and trapping at the grids results in severe losses ($\approx$65%) as shown in section 3. In chapter 2 we showed that the efficiency of the ExB deflection system is rather low, 4% at most. After correction of these losses one obtains a re-emission rate of $\approx 1 \times 10^2$ s^{-1} or $\approx$0.1% of the total beam intensity.

The number of field-moderated positrons was also determined from count rate data from the Ge detector. This detector records the number of annihilation events in the MOS moderator or in the grids. Signal loss associated with charging the islands thus can be attributed to field-assisted moderation. For these experiments we used different settings of the substrate bias and the second grid potential; the voltages for the first and third grid were not altered, respectively -2.5 and 0 kV. A positive substrate bias corresponding with a surface potential of $\approx$130 V was applied to stimulate re-emission. In addition, the middle grid was set to 120 V or 140 V bias. When applying 140V bias, only re-emitted positrons with an escape energy of 10 eV or more are able to leave the moderator region. In contrast, for 120 V all re-emitted positrons can leave. The number of re-emitted positrons with an energy of 10 eV or less thus can be calculated from the difference in both count rates. In Fig. 8 we show for the charged and uncharged moderator the differential signals associated with the re-emitted positrons with energy of 10 eV or less. These curves are qualitatively comparable with the results from the MCP shown in Fig. 7. As in the case of the MCP measurements, the count rate decreases monotonically with the implantation energy due to backscattering. Below 2 keV implantation energy there is
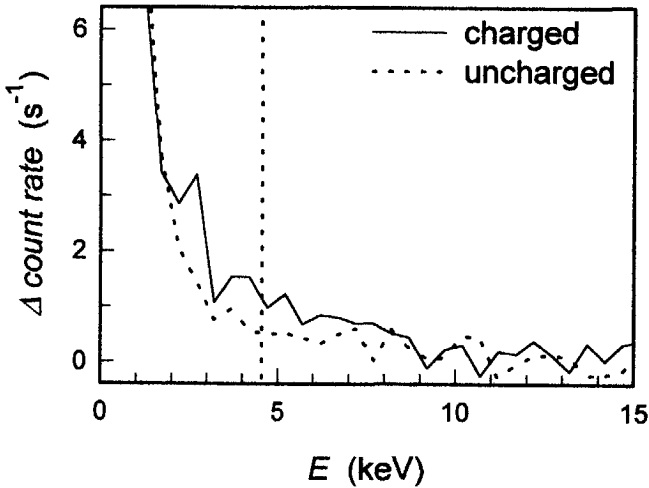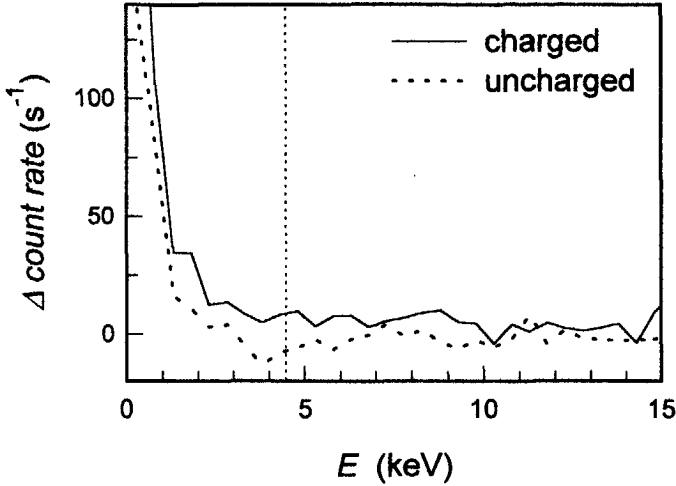
Figure 8: Detection rate of positrons in the range of 0 to 20 eV by the Ge detector versus the implantation energy for the charged and uncharged MOS moderator. The curves were obtained by taking the difference in count rate between the cases of high (140 V) and low (120 V) potential on the second grid. The surface potential of the MOS moderator was kept on 120 V. The vertical dotted line indicates the position of the Si/SiO$_2$ interface.

no substantial difference between the count rates for the charged and the uncharged moderator. Above 10 keV, the signals approach each other again. For implantation into the oxide and into the silicon substrate beneath the oxide (2 keV <E_{imp}< 7 keV), the figure again reveals a small but systematic increase of the number of re-emitted positrons. Hence, we have reproduced the MCP proof of field-assisted moderation using the Ge detector.

The yield of field-moderated positrons for implantation at the Si/SiO$_2$ interface (E_{imp} ≈ 4 keV) as estimated from the data of Fig. 8, approximately is 10 s^{-1} or 0.2% of the total count rate of 6 10^3 s^{-1} of the Ge detector. However, to estimate the efficiency of the field-assisted moderation process one has to correct for 65% grid losses. After such a correction one obtains an efficiency of ≈0.5%.

V DISCUSSION

Our results indicate that the re-emission of positrons from the MOS moderator is indeed stimulated when applying an internal electric field. Although the effect is rather small, the rough qualitative agreement of the MCP and the Ge detector data indicates its reliability. These results provide additional evidence for the concepts on the transport of positrons in the MOS system derived in preceding work. From the MCP data we estimated a re-emission rate in the order of 0.1% of the intensity of the primary beam. From the measurements with the Ge detector we derived a higher re-emission intensity of 0.5% of the incoming positrons.

Although both results are of the same order of magnitude there is a factor 5 difference. The reason for this difference is not clear. Conceivably it is associated with the kinetic energy of the emitted positrons when leaving the moderator region. For the measurements with the Ge detector the surface potential, was 120 V while the MCP measurements the surface potential has a value of about 0.5 V. During the latter experiments the 0.5 eV positrons could be transported less efficiently through the beam system and across the grids on their way as the 120 eV positrons in the experiment with the Ge detector.

From the results in chapter 4 it was shown for large negative fields about 40% of the positrons implanted into the substrate (5 keV) return to the gate[5]. This fraction of 40% heated positrons contrasts with the rather low emission of 0.5% we observed. It shows that only 1% of the heated positrons in the SiO_2 is emitted to the vacuum.

One may attribute this low efficiency to negatively charged defects which would trap the positrons. However, defects in the oxide layer have a small cross section for electron trapping (typical 10^{-17} cm^2). Because of this, only a small fraction of electron traps will be charged during the electron spraying with about 10^{14} cm^{-2} electrons.

Another factor that could affect the emission efficiency is that the charged Au islands may act as very efficient traps for the heated positrons. The trapping at the Au
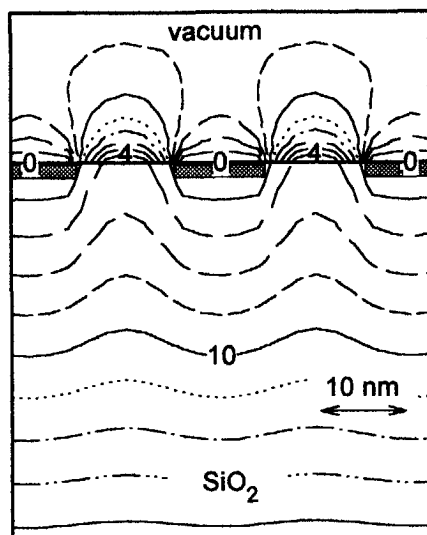
Figure 9: Calculated equipotential lines at the surface of a charged MOS moderator with 10 nm diameter Au islands. The numbers in the figure denote the related potential in V. The islands, indicated with squares, have a potential of 0 V while the substrate potential was 40 V, thus inducing a field of 4 MV/cm in the 100 nm thick oxide layer. Note that in the surface region the field has a significant component parallel to the surface.

islands is enhanced by the coulombic attraction between the positrons and the negative charged islands. This point is illustrated by fig 9 that shows the result of the calculated electric potential around the islands. As can be seen from this figure, the electric field has large tangential components pointing towards the islands. This coulombic attraction may affect the trajectory of the positrons in the SiO_2 such that they hit the metal islands. Furthermore, the field in the vacuum nearby the islands is directed towards the islands so that also re-emitted positrons can be trapped by the islands.

A conceivable solution to improve the emission efficiency is to use smaller islands. In this case the trapping at the islands will be lower because of a smaller surface coverage. Furthermore when reducing the thickness of the islands to a few mono layers of metal atoms the heated positrons could pass through without loosing energy by interactions with electrons or phonons.

Furthermore, the efficiency of the MOS moderator can be improved by optimizing the electric field in the silicon substrate. A first step in this optimization is to use n type silicon substrate with a low doping concentration (10^{15} cm^{-3}). In this way, one obtains a depletion layer of typically 1μm with an electric field in the range of 10^4 Vcm^{-1} when applying a negative bias[8]. From the mobility of positrons in silicon of 120 cm^{2}V^{-1}s^{-1} and their lifetime of 220 ps it follows that at these conditions the positrons drift over a distance of about 2 μm [9,10]. We can thus assume that most of the positrons implanted into the depletion layer will reach the oxide. Another, more effective, way to induce an electric field in the substrate is to create a thin p type doped layer just beneath the oxide in intrinsic silicon substrate. When making electrical contact with the conducting highly doped layer one will be able to apply an electric field over the whole silicon substrate. In this way positrons may be extracted from a layer of several micrometers.

A disadvantage of the MOS moderator is that the SiO$_2$ will degrade because of the implantation of energetic positrons and other ionizing radiation originating from the positron source. The radiation (including the energetic positrons) will damage the SiO$_2$ and can cause local breakdowns. The generated defects may suppress the transport of positrons while the breakdowns will cause local neutralizations of the islands. A typical dose rate of presently used positron sources is 50 mCi or 10^8 positrons per second in the energy range of 0 to 2 MeV. To estimate the radiation damage we can neglect the effect of the γ-quanta because of their relatively low cross section for interaction. From the mean penetration depth of 20 μm of 2 MeV positrons it can be derived that a 100 nm SiO$_2$ layer will dissipate about 5% of their energy. From the dose rate of 10^8 s^{-1} and a generation of about one electron hole pair for each 20 eV dissipated energy one can

estimate a generation rate of 5 10^{11} electron hole pairs per second. These electron hole pairs will be separated efficiently because of the strong electric field. A rough estimation for MOS devices is that degradation occurs after generation of 1 Coulomb charge carriers per cm^2 [11]. With this rule of thumb we estimate that the lifetime of a MOS moderator will be in the range of 1 10^7 s or 50 days.

Furthermore, the electron-hole pairs generated by the energetic positrons will neutralize the charge on the metal islands. In section 2 we derived that the charged moderator will contain a density of trapped electrons of typical 10^{13} cm^{-2}. Above we derived that the radiation induces a generation of 5 10^{11} electron-hole pairs each second. From this it follows that the moderator will be neutralized after 20 s. This means that during operation the MOS moderator has to be charged periodically by exposure with electrons from a filament.

VI CONCLUSIONS

Summarizing our results show that Au islands with 10 nm diameter on a SiO_2 surface do efficiently trap electrons and that by exposure of electrons in the energy range below 3 eV a homogeneous area distribution of charge can be realised. Our data indicate that positron emission from the Si/SiO_2 system indeed occurs, but at a very low level. The presented results may form the starting point from where positron emission for Si/SiO_2 systems can be improved. These improvements may be obtained by using samples with smaller Au islands and by using n-type silicon substrates with low doping concentration. However, although the MOS moderator may open possibilities to realize a improved positron re-emission efficiency, its application will be complicated by the degradation the SiO_2 and the rapid neutralization of the metal islands both caused by the high flux of incoming energetic positrons.

1   P.J. Schultz and K.G. Lynn, Rev. Mod. Phys. **60**, 701 (1988).

2   J. Puska and R.M. Nieminen, Rev. Mod. Phys. **66**, 814 (1994).

3   L.V. Jorgensen, A. van Veen, H. Schut, Nucl. Instr. and Methods in Phys. Research B **119**, 487 (1996).

4   G.R. Brandes, K. Canter, A. Krupyshev, R. Xie, and A.P. Mills, Jr, Mat. Sc. Forum **255-257**, 653 (1997).

5   M. Clement, J.M.M. de Nijs, P. Balk, H. Schut and A. van Veen, J. Appl. Phys. **81**, 1943 (1997).

6   R.I. Simpson, C.D. Beling and M. Charlton, in The Physics and Technology of Amorphous SiO_2, edited by R.A.B. Devine (Plenum Press, New York, 1987), p. 569.

7   M.V. Fischetti, D.J. DiMaria, S.D. Brorson, T.N. Theis and J.R. Kirtley, Phys. Rev. B **31**, 8124 (1985).

8   E.H. Nicollian and J.R. Brews, *MOS Physics and Technology* (Wiley-Interscience, New-York, 1982) p. 60.

9   J. Mäkinen, C. Corbel, P. Hautojärvi, A. Vehanen and D. Mathiot, Phys. Rev. B **42**, 1750 (1990).

10 S. Mäkinen, H. Rajainmäki and S. Linderoth, Phys. Rev. B **42**, 11166 (1990).

11 V.V. Afanas'ev, J.M.M. de Nijs, P. Balk and A. Stesmans, J. Appl. Phys. **78**, 6481 (1995).

Chapter 7

Relation between defect structure and VUV radiadion hardness

I INTRODUCTION

It has been well established that the radiation-hardness of the metal-oxide-semiconductor (MOS) system is strongly affected by the details of the fabrication procedure [1,2]. Since hydrogen is a notorious intermediate in the generation of interface traps, it is quite obvious that as a rule the incorporation of this species during device fabrication should be minimized. It is also known that post oxidation anneals (POA) at temperatures above 900°C in an inert ambient should be avoided. As shown by Warren et al., such an anneal enhances positive charging of the bulk oxide and the generation of Si/SiO$_2$ interface and border traps upon exposure of the MOS system to ionizing radiation [3,4]. According to their opinion, these effects are caused by the formation of O vacancies and O vacancy-related complexes in the oxide network at or close to the Si/SiO$_2$ interface during the high temperature anneal. Such a creation of additional O vacancies would immediately explain the correlation between the positive charging of the bulk oxide and the POA treatment since the vacancies constitute trapping centers for holes [5]; however, it does not offer a straightforward explanation for the enhanced generation of interface and border traps upon irradiation.

Several techniques have been used to investigate the structure of the Si/SiO$_2$ system. Electron spin resonance studies have greatly contributed to our knowledge by resolving the microscopic structure of a number of electrically active point defects such as the O vacancy center [5,6]. The structure of the interfacial region has also been investigated by high resolution transmission electron microscopy [7] and, indirectly, by X-ray photoemission spectroscopy [8,9]. Although the results from these latter studies have contributed to the general understanding, they have not provided specific insights in the relation between the structural and electrical properties of the interface. Positron annihilation (PA) is an alternative technique that could also provide structural information but whose possibilities have not been sufficiently explored thus far [10,11]. For the Si/SiO$_2$ system, the nature of the positron trapping centers has not been unambigiously established; however, in line with the trapping centers in metals and semiconductors one would expect that the positrons are trapped by open spaces in the oxide network thus providing information on such spaces.

In this investigation we have studied the effect of POA at 1000°C in N$_2$ of various times. On the one hand, such an treatment provides a promising test case for PA spectroscopy and in particular its sensitivity to structural changes of the Si/SiO$_2$ system. On the other hand, it could produce new insights on the effect of POA on the susceptibility for the generation of interface traps.

Like results of capacitance-voltage (C-V) measurements but unlike electron spin resonance data, the PA measurements do not provide direct structural information. The understanding and the interpretation of the results of PA measurements thus have to be derived from correlations between PA data and other system properties. Therefore, we have studied the influence of POA on the bulk oxide electron and hole traps and interface traps in the as-grown system and on the generation of interface traps by vacuum ultraviolet (VUV) irradiation [12].

Doing our PA experiments, we learned that the positrons can be preferentially driven towards the SiO$_2$ region bordering the Si substrate, thus providing valuable information on the positron trapping sites in this border region. The PA data show that

already a short POA significantly changes the oxide network. This change does not correlate with the more gradual evolution observed for the interface traps and bulk oxide traps in the as-grown system, but it does correlate with the generation of interface traps by VUV radiation. In our irradiation experiments only a neutral metastable species, such as excitons or hydrogen atoms, which have to traverse the oxide layer from gate to substrate could produce the interface traps. The PA data suggest that the samples not subjected to a POA contain relatively large interstices in the oxide network near the Si substrate that account for the trapping and annihilation of the positrons. POA removes these larger interstices. Possibly, they act also as a scavenger for the metastable species that produce interface traps when arriving at the Si/SiO_2 interface, which would explain the observed correlation between PA and the generation of interface traps.

In the following section we will describe the preparation of the oxides and the techniques used for their electrical characterization. Next, PA spectroscopy is briefly introduced and it is shown that this technique indeed may provide information from the oxide network near the substrate. In further sections we present the experimental results and a discussion.

II. EXPERIMENTAL

For our studies we have used MOS capacitors on 0.05-0.2 Ωcm p-Si(100) substrates with a 105nm thick gate oxide prepared by oxidation in dry O_2 at 1000°C. Following the growth, the process was quenched by changing the gas flow from O_2 to Ar or N_2, thus subjecting the oxides to POA. After a certain time, the POA time, the furnace was ramped down to 800°C, whereafter the wafers were unloaded. The system is equipped with a special unloading tube to allow the wafers to cool down in a pure N_2 ambient. With the aid of this tube, passivation of as-grown interface traps is avoided [12]. Transparent (15 nm) Al gates were deposited by evaporation from a resistively heated W

boat. The capacitors were subjected to a 30 minute post-metallization anneal (PMA) in forming gas (10% H_2 and 90% N_2) at 400°C.

The density of interface traps was measured using combined quasi-static and high frequency C-V measurements. Avalanche electron injection was applied to study the bulk oxide electron traps. For the hole trapping experiments we used the technique of VUV hole injection: the capacitor is exposed to the irradiation from a Kr source (hv = 10 eV, 10^{15} photons $cm^{-2}s^{-1}$) while a positive gate bias is applied corresponding to a 1 MV cm^{-1} electric field in the oxide. Electron-hole pairs are generated just beneath the gate [13], the electrons being swept towards the gate whereas the holes being transported through the oxide layer towards the Si substrate, thus filling the hole traps in the oxide. For both types of injection experiments, the amount of trapped charge carriers was calculated from the midgap voltage shift (ΔV_{mg}).

The susceptibility for the generation of interface traps was studied by exposure of the MOS capacitors to VUV radiation at negative bias conditions. At this condition, positive charging of the oxide is avoided because the holes will not appear in the region near the Si/SiO_2 interface where the dominant hole trapping centers are located [5]. Bulk oxide electron trapping is also avoided since we used a rather limited exposure ($<10^{16}$ cm^{-2}). The oxide remains uncharged; however, large numbers of H-induced fast donor-type traps at the Si/SiO_2 interface are generated [12,14-16]. The number of the radiation-induced interface traps above midgap was calculated from the stretch-out of the C-V curves.

The Delft Variable Energy Positron beam (VEP) was used for the positron annihilation Doppler broadening measurements [17]. This system produces a collimated beam of monoenergetic positrons with energy ranging from 0 up to 30 keV with a typical flux of $\approx 10^4$ $cm^{-2}s^{-1}$. The positrons are extracted from a ^{22}Na source. The γ-photons that result from the annihilation of the positrons are detected by a Ge detector.
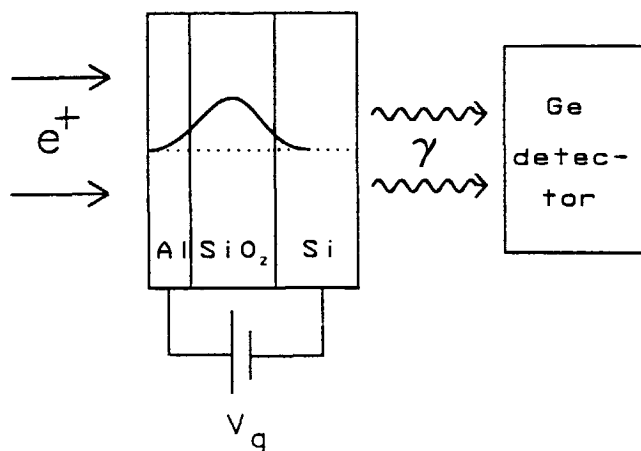
Figure 1. Schematic illustration of the experimental arrange-ment for PA measurements. Positrons are implanted into the MOS capacitor. After thermalization they will be trapped at defects in the system. Next, they annihilate with an electron thus producing two γ photons that are detected by the Ge detector. In the case of a MOS system, the thermalized positrons can be driven towards the gate or the Si substrate by applying an external gate bias.

III. POSITRON ANNIHILATION

In the following we will present a brief discription of the positron annihilation (PA) Doppler broadening measurements, followed by a more detailed discussion on the experimental approach developed for MOS systems. A more extended treatment of PA spectroscopy can be found in the review paper of Asoka-Kumar et al. [10].

For the PA experiments, accelerated positrons are implanted into the system [10,11]. Figure 1 gives a schematic illustration of the experimental set up. By varying their kinetic energy the positrons can be implanted at a pre-defined depth. For the lower energies they are implanted into the gate; for the higher values they are deeper implanted, into the oxide

or into the substrate. After thermalization, the positrons will diffuse until being captured at a defect.

The trapped positron ultimately annihilates with an electron, thereby producing two 511 keV γ quanta. The energy of the γ quanta is slightly affected by the momentum of the annihilated particles. This variation is reflected in the spectral shape of the γ peak, which thus contains information about the electronic environment of the defect. The resolution of the γ detector is too low to obtain a detailed momentum distribution; however, it is sufficient to study the broadening of the peak. This broadening is expressed with the aid of the so-called shape parameters S and W. The definitions of S and *W* are given in figure 2. One should note that this figure shows an as-measured spectrum.
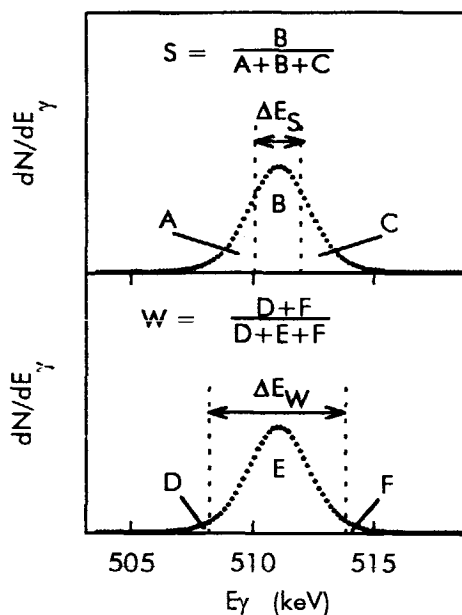

Figure 2. Definition of shape parameters S and W of the γ-peak. The indicated area's (A, B,.. , F) denominate sections defined with the aid of a fixed integration window (ΔE_S and ΔE_W). The figure shows a typical experimental spectrum.

The introduction of these particular definitions of S and W to parameterize the γ peak offers the advantage of a linear formalism: if annihilation takes place at two defects, A and B, characterized by (S_A, W_A) and (S_B, W_B) and with trapped fractions f_A and f_B, f_B = 1- f_A, then the measured parameters (S_M, W_M) will be given by:

$$S_M = f_A S_A + f_B S_B \qquad \text{(1a)}$$

and

$$W_M = f_A W_A + f_B W_B \qquad \text{(1b)}$$

The peak shape that is actually measured, not only depends on the microscopic structure of the defects, but also on the geometry of the detection system. This feature makes it difficult to directly compare S and W data from different laboratories. To circumvent this drawback, some well-defined reference systems are used to characterize the equipment. Bulk crystalline Si is such a reference, and therefore we could very conveniently use the S and W values measured for large implantation energies for the normalization.

Earlier PA studies on metals and semiconductors have taught that the positrons have a preference to occupy the so-called 'open-volume defects' such as vacancies, clusters of vacancies or voids [18,19]. In the relatively large open-volume defects, there is little overlap of the trapped positron with the high momentum core electrons. Annihilation mainly takes place with the low momentum valence electrons which results in a narrow γ peak with a large S and a small W value. With decreasing volume, the positron will become more enclosed which causes a stronger interaction with the core electrons of the confining atoms. The enhanced interaction with the high momentum core electrons broadens the γ peak. This results in a smaller S and a larger W value; i.e., S in-creases and W decreases with the "volume" of the defect [20]. The experience from PA studies of the past decade shows that defects can be characterized by means of an S parameter. The work of Liskay et al. [21] and the results presented in this paper show that the W parameter

may contain independent information. Because of this it is favorable to use the *S-W* pair as a fingerprint of a particular defect.

If positrons are implanted in an insulating layer such as an oxide, it is possible to control their transport after therma-lization by applying an electric field. Figure 3 schematically shows the electrochemical potential for the positrons in a MOS system for different signs of the bias voltage. Opposite to the case of electron affinities, the positron affinity of the oxide is larger than that of the Si or the Al. In the case of a bias more positive then the flatband voltage, the positrons that are implanted into the oxide are driven towards the Si/SiO$_2$ interface. However, these positrons can not enter the Si because of the potential barrier; they are confined to the oxide region bordering the substrate.
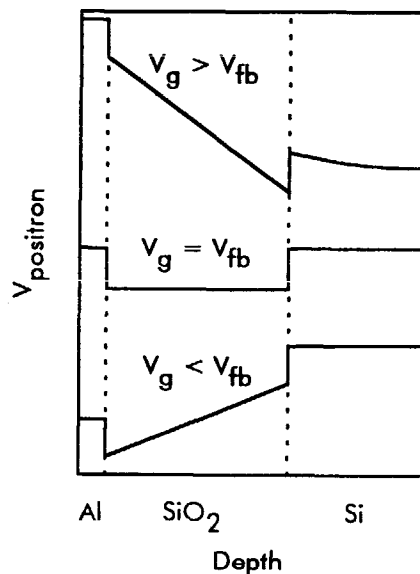

Figure 3. Electrochemical potential for positrons in MOS system at positive bias, flatband voltage or negative bias. Opposite to the case of electron affinities, the positron affinity of the oxide is larger than that of Si or Al.

Figure 4 shows the S-value normalized with respect to that of Si as a function of the implantation depth for a MOS system subjected to different positive bias voltages. In the case of implantation into the Al we obtained an S-value of about 1.075. Implantation into the oxide layer results in an S-value exhibiting a minimum. However, this minimum depends upon the field strength: for increasing fields it can be seen that it approaches an absolute minimum (S_{min}) of about 0.973.

For the interpretation of the PA measurements it is often helpful to plot the data as trajectories in the S-W plane, using the implantation energy as a running parameter. Such a plot is shown in figure 5. The direction of increasing implantation energy is indicated by the arrows in the figure. The annihi-lation at different sites can now be represented by trap coordinates in this plane. For example, annihilation in the Si substrate is represented by the S-W coordinate ($S_{Si} = 1$, $W_{Si} = 1$) and annihilation in the Al by ($S_{Al} = \approx 1.08$, $W_{Al} = \approx 0.84$). In most cases we will have to deal with the involvement of three or more centers, located at different depth. The coordinates of the defects then define a polygon in the S-W plane. From the linearity property of the S and W parameters (Eqs. 1a and 1b) it immediately follows that in this situation the trajectory is confined to this polygon. If annihilation is determined by two distinguishable sites only, the trajectory is given by a straight line connecting the two defect coordinates; changing the implantation energy only changes the distribution of the positrons over the two traps. Such an effect is seen twice in figure 5; the trajectory can be quite satisfactorily approximated by two straight lines. Moreover, within the experimental error, the trajectories always run at the 'inner' side. This shows that at this particular positive bias condition at least three sites are involved but that there are no indications for the presence of a fourth. The trap coordinate of the third center is given by the point where the two straight lines cross.

The trajectory of figure 5 closely approaches the crossing of the two lines, but does not reach this point completely. This feature shows that although a large fraction of the positrons is trapped at the third trap, there is always a small fraction that annihilates in the Al or the Si. This agrees with numerical simulations of the implantation made
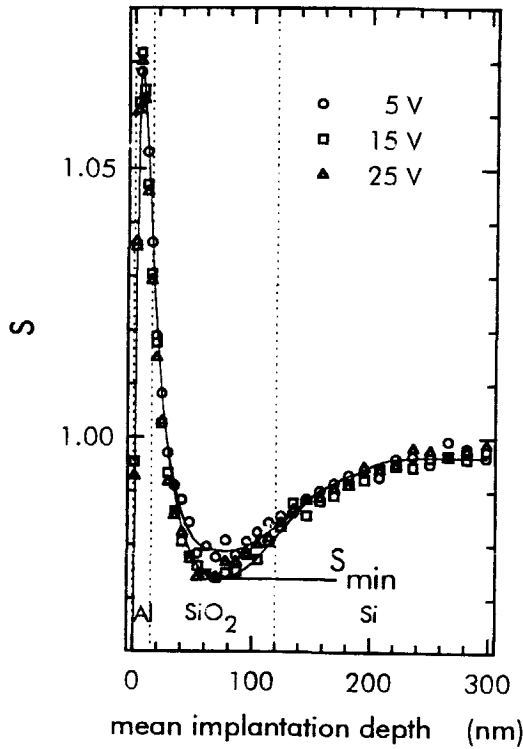
Figure 4. S parameter versus mean implantation depth of positrons in a Al/SiO2/Si system for various positive gate bias voltages. All data have been normalized to S_{Si}.

with the variable energy positron fitting program (VEPFIT) [11] which show that the implantation profile is stretched-out, with tails extending into Si and Al.

Above we have argued that, if a positive bias of 15V is applied during the PA depth scan, effectively only three sites play a role in the trapping of the positrons. Considering this feature, we may also understand the approach of the absolute minimum S value (S_{min}) for an implantation in the middle of the oxide for increasing positive bias

Figure 5. S-W trajectory for positrons implanted in a Al/SiO$_2$/Si system for 15V positive gate bias. The arrows indicate the direction of increasing implantation energy.

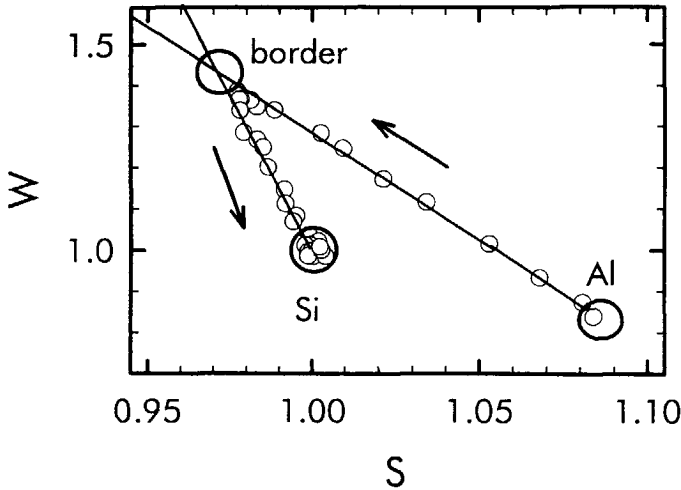(figure 4). Due to the electric field, the positrons implanted in the oxide will be transported towards the Si/SiO$_2$ interface. When this field has moderate values, the positrons will reside sufficiently long in the oxide to have an appreciable fraction trapped at sites in the bulk of this layer; those not trapped in the oxide will be first driven into the triangular potential well at the Si/SiO$_2$ interface and next captured at sites in this well. Changing the magnitude of the electric field thus changes the ratio between positrons trapped at sites in the bulk of the oxide layer and those captured by centers in the potential well. For the +15V bias, trapping at centers in the bulk of the oxide layer becomes negligible and all positrons are collected in the potential well. Thus, applying such a gate bias allows us to exclusively probe the sites in the oxide close to the substrate. For convienience, we will in the following refer to this region as the 'oxide border region'; the corresponding S-W coordinate will be denoted as (S_{border}, W_{border}).

IV. RESULTS

Using the insights discussed in the foregoing section, we have first verified whether or not PA at a positive gate bias is suited to monitor the structural changes induced by POA of various times in N_2. The result revealed a clear distiction between the samples with POA shorter than 4 min. ('short POA') and those with POA of 4 min. or longer ('long POA'). Within experimental error, identical trajectories were obtained for all specimens with a short POA. The systems subjected to a long POA also produced approximately equal trajectories; however, these latter were quite different from the trajectories of the specimens with a short POA, without any indication of a gradual transition between the short and long POA. In figure 6 we present typical trajectories for each case. The data clearly show a distinct shift of the trap coordinate from (S_{border} =0.973, W_{border} =1.45) to (S_{border} =0.960, W_{border} =1.50).
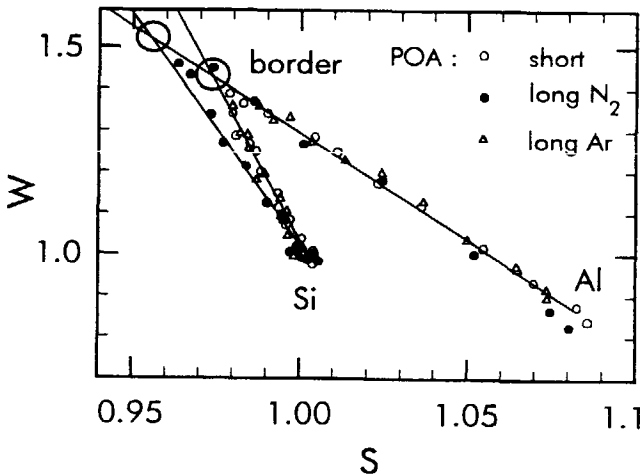

Figure 6. S-W trajectories of a specimen with a long (20 min.) POA in N_2, of one with a short (0 min.) POA in N_2 and of one with a long (20 min.) POA in Ar. The trajectories are recorded at 15V positive gate bias.

To further explore the capabilities of PA we also studied a sample subjected to POA in Ar. Figure 6 shows the trajectory of a specimen with a 20 min. Ar anneal. The data do not exhibit a shift as observed for the N_2 anneal; this shows that the Ar anneal does not affect the positron trapping centers in the oxide border region. Apparently, the annealing effect is element specific.

Next we investigated whether or not POA in N_2 also affects the generation of interface traps. For this purposeF we irradiated a set of capacitors at negative bias voltage. Figure 7 shows the number of radiation-induced interface traps above midgap versus the VUV doses. The data again reveal two clearly distinguished groups of data points: all specimens that had received a long POA in N_2 of four minutes or more show a generation rate about a factor ten larger than those samples that had received a short POA. Again, no transition regime was found.

For the sample with a 20 min. POA in Ar we also studied the generation of interface traps. The result is shown in figure 7. For this specimen the data reveal a low generation rate. The Ar anneal did not notably change the susceptibility of the system towards interface state generation, in contrast to an equally long POA in N_2.

In figure 8 we have made a comparison of the PA and the VUV data. One should note that we have used here S_{min} instead of S_{border} for representing the PA data, however, this does not affect the observations. The number of interface traps generated by VUV exposure of 5×10^{15} photons cm^{-2} is plotted as function of POA time in N_2 together with the S_{min}. As can be seen, interface state generation and S_{min} are correlated. Recalling the experiments on specimens with a 20 min. POA in Ar, large S_{min} and small generation rate, one should note that this result perfectly fits the correlation.

Although the data reveal a clear correlation between S_{min} and interface trap generation, it is important to verify whether the sites measured with PA could not also be associated with point defects in the as-fabricated Si/SiO_2 system. The results of these measurements are shown in figure 8. The effect of POA in N_2 can be summarized as follows: Bulk oxide electron trapping centers show no dependence at all. For this reason these data are not shown in figure 8. The number of the as-grown interface traps associated

with trivalent Si or P_b centers [22], established on capacitors without PMA, decreases continuously with POA time. The density of hole traps with large cross section (≈ 3 x 10^{-14} cm^2) increases gradually with the anneal time. This latter large cross section hole trap has been attributed to near-interfacial O vacancies, which after hole capture produce the well-known E'_γ signal [5]. Apparently, none of these defects shows a correlation with S_{min}.
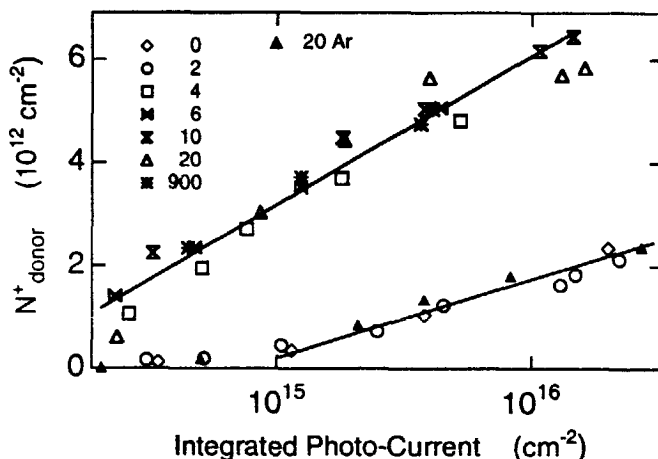
Figure 7. Density of VUV-induced interface traps above midgap versus the exposure. The oxides had received POA in N_2 or in Ar. The POA times are indicated in the figure in minutes.

Comparing the results of figure 8 with the data from the electrical measurements presented by Warren et al. for metal gate systems with and without POA in N_2 at 1000°C, it appears that our results are qualitatively the same: they too found a strong enhancement of the susceptibility for the generation of interface traps and positive charging of the bulk oxide when applying POA [3,4].

Also for the sample subjected to the 20 min POA in Ar we have measured the trap densities; the specimen contained ≈ 3.5 x 10^{12} cm^{-2} hole traps with $\sigma \approx 3$ x 10^{-14} cm^2 and

$\approx 2 \times 10^{11}$ cm^{-2} interface states. Within experimental error these data agree with the numbers obtained for a sample subjected to a 20 min POA in N$_2$. Apparently the evolution with POA time of the O vacancies and that of the as-grown interface states does not depend on the annealing ambient, in contrast to the susceptibility for the generation of interface traps and the positron trapping centers.
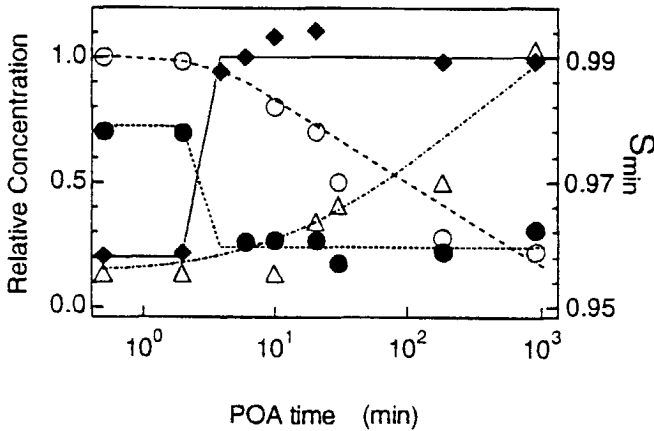
Figure 8. Evolution with POA time of S_{min} ($\bullet$), interface traps produced upon VUV irradiation ($\blacklozenge$), O vacancy-related hole traps ($\triangle$), interface traps in the as-grown oxide (P_b, o). The right-hand axis applies to S_{min} whereas the opposite scale denotes the relative concentrations of defects. The maximum values are: 5×10^{12} cm^{-2} for interface traps generated upon a VUV dose of $\approx 4 \times 10^{15}$ photons cm^{-2}; 9×10^{12} cm^{-2} for the O vacancies; and 5×10^{11} cm^{-2} for interface traps in as-grown capacitors.

V. DISCUSSION

As shown in section III, at the positive bias condition, the positrons implanted into the middle of the oxide layer provide information on the oxide border region close to the Si substrate. From the PA measurements it follows that POA in N_2 removes certain positron traps located in this region and that their removal only correlates with an enhancement of the susceptibility of the system for the generation of interface traps.

For metals and semiconductors it has been well established that the positrons are trapped by defects such as vacancies or clusters of vacancies [18,19]. However, for the less studied SiO_2 layers the nature of the positron traps is still an open question. Work of Uedono et al. [23] has convincingly shown that positron annihilation at the SiO_2 border region is not preceeded by the formation of positronium, that is, a bound electron-positron pair, which shows that the positron traps have a diameter of less than 1nm [20]. Our PA data agree with theirs and therefore we can safely assume that also in our
samples the positrons are captured at sites smaller than 1nm. Furthermore, the data presented in figure 8 exclude the possibility that the positrons are captured by the O vacancies, hydroxyl groups or Si dangling bonds; these centers constitute the most important point defects in the Si/SiO_2 system as identified thus far. In our opinion, it is unlikely that there are other structural and compositional defects in the Si/SiO_2 system. However, thermally grown vitreous SiO_2 has a chemically saturated but very open network structure. Conceivably, the positrons are easily accomodated by the regular open spaces between the network atoms, the interstices. These interstices are interconnected by narrower openings (bottlenecks), thereby forming channels. Thus, most likely the thermalized positrons would not be really trapped in the interstices because they would be able to move from the one interstice to the other through the bottlenecks. When applying a positive bias, the positrons are driven towards the Si substrate. At the interface they are confined in one dimension by the triangular potential well but they will be still able to laterally move around, in search of a trapping site. Because of the flexible nature of the

oxide network, the interstices will have a certain size-distribution. The Si substrate, to which the network is tied-up, could broaden this size distribution. Unable to escape from the triangular potential well, the positrons would become ultimately trapped by the larger near-interfacial network interstices.

In section III, it was argued that at the proper positive bias conditions, most of the positrons are collected in the oxide border region. This, however, does not exclude the possible presence of two or more positron traps, say A and B, in this region. The positron trapping probability for the A and B type centers (p_A and p_B) is given by the product of their respective concentrations (C_A and C_B) and capture cross sections (σ_A and σ_B)[24]:

$$p_A = \frac{\sigma_A C_A}{\sigma_A C_A + \sigma_B C_B}. \tag{2a}$$

and

$$p_B = \frac{\sigma_B C_B}{\sigma_A C_A + \sigma_B C_B}. \tag{2b}$$

The shape of the γ-peak is determined by the contributions of each of the positron trapping centers. The shift observed in figure 6, thus has to be explained in terms of a change of the concentration of the dominant sites. The decrease in S_{border} and the increase in W_{border} after POA in N_2, suggests that after annealing the mean size of the interstices at the interface has decreased. Subsequently, trapping is governed by those interstices with smaller volume.

The decrease of S_{border}, shown in figure 6, indicates that positron trapping sites with a larger volume are removed when applying POA of four minutes in N_2. This 4 minutes period roughly corresponds to the typical time constant for the refreshment of the ambient of the furnace. Because of this we believe that this 4 minute limit only shows that already a (very) short exposure of the grown oxide at a temperature of 1000 °C to N_2 substantially alters the structural properties of oxide network bordering the Si substrate.

POA in Ar did not remove the larger interstices in the oxide border region. This illustrates that the structural change is element specific. A straightforward explanation would be that nitrogen is chemically incorporated. However, in the case of such a

chemical incorporation, which is easily accomplished by an anneal in ammonia or N_2O, we would expect a suppression of the generation of interface traps, and not an enhancement as presently observed [25]. Another explanation would be that larger interstices near the Si/SiO_2 interface are filled with N_2 molecules which would reduce the trapping probability for the positrons. However, this does not immediately explain our main observation regarding the correlation between S_{min} and interface trap generation.

As stated before, Warren et al. observed for the metal gate MOS system a strong enhancement of the susceptibility for the generation of interface traps and positive charging of the bulk oxide when applying POA [3,4]. Both effects were attributed to the creation of O vacancies due to the out-diffusion of O atoms from the oxide network into the Si substrate. Our data also reveal an enhancement of both effects when applying POA, in agreement with the data of the aforementioned authors; however, the abrupt increase of the interface trap generation rate does not correlate with the more gradual development of the areal density of O vacancies. Moreover, in the case of the Ar annealed samples, the results indicate that O vacancies are still created but without affecting the generation rate of interface traps. Apparently we can not ascribe the enhanced interface trap generation rate to the formation of O vacancies, as proposed by Warren et al [3,4].

It has been well established that in the case of Al gated systems atomic hydrogen plays a major role in the generation of interface traps. One mechanism for their production is the depassivation of substrate trivalent Si centers [16]. However, recent studies have also revealed the excistence of another type of defect, the so-called donor interface trap which has been associated with the presence of hydrogen atoms in the proximity of the Si/SiO_2 interface [12,14-16]. It has been proposed that the H atoms are weakly bonded at bridging O atoms in a strained situation close to this interface. The whole configuration would constitute a localized electronic state with an energy level within the forbidden bandgap of Si. Earlier work of our group has clearly shown that VUV irradiation produces predominantly large numbers of such donor traps [12].

In the present case we used 105 nm thick oxides for our experiments. The penetration depth of 10 eV photons is approximately 10 nm [13], thus excluding the

possibility that the H-induced interface traps are produced by a direct action of photons, for example by direct cracking of H_2. Instead, a mobile intermediate is needed to bridge the distance between the point where the photon is absorbed and the Si/SiO_2 interface. The absorption of the photon takes place by the generation of an electron-hole pair, most likely bonded as an exciton. During the irradiation an electric field of -1MV cm^{-1} was applied. Thus, it appears that only a mobile neutral species could take care of the transport. Atomic H itself will play such a role; it is well established that such H is released from the SiO_2/Al interface by the interaction of the radiation-induced charge carriers and that such H can migrate through the oxide. However, excitons are also a possible candidate for this role. Upon arrival at the Si/SiO_2 interface such excitons could crack H_2.

Both the H atoms and exitons are rather unstable species; in both cases their numbers may be strongly reduced during transport through the oxide layer: excitons may recombine and atomic H may dimerize when meeting another H. Because of their metastable nature, the transport of both species and the probability of arriving at the Si/SiO_2 interface will be strongly affected by the presence of sites in the oxide layer that could trap such species.

If we ascribe the positron traps with large S_{min} to relatively large interstices in the oxide network in the vicinity of the Si substrate that can be filled with N_2 but not with Ar, this would offer also a straightforward explanation for the reduced build-up of interface traps for samples with a short POA in N_2 or an anneal in Ar: The open network spaces would also efficiently trap the metastable intermediate involved in the generation mechanism.

Warren et al. also presented data on the generation rate of border traps, which again is enhanced when applying POA in N_2 [3,4]. According to their opinion, this enhancement is also caused by the creation of O vacancies; however, for the metal gated capacitors in which release of atomic H plays a promi-nent role, this observation can be alternatively interpreted within our framework of H-induced donor traps. As argued elsewhere, some of the H atoms would be weakly bonded at bridging O atoms in a strained situation further

away from the interface; the whole configuration would be observed as a slow state or a border trap [26,27]. Thus the density of such H-related border traps would always track that of the donor-type interface traps. Their enhanced generation when applying POA in N_2 could then be explained by the same mechanism as proposed for the H-induced interface traps.

VI. CONCLUSION

The results of our study show that PA is a promising technique for the investigation of thermally induced changes of the Si/SiO_2 system, providing information that is not obtained by other experimental methods. Moreover, when implanting the positrons in the middle of the oxide layer and applying a positive bias, it is possible to drive the positrons to the oxide region close to the Si substrate, thus allowing one to focus on positron trapping sites in this region.

For the present case of POA in N_2 at a temperature of 1000°C, the PA data show that such an anneal removes sites with a large S_{min} located in the oxide close to the substrate. Their removal is correlated with an enhanced generation of interface traps upon VUV irradiation. Apparently, the positron trapping sites are actively involved in the suppression of the generation of interface traps by trapping and removing mobile intermediates such as atomic H or excitons. The association of the positron trapping sites with relatively large network interstices would fit with this explanation.

Although we have no direct evidence, we believe that the observed correlation between S_{min} and interface state generation, which requires the transport of a metastable intermediate, supports the association of the positron traps with regular but relatively large oxide network interstices.

1   "Ionizing radiation effects in MOS devices and circuits",Eds. T.P. Ma and P.V. Dressendorfer, J. Wiley & Sons, NY, (1989).

2   P.S. Winokur, E.B. Erret, D.M. Fleetwood, P.V. Dressendorfer and D.C. Turpin, "Optimizing and controlling the radiation hardness of a Si-gate CMOS process", IEEE Trans. Nucl. Sci., NS-32, 3954 (1985).

3   W.L. Warren, M.R. Shaneyfelt, D.M. Fleetwood, J.R. Schwank, P.S. Winokur and R.A.B. Devine, "Microscopic nature of border traps in MOS oxides", IEEE Trans. Nucl. Sci, NS-41, 1817 (1994).

4   W.L. Warren, D.M. Fleetwood, M.R. Shaneyfelt, J.R. Schwank, P.S. Winokur, R.A.B. Devine, and D. Mathiot, "Links between oxide, interface, and border traps in high-temperature annealed Si/SiO$_2$ systems", Appl. Phys. Lett., 64, 3452 (1994).

5   Y.Y. Kim and P.M. Lenahan, "Electron-spin-resonance study of radiation-induced paramagnetic defects in oxides grown on (100) Si substrates", J. Appl. Phys., 64, 35576 (1988).

6   P.M. Lenahan, "Electron spin resonance and instabilities in metal insulator semiconductor systems", Microelectron. Eng. 22, 129 (1993).

7   G. Hollinger, R. Saoudi, P. Ferret and M. Pitaval, "The microstructure of the Si/SiO$_2$ interface investigated by XPS and HRTEM", in "The Physics and Chemistry of SiO$_2$ and the Si/SiO$_2$ interface", eds. C.R. Helms and B.E. Deal (Plenum Press, New York, 1988) pp. 211-218.

8   F.J. Grunthaner and P.J. Grunthaner, "Chemical and electronic structure of the Si/SiO$_2$ interface", Mat. Sc. Rep., 1, 65 (1986).

9   F.J. Himpsel, F.R. McFeely, A. Taleb-Ibrahimi, J.A. Yarmoff and G. Hollinger, "Microscopic structure of the Si/SiO$_2$ interface", Phys. Rev. B , 38, 6084 (1988).

10   P. Asoka-Kumar, K.G. Lynn and D.O. Welch, "Characteri-zation of defects in Si and Si-SiO$_2$ using positrons", J. Appl. Phys., 76, 4935 (1995).

11   A. van Veen, H. Schut, M. Clement, J.M.M. de Nijs, A. Kruseman and M.R. IJpma, "VEPFIT applied to depth profiling problems", Appl. Surf. Sc., 85, 216 (1995).

12   K.G. Druijf, J.M.M. de Nijs, E. van der Drift, E.H.A. Granneman and P. Balk, "The nature of defects in the Si-SiO$_2$ System generated by VUV Irradiation", Appl. Phys. Lett., 65, 347 (1994).

13   Z.A. Weinberg, G.W. Rubloff and E. Bassous, "Transmission, photoconductivity and the experimental band gap of thermally grown SiO$_2$ Films", Phys. Rev. B , 19, 3107 (1979).

14   J.M.M. de Nijs, K.G. Druijf, V.V. Afanas'ev, E. van der Drift and P. Balk, "Hydrogen induced donor-type Si/SiO$_2$ interface states", Appl. Phys. Lett., 65, 2428 (1994).

15   K.G. Druijf, J.M.M. de Nijs, E. v.d Drift, V.V. Afanas'ev, E.H.A. Granneman and P. Balk, "On the microscopic nature of donor-typeSi/SiO$_2$ interface states." J. Non-Crystal. Solids, 187, 206 (1995).

16   E. Cartier, J.H. Stathis and D.A. Buchanan, " Passivation and depassivation of Si dangling bonds at the Si/SiO$_2$ interface by atomic hydrogen", Appl. Phys. Lett., 63, 1510 (1993).

17   A. van Veen, "Positron beam analysis techniques and gas desorption spectrometry for the characterization of defects in materials", J. Trace Microprobe Techn., 8, 1 (1990).

18   M. Eiduys, "Positron methods for the study of defects in bulk materials", J. de Physique, 5, C1-93 (1995).

19   M.J. Puska and R.M. Nieminen, "Theory of positrons in solids and on solid surfaces", Rev. Mod. Phys., 66, 814 (1994).

20   R.A. Hakvoort, A. van Veen, P.E. Mijnarends, H. Schut, "Helium and hydrogen decorated cavities in Si", Appl. Surf. Sc., 85, 271 (1995).

21   L. Liszkay, C. Corbel, L. Baroux, P. Hautojärvi M. Bayhan, A.W. Brinkman and S. Tararenko, "Positron trapping at divacancies in thin polycrystalline CdTe films deposited on glas", Appl. Phys. Lett., 64, 1380 (1994).

22   G.J. Gerardi, E.H. Pointdexter and P.J. Caplan, "Interface states and P$_b$ centers in oxidized (100) Si wafers", Appl. Phys. Lett., 49, 348 (1986).

23 A. Uedono, L. Wei, S. Tanigawa, R. Suzuki, H. Ohgaki, T. Mikado, T. Kawano and Y. Ohji, "Positronium formation in SiO_2 films grown on Si substrates studied by monoenergetic positron beams", J. Appl. Phys., 75, 3822 (1994).

24 For didactical reasons, we have deviated from the terminology used in PA. In this field, a 'positron trapping rate' (R) is used instead of a 'trapping probability' (p) whereas a 'positron capture cross section' (σ) is replaced by a 'specific positron trapping rate' (κ).

25 E. Cartier, D.A. Buchanan and G.J. Dunn, "Atomic Hydrogen-induced interface degradation of reoxidized-nitrided Si dioxide on Si," Appl. Phys. Lett., 64, 901 (1994).

26 K.G. Druijf, J.M.M. de Nijs, E. v.d Drift, E.H.A. Granneman and P. Balk, "Recovery of VUV irradiated MOS systems" J. Appl. Phys., 78, 306 (1995).

27 R.E. Stahlbush, E. Cartier and D.A. Buchanan, "Anomalous positive charge formation by atomic hydrogen exposure", Microelectronic Eng., 28, 15 (1995).

Chapter 8

Electron momentum distribution at defects in the Si/SiO$_2$ system

I INTRODUCTION

Positron annihilation Doppler broadening measurements have been applied successfully to study defects in materials [1,2,3]. In principle, the shape of the photo peak in the γ-spectrum reflects the momentum distribution of the electrons that surround the defects. Because of their low momentum, valence electrons cause only a small Doppler shift; they have a major contribution close to the center of the 511 keV photo peak. The contribution of the core electrons extends to higher momenta and will therefore be observed at the side wings of the photo peak. Defects do affect the momentum distribution of the valence electrons in their surrounding. Therefore, the low momentum part of the γ-spectrum contains information on the defect structure of the material. In contrast, the contribution of core electrons is not affected by the structure but by the type of atoms at the defect site [4,5]. Hence, the atomic composition of the defect site is reflected by the high momentum contribution.

Usually, only the relative contribution of the low momentum electrons, expressed in the so called shape-, or *S parameter*, is used to characterize defects. However, in the last years also information from the side wings of the photo peak, related to interactions with core electrons was successfully used to characterize defects in more

detail. To this end the *W parameter* was used as a simple way to quantify information from the high momentum part of the spectrum [6,7,8]. To obtain more specific information one has to focus on details in the spectrum in the high momentum range[4,5].

For the study of detailed features of the side wings, one has to suppress the background signal by using coincidence measurements instead of the commonly used single detector analysis[4]. In such coincidence measurements only events are included that are simultaneously detected and that fulfil within predefined limits the energy conservation law for 2 γ annihilation. In this manner the momentum range in which a significant signal can be observed can be extended from about 5 keV Doppler shift for the single detector measurements to about 12 keV for the 2 detector set-up[4].

To obtain more insight in the relation between the structure of defects, the atomic composition of their surrounding, and the positron beam data we have studied some well-documented types of defects in the Si/SiO_2 system. First, we will present and discuss, in section 3, data from SiO_2 layers grown by wet oxidation that were negatively charged by exposure to low energy electrons. The literature on charge trapping strongly indicates that upon electron injection of wet grown oxide layers Si-O-H (hydroxyl) groups are charged after which negatively charged Si-O⁻ groups are formed[9]. Because of their negative charge the Si-O⁻ groups will efficiently trap positrons. We will show that the specific contribution from core oxygen electrons in the γ-spectrum increases upon charging the Si-O⁻ groups.

In the following section (4) we will discuss results from defects at the Si/SiO_2 interface of Al gated MOS capacitors that were subjected to a so called post metalization anneal (PMA) in a hydrogen containing ambient. Such an anneal is known to passivate unsaturated dangling silicon bonds with hydrogen atoms[10,11,12]. We will show that the passivation changes the contribution of valence electrons to the Doppler broadening spectrum without affecting the ratio between the core oxygen and the core silicon contribution to the spectrum.

II EXPERIMENTAL

For the investigation of defects in the bulk SiO_2 we used samples with 1 μm thick oxide layers on 80-125 Ωcm n-Si(100) substrates prepared by wet oxidation at 1050°C. The oxides were exposed to a low energy electron beam to charge the Si-OH (hydroxyl) groups. The electrons are obtained from a W filament situated behind an ExB deflector (see chapter 2) which is used to inject the electrons into the beam system. To spread the electrons over the sample surface, the last coil of the positron beam system is switched off thus creating a locally divergent magnetic field near the sample.

For the studies of the defects at the Si/SiO$_2$ interface, we have used MOS capacitors with a 105 nm thick gate oxide prepared on 0.2-0.05 Ωcm p-Si(100) substrates by oxidation in dry O_2 in a double walled furnace at 1000°C. After oxidation, the samples were subjected to a 30 minute post oxidation anneal in N_2 at the same temperature. The system is equipped with a special unloading tube to allow the wafers to cool down in a pure N_2 ambient. With the aid of this tube passivation of as-grown interface states is avoided[11]. Thin (15 nm) Al gates were deposited by evaporation from a resistively heated W boat. Some of the capacitors were subjected to a 30 minute post-metalization anneal (PMA) in forming gas (10% H_2 and 90% N_2) at 400°C. Using combined high-frequency (1 MHz) and quasi-static capacitance-voltage measurements it was established that the capacitors that were not subjected to a PMA contained $\approx 3 \times 10^{11}$ cm^{-2} interface states whereas the samples with PMA had a density of interface states below 1×10^{10} cm^{-2}.

III NEGATIVELY CHARGED DEFECTS IN SiO$_2$

A. *S-W* data

To charge the electron traps we exposed the SiO_2 to electrons with a maximum energy of 6 eV. When arriving at the SiO_2 surface the electrons are injected

into the conduction band which is 1.0 eV below the vacuum level[13], (see also appendix A)[13]. The injected electrons traverse the oxide layer to the substrate, however some are trapped at defects. The density of trapped charge was derived from the change in the surface potential during the electron exposure. Appendix A describes how the surface potential was determined from the reflection of a 12 eV positron beam. We observed that the trapped charge has a homogeneous area distribution and we calculated its density assuming a depth distribution centered at the oxide layer. By continuing the electron exposure, a maximum charge density of 6×10^{12} cm^{-2} could be reached.
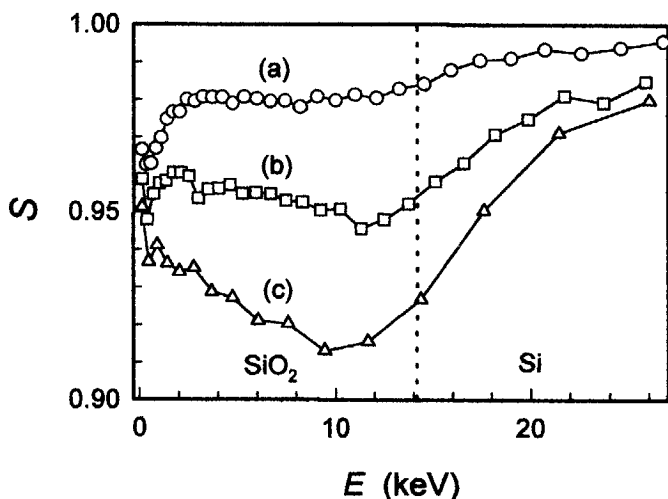

Figure 1. S parameter versus implantation energy E_{imp} for the as grown bare oxide sample (a) and after charging the SiO_2 to 1×10^{12} cm^{-2} (b) and 6×10^{12} cm-2 (c).

Between the different electron exposures we applied Doppler broadening measurements on the sample. Fig. 1 shows the resulting S parameter versus implantation energy curves recorded for different charge densities. The $S(E)$ data for the as-grown sample (a) exhibit a dip for shallow implantation at $E_{imp} \approx 0.3$ keV that can be ascribed to annihilation in the surface region. For implantation in the bulk of the oxide layer, the curve shows a constant value of S=0.98. For implantation into the

substrate the curve increases to the level of bulk Si. Because of the broad implantation profile and the thick oxide layer, the S value for bulk Si is not reached.

The curves b (Q_{ox} = 1.2x10^{12} cm^{-2}) and c (Q_{ox} = 6x10^{12} cm^{-2}) show that the electron exposure causes a decrease of the S value of the oxide layer. Furthermore, the decrease in S is stronger for implantation deeper into the oxide layer. Apparently the effect of the charging is larger in the region close to the Si/SiO$_2$ interface. This effect may be due to a locally stronger electric field which will enhance the field-induced transport of positrons to the negatively charged centers. Also for implantation in the substrate the S value decreases. This effect can be ascribed to an increased drift of the positrons from the substrate to the negatively charged SiO$_2$.
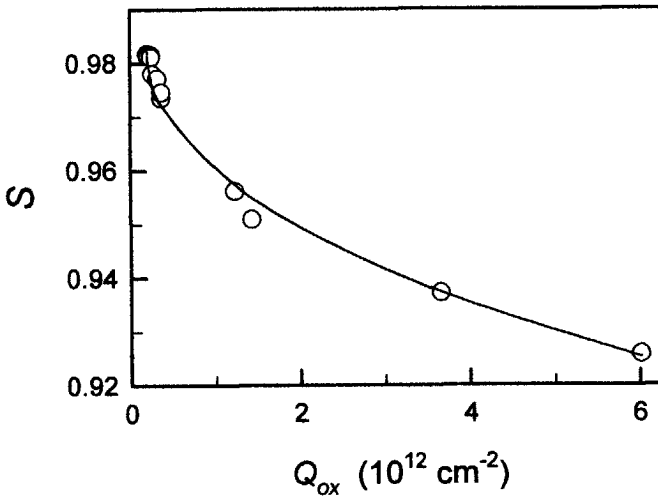

Figure 2. S- parameter for implantation in the center of the oxide layer (E_{imp} = 5 keV) as function of the charge density .

Fig. 2 shows the S value for implantation with 5 keV as function of the density of trapped charge. As can be seen from this curve, the decrease of S starts to saturate when reaching a charge density of 5x10^{12} cm^{-2}. However, a complete saturation was not reached yet which indicates that at this charge density still not all positrons are

trapped. Hence one still observes annihilation events from other defects than the negatively charged centers.

The results of the Doppler broadening measurements are shown in Fig. 3 as a trajectory in the S-W plane using the charge density as a running parameter. As can be seen from this picture, the data follow within experimental error a straight line in the S-W plane. The starting point of this straight trajectory is the (S, W) point of the as-grown SiO_2. For increasing charge density the straight trajectory approaches the (S, W) co-ordinates of the charged electron traps, which has thus to be located on the straight line through the data. The shape of the S-W trajectory provides information about the number of different electron traps. When more types of defects with different cross section for electron trapping are involved the data would follow a curved S-W trajectory determined by the (S, W) co-ordinates of the subsequently charged trapping sites. Thus, the straight S-W trajectory in Fig. 3 indicates that only one type of electron trap is charged during the electron exposure.
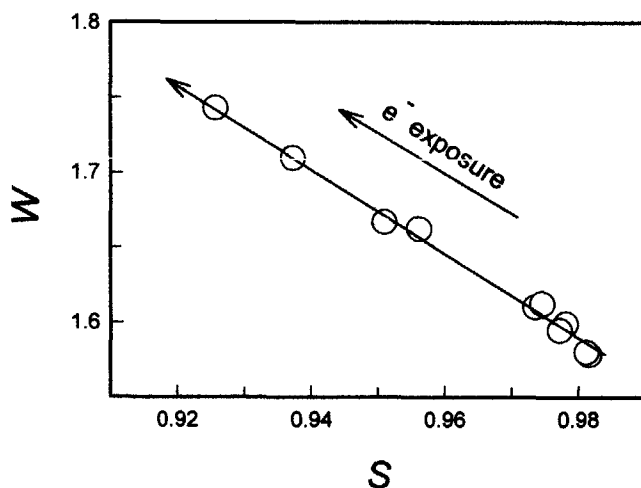

Figure 3. S-W trajectory for positron annihilation at implantation energy $E_{imp} = 5\ keV$ recorded during the electron exposure. The arrow indicates the direction of increasing charge density caused by the exposure.
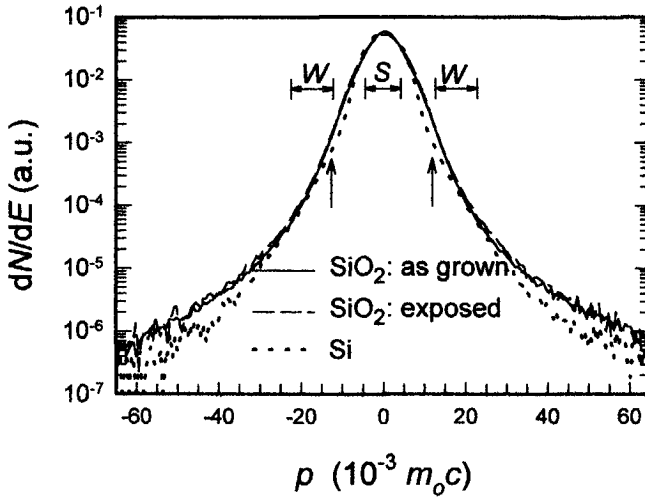
Figure 4. The γ-spectra at Eγ = 511 keV related to annihilation in the as grown SiO_2 (E_{imp} = 5 keV) (a), after charging to $6x10^{12}$ cm^{-2} (b) and from the bulk of a Si reference sample (c). The horizontal shows the electron momentum derived from the Doppler shift expressed as a fraction of m_0c, with m_0 the rest mass of the electron and c the velocity of light. Also the integration intervals used for the calculation of the S- and W parameter are indicated in the figure. The vertical arrows marks sites with a relative low signal from bulk Si at p = 10^{-3} m_0c.

B. Coincidence measurements

Fig. 4 shows the photo peak at 511 keV as determined with the two-detector set-up for crystalline Si and for implantation into the middle of the 1 μm wet grown SiO_2 layer (5 keV). The measurements for the SiO_2 were performed before and after charging the electron traps. As shown by this figure, there are clear differences between the spectra for bulk silicon and for SiO_2. However, there are only minor differences between the spectra of the as-grown and the electron exposed SiO_2. The changes induced by the

electron exposure in the SiO_2 are thus much smaller than the differences in electron structure between Si and SiO_2.

To better reveal the details of the shape of the photo peak, the data from the coincidence measurement are divided by the spectrum from a well-defined reference material[4]. Most times, bulk silicon is used as reference. Fig. 5 shows the so-called ratio curves obtained by dividing the data from the as-grown and the electron exposed SiO_2 by the spectrum for Si. We express the Doppler shift in this chapter in terms of momentum with conversion factor of 10^{-3} m_Oc to 390 eV where m_O denotes the rest mass of the electron and c the velocity of light.
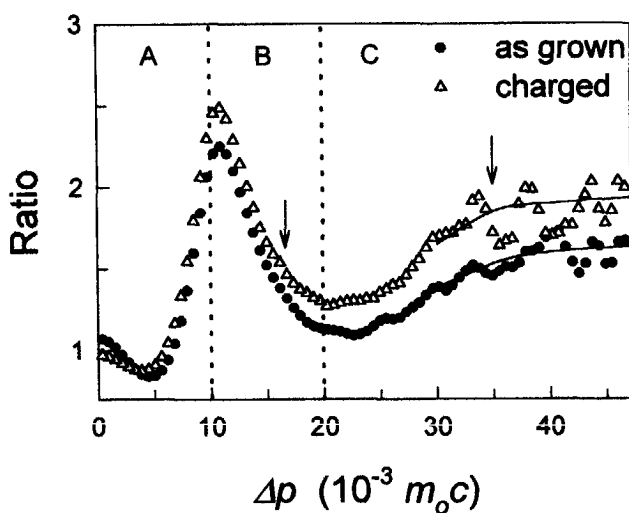
Figure 5. Ratio curves obtained after dividing the spectrum of as grown and charged SiO_2 by the bulk Si spectrum. Previous to the division the SiO_2 and the Si data were smoothed by a three point moving-average filter. The solid curves through the data are drawn to guide the eye. The vertical dotted lines indicate the intervals dominated by valence electrons (A), by a mixture of valence and core electrons (B) and by core electrons only. The vertical arrows mark specific parts of the signal related to core electrons of oxygen.

To reduce the noise, related to the statistic of the detection events, data were smoothed using a three-point moving-average filter. This filtering removes the high frequency components of the noise but, as can be seen in Fig. 5, above $30 \times 10^{-3}\ m_0 c$ there still are fluctuations with a periodicity of about 8 data points. The width of the fluctuations ($2 \times 10^{-3}\ m_0 c$) is smaller than the detector resolution ($\sim 4 \times 10^{-3}\ m_0 c$) and consequently they can be attributed to noise. To guide the eye, we plotted curves through the data that neglects the noise fluctuations.

To interpret the information in the ratio curves of Fig. 5 it is helpful to make a rough classification of the different momentum ranges that are dominated by valence or by core electrons. In Fig. 5 the momentum ranges are indicated with vertical dotted lines. On the basis of model calculations made for silicon, germanium and aluminium we can describe the momentum range 'A' below $10 \times 10^{-3}\ m_0 c$ to interactions with valence electrons[4,5]. The area C, above $20 \times 10^{-3}\ m_0 c$, is related to core electrons. The intermediate range B exhibits a mixture of contributions from core and valence electrons.

C Annihilation spectrum from as grown SiO_2

We will first discuss the data from the as-grown SiO_2. We will do so separately for different regions on the momentum scale.

$p\ <\ 8 \times 10^{-3}\ m_0 c$:

For very low momenta, $p < 2 \times 10^{-3}\ m_0 c$, the ratio curve for the as-grown SiO_2 (Fig. 5) is somewhat higher than 1 indicating that there is more interaction with very low momentum valence electrons than in bulk Si. However, for the momentum range of 2 to 6 $\times 10^{-3}\ m_0 c$ the ratio curve is lower than 1 which shows that for the valence electrons with intermediate momentum the signal is lower.

The relatively high and sharp contribution at zero momentum points to annihilation in so called open volume sites that consists of cavities with a diameter of several atom distances. Positrons in large open volume sites have a very weak

interaction with core electrons in the surrounding material. Annihilation mainly occurs with valence electrons at the edge of the open volume site that have low momentum.

In literature, results are presented from lifetime- and 2D-ACAR- measurements on thermally grown SiO_2 layers with an S value comparable to that of our samples[14,15]. These results indicate that the positron annihilates in open volume sites, in agreement with our data. These results show further that typically 20 % of the positrons annihilate as positronium, a hydrogen like bound state between a positron and an electron with approximately zero momentum. Positronium is stable only in cavities with a diameter larger than 1 nm[15,16]. Hence about 20% of the probed defects are larger than 0.9 nm.

$8x10^{-3} m_0c < p < 15x10^{-3} m_0c$:

This range is dominated by a peak with a maximum at $12x10^{-3} m_0c$. Unfortunately, this peak does not contain any information on the SiO_2 but it is an unwanted result of the presentation of the data in ratio curves obtained by division by the Si data. As can be seen from Fig. 4, the peak at $12x10^{-3} m_0c$ is caused by a relatively low value of the bulk Si spectrum at this momentum. When positrons are trapped at defects in the Si the low momentum contribution is not observed[17]. Therefore this specific feature of the Si spectrum can be attributed to annihilation of valence electrons with delocalized positrons.

$15x10^{-3} m_0c < p < 20x10^{-3} m_0c$:

Above $15x10^{-3} m_0c$ the signal decreases slowly, reaching a minimum at $20x10^{-3} m_0c$. Kruseman et al, observe a comparable 'shoulder' in ratio curves for oxygen-related defects in Si. In contrast, in the case of vacancy clusters in silicon the ratio curve decreases faster. Because of this, these authors attributed the slowly decreasing signal to oxygen core electrons.

$p > 20x10^{-3} m_0c$:

In this range the signal increases again and approaches a constant value of about 1.5. The shape of the curve contains information on the specific contributions of core Si

or of core O electrons. The contribution from core Si electrons in ratio to bulk Si spectrum curves, may be low or high but is by definition constant over the whole high momentum range ($p > 20 \times 10^{-3}\ m_0c$). The increase in the signal in Fig. 5 above 20×10^{-3} m_0c has thus to be ascribed to core O electrons. Earlier published data for oxygen related defects in silicon exhibit a comparable core O contribution in the high momentum range[17].

D annihilation spectrum from charged SiO₂

The ratio curve for the electron exposed SiO_2 (Fig. 5) exhibits a slightly different shape. To visualise the difference between both curves the ratio of the spectrum of the charged to that of the as-grown SiO_2 is plotted in Fig. 6. Again we will discuss the charging induced changes separately.

$p < 5 \times 10^{-3}\ m_0c$:

As can be seen from Fig. 6, the charging causes a 10% signal reduction for low momenta. This difference is also reflected by the S parameter that is lower for the exposed sample, see Fig. 2. The reduction indicates that in the electron exposed SiO_2 fewer positrons are trapped in large open volume sites.

Alternatively, one could propose that the negatively charged centers are identical with the open volume sites, and that charging them changes the positron-electron interaction. Although our experiments can not exclude this possibility, it appears unlikely when considering the literature on lifetime studies: Uedono et al showed that for SiO_2 layers grown by wet oxidation and chemical vapour deposition (CVD) trapping of positrons at large open volumes is inversely proportional with the concentration of electron traps as Si-O-H groups and H_2O molecules[14].

$5 \times 10^{-3}\ m_0c$: $< p < 20 \times 10^{-3}\ m_0c$:

As can be seen from Fig. 5 the exposure causes an increase of the peak at $10 \times 10^{-3}\ m_0c$. However, this peak is not visible in the relative changes shown in Fig. 6. Instead, the curve in Fig. 6 shows a peak at $8 \times 10^{-3}\ m_0c$ and a minimum at
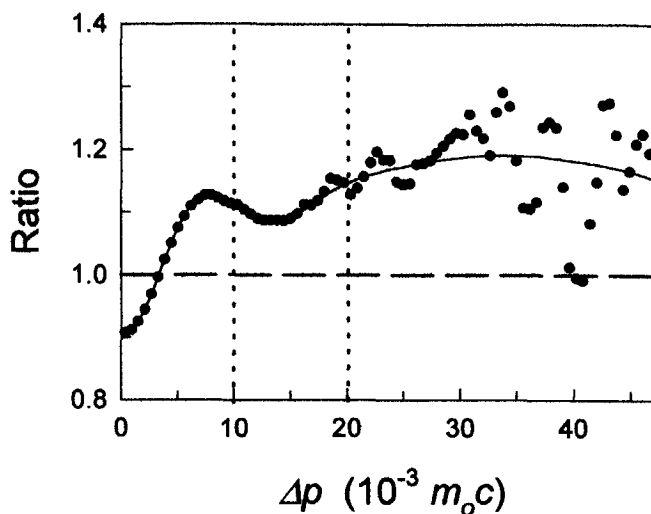
Figure 6. Ratio curve obtained after division of the spectrum of charged by that of as grown SiO$_2$. The solid curve through the data is drawn to guide the eye.

14×10^{-3} m_oc. The differences between Figs. 5 and 6 show that the charge induced changes in the intermediate momentum range can not be simply treated as an increase of an oxygen-related signal. Apparently, the positrons in the charged oxide are trapped at another defect with a stronger interaction with valence electrons with momentum of 8×10^{-3} m_oc

$p > 20 \times 10^{-3}$ m_oc:

Fig. 5 shows that the charging causes an increase in the signal in the high momentum range. Above, this high momentum contribution was described to interaction with core oxygen electrons, and this observation does thus point to a higher core oxygen contribution.

The ratio curves in Fig. 5 thus show that the contribution from core oxygen increases in absolute sense due to the electron exposure. However, they do not show whether the contribution from core oxygen increases also in relation to the core silicon contribution; i.e. whether only the core oxygen signal is affected or that the core

oxygen and core silicon contribution increases proportionally. To obtain information on the ratio between the different core contributions it is helpful to use the ratio to the as-grown SiO_2 spectrum curve in Fig. 6. In the case of a proportional increase of the core oxygen and core silicon contributions, the high momentum part of the spectrum will change in intensity, but its shape will not be affected. In the ratio of the charged to the as-grown SiO_2 this would result in a constant value in the high momentum part. However, the ratio curve in Fig. 6 exhibits a structure at high momentum, comparable with that in Fig. 5 related to core oxygen electrons. This observation shows that the changes at high momentum are mainly due to an increased core oxygen contribution.

The high momentum data does thus show that positrons are trapped at defects where they have a strong interaction with core oxygen electrons. It should be in line with our results to ascribe the probed defects to charged Si-O⁻ groups that are supposed to be created after electron trapping at Si-O-H groups[9]. Positrons are bound at negatively charged Si-O⁻ groups and do strongly overlap with the wavefunction of the core oxygen electrons.

Summarizing, we ascribe the trapping sites probed in the as-grown SiO_2 to relatively large open volumes (~1 nm) in a saturated SiO_2 network. Positrons trapped at the open volumes have a weak interaction with core electrons resulting in a sharp contribution in the low momentum range ($p < 5 \times 10^{-3} \, m_O c$). However, when applying an electron exposure, trapping at negatively charged Si-O⁻ groups will be favoured because of the coulomb attraction. We observed for the negatively charged Si-O⁻ centers a relatively high core oxygen contribution in the high momentum range ($p > 20 \times 10^{-3} \, m_O c$).

IV INTERFACE STATES IN THE MOS SYSTEM

A. *S-W* data

The defect structure in the MOS system is known to depend on the different annealing steps that are applied during the fabrication. When applying a so called post metalization anneal (PMA) after deposition of the Al gate, unsaturated hydrogen bonds are passivated with hydrogen[10,11]. To investigate the relation between this passivation and the positron beam data we applied Doppler broadening measurements at MOS capacitors before and after applying such PMA.
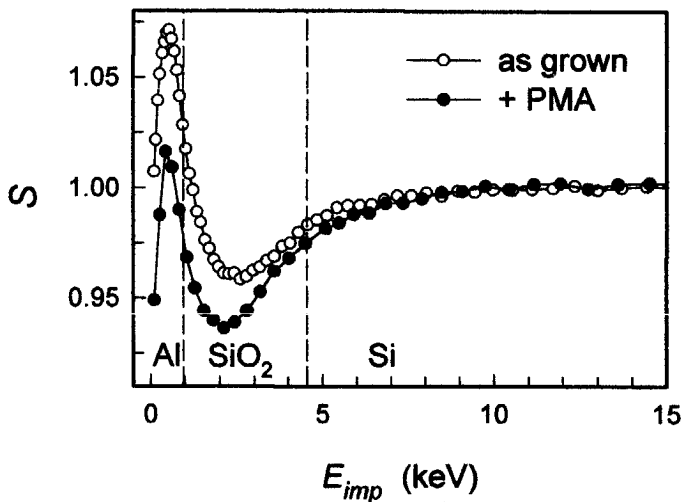

Figure 7. S versus implantation energy E_{imp} for an MOS capacitor before (a) and after (b) applying a post metalization anneal (PMA) at 400 °C in forming gas. The vertical lines indicates the position of the interfaces between the Al gate, the SiO_2 layer and the Si substrate.

Fig. 7 shows the $S(E)$ curves recorded at positive gate bias condition before and after the PMA. The $S(E)$ curve for the as-grown capacitor exhibits a high S value for implantation in the Al gate and a low one for implantation in the oxide layer. These data are comparable to those discussed in chapter 3[6,18]. In this chapter we argued that the positrons implanted in the oxide layer are pushed by the applied electric field to the substrate and that they are all trapped at the Si/SiO_2 interface. The curve for positive bias is thus determined by three defect layers only. The Al gate is probed for shallow implantation below 1 keV, for implantation into the oxide (1 keV $< E_{imp} <$ 4.5 keV) the S parameter yield information about defects at the Si/SiO_2 interface and the silicon substrate is seen for deep implantation (E $>$ 5 keV).

After a PMA the S parameter decreases for implantation into the Al gate and for implantation into the oxide layer. The decrease of S for the thin Al gate can be ascribed to the annealing of defects in this metal layer. The Al is deposited at room temperature and the anneal at 400°C affects the defect structure and the grain boundaries. Furthermore, a thin Al_2O_3 layer is formed during this anneal at the SiO_2/Al interface[11]. The decrease in S for implantation into the oxide layer has to be ascribed to changes in the defect structure at the Si/SiO_2 interface. Apparently, the PMA causes a decrease of the specific S value of the defects at the interface.

The specific S value of the defects at the interface can be derived when not only the S parameter is used but also the additional information provided by the W parameter. Fig. 8a shows a so called S-W plot which presents the data for the as-grown capacitor as a trajectory in the S-W plane using the implantation energy as a running parameter. As can be seen from this figure the data follow an S-W trajectory that can be approximated by two straight lines. The specific (S,W) point of the Si substrate is seen as a clustering of data points for high implantation energy while the (S,W) position of the Al gate is situated somewhere on the straight line through the data for shallow implantation. In chapter 3 we argued that the (S,W) co-ordinates of the Si/SiO_2 interface are determined by the intersection point of the straight lines through the low and the high energy parts of
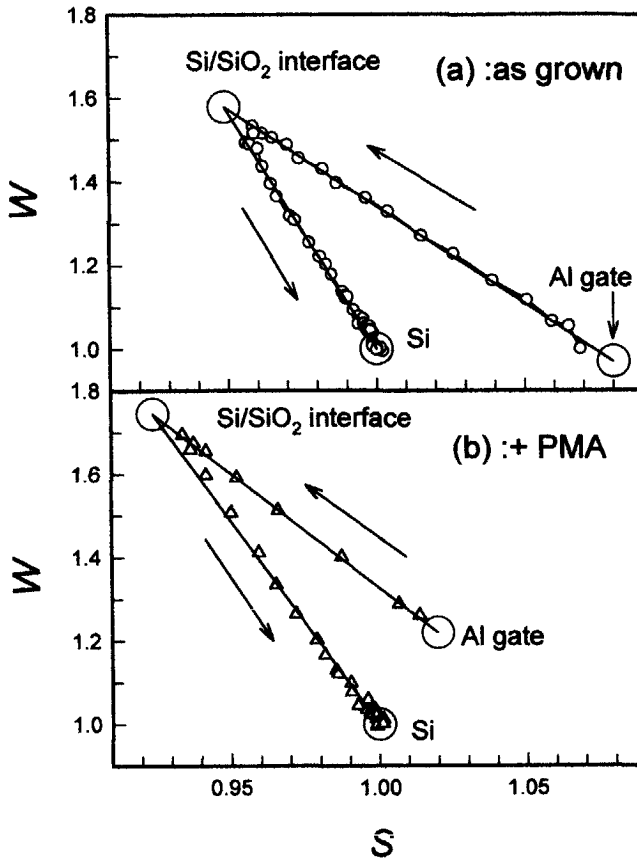
Figure 8. S-W trajectories of an MOS system subjected to + 15 V bias before (a) and after applying a PMA treatment. The large circles correspond with the points of the Al gate, the Si/SiO2 interface and the Si substrate.

the *S-W* trajectory. This intersection point is approached for implantation in the middle of the oxide layer and is related to the minimum in the *S(E)* curves in Fig. 7.

Fig. 8b shows the *S-W* trajectory recorded after the PMA. Because the (*S,W*) co-ordinates of the Si/SiO2 interface and the Al gate are changed, the data follow a different *S-W* trajectory. However, basically the *S-W* data exhibits the same type of trajectory that

can be approximated by two straight lines intersecting at the specific (S, W) point of the Si/SiO$_2$ interface. From Fig. 8 it can be seen that the PMA causes for the Si/SiO$_2$ interface a shift from $(S, W) = (0.950, 1.57)$ to $(S, W) = (0.924, 1.74)$.
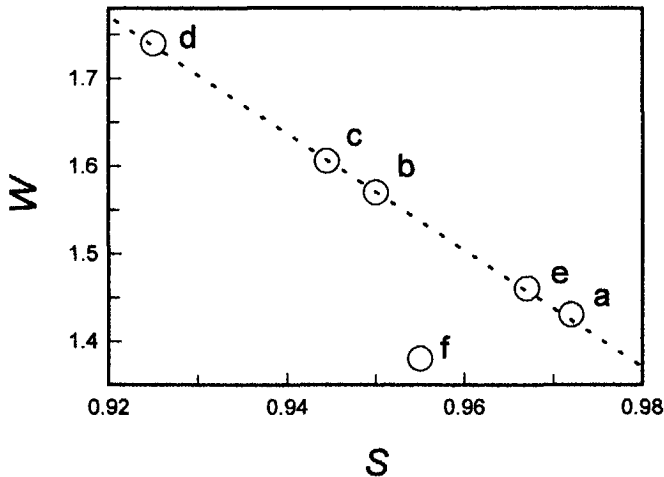

Figure 9. Map of specific (S,W) positions of the SiO$_2$/Si interface of MOS capacitors subjected to different annealing treatments during fabrication. The figure shows results obtained from capacitors subjected to: no extra anneal (a)[8], applying a post oxidation anneal (POA) in N$_2$[8] (b), an anneal at 400°C in H$_2$ containing ambient (10%H2/90%N2) before metalization (c), both a POA and a PMA treatment (d), preparation of 350 nm SiO$_2$ instead of 100 nm followed by a POA (e)[18], and deposition of a polysilicon gate instead of an Al one (f) [19].

When applying a positive gate bias one can thus easily detect changes in the (S, W) co-ordinates of the Si/SiO$_2$ interface. We have performed similar measurements on capacitors subjected to different treatments during their fabrication. The (S, W) co-ordinates of the Si/SiO$_2$ interface recorded after applying different annealing treatments are plotted in Fig. 9. As shown by this figure, most samples yield for the interface an

(S, W) position situated on one single straight line. Although we have no explanation for this, it indicates that Doppler broadening can offer interesting information on the effect of annealing treatments on the defect structure at the interface.
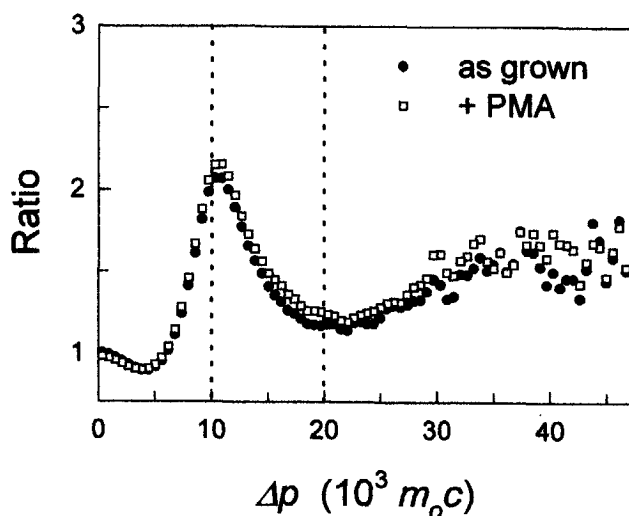
Figure 10. Ratio curves obtained after dividing the spectrum of the Si/SiO₂ interface before and after a PMA treatment by the bulk Si spectrum.

B Coincidence measurements

To study in more detail the defects at the Si/SiO_2 interface we applied coincidence measurements while implanting positrons in the middle of the oxide layer ($E_{imp} = 2.5$ keV) and applying positive gate bias. Under these conditions more than 95% of the positrons are implanted into the oxide layer after which they are collected at the Si/SiO_2 interface where they probe the defect structure[18]. Fig. 10 shows the resulting ratio to the bulk Si spectrum curves of the Si/SiO_2 interface for the as-grown and for the hydrogen passivated capacitor. These ratio curves are qualitatively comparable with those obtained

for bulk SiO_2 discussed above. Furthermore, there are only minor differences between the ratio curves from the passivated and the as-grown MOS capacitors.

First we will discuss the general shape of the ratio curve for the as-grown capacitor. We will do so separately for different momentum intervals.

$p < 5x10^{-3} \ m_0c :$

The contribution at zero momentum equals one which is comparable with that in Fig. 5 for the electron exposed SiO_2, but lower than for as-grown SiO_2. Above we described the high signal for the as-grown SiO_2 at zero momentum to large open volumes (~1 nm). Apparently, such open volumes are not present at the Si/SiO_2 interface.

$5x10^{-3} \ m_0c: < p < 20x10^{-3} \ m_0c:$

The peak at $12x10^{-3} \ m_0c$ discussed in section 3 is also present in Fig. 10, but it has a lower intensity. This peak was ascribed to the low contribution of valence electrons at $12x10^{-3} \ m_0c$ in the silicon reference spectrum. The lower magnitude of the peak for the Si/SiO_2 interface can be explained straightforwardly by a larger bulk silicon component due to interaction with the substrate.

$p > 20x10^{-3} \ m_0c:$

The contribution in momentum range above $20x10^{-3} \ m_0c$, related to interaction with core electrons, is comparable with as-grown bulk SiO_2. This indicates that the core oxygen contribution does not really differ for the bulk SiO_2 and the interface region.

To compare the data from the as-grown and the hydrogen passivated interface we divided the spectrum of the as-grown sample by that from the hydrogen passivated one. The corresponding ratio curve is shown in Fig. 11 for both sides of the photo peak. Note that the magnitude of the signal in this curve is rather low in comparison with that in Fig. 5,6 and 10. Again we will discuss the changes separately.
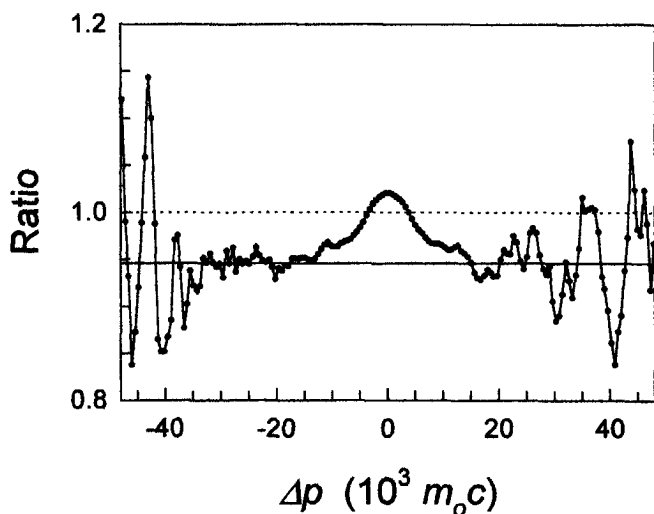
Figure 11. Ratio curve obtained after division of the spectrum of the Si/SiO$_2$ interface obtained for the as grown MOS system divided by the spectrum recorded after the PMA treatment.

$p < 15 \times 10^{-3} \, m_0 c$:

The ratio curve in Fig. 11 exhibits a peak at zero momentum. This shows that the as-grown capacitor has a higher contribution of valence electrons. The PMA induced change in the valence electron contribution can very well be attributed to the hydrogen passivation of dangling silicon bonds. Non passivated silicon bonds are negatively charged due to the electric field and thus constitute traps for positrons. A positron will, like a hydrogen atom (or proton), strongly interact with the valence electrons of an unsaturated silicon bond. After hydrogen passivation these interactions disappear.

$p > 15 \times 10^{-3} \, m_0 c$:

Fig. 11 exhibits a lower level in this range. When neglecting the noise, the signal can be considered as a constant value of about 0.94. The PMA thus causes an

increased contribution from core electrons. The constant level in the high momentum range of Fig. 11 shows that the ratio between the core oxygen and the core silicon contributions was not affected by the PMA.

Summarizing, our data indicates that, in contrast to bulk SiO_2, positrons do not detect large open volumes at the Si/SiO_2 interface. A PMA treatment reduces the contribution of valence electrons and causes a proportional increase of the core oxygen and core silicon signal. For as-grown capacitors the relatively large contribution of valence electrons is ascribed to negatively charged dangling bonds centers at the Si/SiO_2 interface. When the dangling bonds are passivated with H, the positrons probe H passivated silicon bond centers or other sites with a larger interaction with core electrons. The dangling bond centers and the sites probed after applying the PMA exhibit an equal ratio between the core oxygen and the core silicon signal.

V CONCLUSIONS

The results presented in this chapter demonstrate that a detailed analysis of positron annihilation spectra yield information on the configuration of defects in the Si/SiO_2 system that can not be extracted from the S- and W-parameter. For charged electron traps in SiO_2 we observed an increased interaction with oxygen core electrons. This observation shows that these charge traps can be ascribed to Si-O⁻ centers. Our data reveals for the Si/SiO_2 interface a decreased signal from valence electrons at dangling silicon bond centers due to a passivation anneal while the ratio between the contributions of core electrons of oxygen and silicon was not affected.

[1] P.J. Schultz and K.G. Lynn, Rev. Mod. Phys. **60**, 701 (1988).
[2] M.J. Puska and R.M. Nieminen, Rev. Mod. Phys. **66**, 814 (1994).
[3] A. van Veen , A.C. Kruseman, H. Schut, M. Clement, P.E. Mijnarends, B.J. Kooi and J.Th.M. de Hosson, Mat. Sc. Forum **255-257**, 76 (1997).
[4] P. Asoka-Kumar, M. Alatalo, V.J. Ghosh, A.C. Kruseman, B. Nielsen and K.G. Lynn, Phys. Rev. Let. **77**, 2097 (1996).

5   P.M. Alatalo, B. Barbiellini, M. Hakala, H. Kauppinen, T. Korhone, M.J. Puska,
    K. Saarinen, P. Hautojärvi and R.M. Nieminen, Phys. Rev. B **54**, 2397 (1996).

6   M. Clement, J.M.M. de Nijs, P. Balk, H. Schut and A. van Veen, J. Appl. Phys.
    79, 9029 (1996).

7   L. Liszkay, C. Corbel, L. Baroux, P. Hautojärvi, M. Bayhan, A.W. Brinkman and
    S. Tararenko, Appl. Phys. Lett. **64**, 1380 (1994).

8   M. Clement, J.M.M. de Nijs, A. van Veen, H. Schut and P. Balk, IEEE Trans. on
    Nucl. Sc. **NS-42**, 1717 (1995).

9   E.H. Nicollian and J.R. Brews, MOS (Metal Oxide Semiconductor) Physics and
    technology (Wiley-Interscience, New York, 1982), p. 538 and p. 657.

10 P. Balk, Extended abstract of papers, presented at the Electrochemical Society
    Meeting, Buffalo, NY 10-14 October 1965 (The Electrochemical Society, New York,
    N.4., 1965), paper 111.

11 E.H. Nicollian and J.R. Brews, MOS (Metal Oxide Semiconductor) Physics and
    technology (Wiley-Interscience, New York, 1982), p. 782.

12 E.H. Pointdexter, P.J. Caplan, B.E. Deal and R.R. Razouk, J. Appl Phys. **52**, 879
    (1981).

13 E.R. Williams, Phys. Rev. A **140**, 569 (1965).

14 A. Uedono, L. Wei, S. Tanigawa, R. Suzuki, H. Ohgaki, T. Mikado and K. Fujino,
    J. Appl. Phys. **75**, 216 (1994).

15 J.P. Peng, K.G. Lynn, P. Asoka-Kumar, D.P. Becker, and D.R. Harshman, Phys.
    Rev. Lett. **76**, 2157 (1996).

16 R.A. Hakvoort, *thesis*, Delft University of Technology, Delft (1993).

17 A.C. Kruseman, H. Schut, M. Fujinami, and A. van Veen, Mat. Sc. Forum **255-
    257**, 793 (1997).

18 M. Clement, J.M.M. de Nijs, P. Balk, H. Schut and A. van Veen, J. Appl. Phys.
    81, 1943 (1997).

19 M. Clement, J. M. M. de Nijs, H. Schut, A. van Veen and P. Balk, Mat. Sc.
    Forum **255-257**, 718 (1997).

Appendix A

Charging of bare SiO₂ layers by electron exposures

To charge electron traps in bare oxide layers we exposed them *in situ* to electrons obtained from a filament behind an ExB deflection system (see chapter 2). For this purpose, the filament leads are set to -5 V and 0 V respectively. Because of this low potential on the filament, the emitted electrons have an energy of 6 eV at most, i.e. the sum of thermal energy and the kinetic energy obtained by the repulsive potential. When arriving at the SiO₂ surface the electrons are injected into the conduction band which is 1.0 eV below the vacuum level, see Fig. 1 [1]. The injected electrons traverse the oxide layer to the substrate, however some are trapped at electron traps. Charging the oxide raises the surface potential experienced by electrons, thus preventing further their injection, i.e., the charging is a self limiting process. To continue charging we applied a positive bias on the substrate (V_{sub}) which lowers the surface potential again. The potential diagram of Fig. 1 illustrates this point.

When charging the SiO₂ we noticed that one should not use a too large positive bias on the substrate. For example, for an electron energy of 20 eV at the surface we observed a rapid decrease of the negative oxide charge. For such energies, the electron energy is dissipated by generation of electron-hole pairs in the oxide layer. The holes do efficiently drift to the negatively charged centers thus causing a rapid neutralization. To avoid such neutralization, one has to limit the positive substrate potential such that the energy of the arriving electrons remains below 9 eV, the excitation energy for electron-hole pairs. Because of this, the SiO₂ was charged in
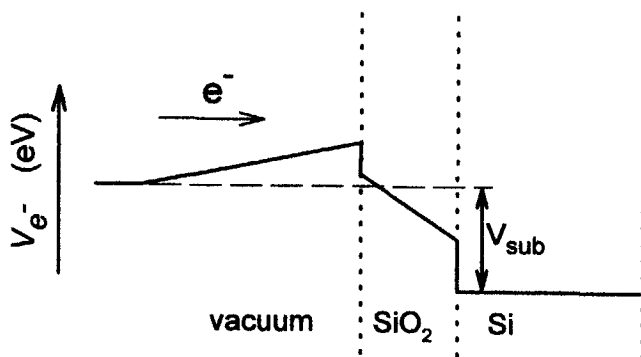
Figure 1. Potential diagram for electrons entering the bare SiO$_2$ layer from the vacuum.

subsequent steps in which V_{sub} was increased with 1 V. During each step the sample was exposed to about 5×10^{11} cm^{-2} electrons.

Unfortunately, the positive potential on the substrate causes, in combination with the broad diverging electron beam, an additional electron exposure at the backside of the sample. Because of this additional backside exposure, the total amount of charge injected into the oxide could not be determined.

We analyzed the charging of wet grown 1 μm thick SiO$_2$ layers, described in chapter 8, by the reflection of a 12 eV positron beam as a function of the external applied substrate potential V_{sub}. The reflection can be deduced from the rate of annihilation events in the sample. Fig. 2 curve "a" shows the detected annihilation rate versus V_{sub} for the case of the as grown SiO$_2$. For $V_{sub} < 11$ V the positrons are implanted in the sample. When raising the bias above a certain value, the positrons are reflected at the surface and their annihilation does no more contribute to the detector signal. This effect is clearly seen as a decrease in the count rate.
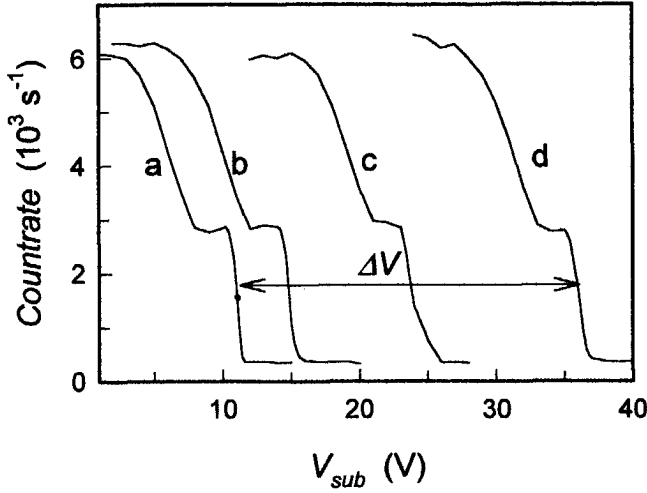
Figure 2. Countrate in the Ge detector versus substrate bias V_{sub} for the as grown SiO_2 (a) and after charging by electron exposure (b, c and d). The shift ΔV of curve 'd' corresponds with a charge density of $1x10^{12}$ cm^{-2} assuming a depth distribution centered

Note that the curves in Fig. 2 decrease in two separated steps. At $V_{sub} = 3$ V curve "a" starts to decrease, reaching constant level of 0.4 times the initial intensity. The signal is constant between 8 and 10 V after which it decreases suddenly to the background level. The stepwise decrease can be explained by the scattering of positrons in SiO_2. At $V_{sub} > 3$ V the positrons enter the sample with an energy below 9 eV. This energy is too low for the creation of electron hole pairs in SiO_2, hence the positrons can only cool down by interaction with phonons. Phonon scattering is a low efficient energy loss mechanism and therefore a large fraction of the positrons escapes from the SiO_2 surface before thermalization. The first decrease at $V_{sub} \approx 5$ V can be explained by such "backscatering" of non-thermalized positrons. In the range 8V < V_{sub} < 10 V all positrons cool down via the phonon interaction process resulting in about 40% backscatering to the vacuum. The constant signal in this range indicates that the backscatering process is scarcely affected by the small differences in implantation depth caused by the change in substrate potential. At $V_{sub} > 11$ V the positrons are reflected before entering the sample, thus causing the second decrease.

Charging the electron traps changes the surface potential of the SiO_2 according to

$$\Delta V_{surf} = \frac{d\, Q_{surf}}{\varepsilon_{ox}} , \qquad (1)$$

where d is the mean distance between the charged traps and the Si/SiO_2 interface, ΔV_{surf} the change in surface potential , Q_{surf} the area density of trapped charge and ε_{ox} the dielectric permittivity of SiO_2. The effect of charging is shown by curves "b", "c" and "d" in Fig. 2: the curve is shifted by 25 V. Furthermore, it can be seen that the shape of the curve is conserved, which indicates that the charging only affects the surface potential. Because of this we can use the shift as a measure for the trapped charge. The shift of 25 V in Fig 2 corresponds according (1) to a charge density of about 1×10^{12} cm^{-2} when assuming a depth distribution centered at the oxide layer.

The observation that the shape of the curve is conserved indicates that the charge is homogeneously distributed over the surface. A homogeneous distribution is expected due to the self-limiting property of the charging process.

We continued the charging of the SiO_2 by further electron exposure while stepwise increasing the bias on the substrate. After reaching a voltage shift of 140 V, corresponding to a charge density of about 6×10^{12} cm^{-2}, it was not possible to induce any additional charging. The reason of this saturation effect is not clear. Because wet grown SiO_2 layers are known to contain more than 10^{18} cm^{-3} electron traps, it is excluded that they are all charged[2]. One can propose that the saturation is due to impact ionization caused by ballistic electrons heated by the electric field. The created holes will efficiently neutralize the trapped negative charge. However, one can also explain the stopping of the charging process as follows: the injection of electrons in the oxide layer is prevented because the trajectories of low the energetic electrons in the vacuum are disturbed by stray fields originating from the high potential on the substrate.

[1] E.R. Williams, Phys. Rev. A **140**, 569 (1965).

[2] E.H. Nicollian and J.R. Brews, MOS (Metal Oxide Semiconductor) Physics and technology (Wiley-Interscience, New York, 1982), p. 541.

Summary

presence of defects in the MOS system causes the degradation of its electric characteristics. To reduce the density of defects in the Si/SiO$_2$ system a good insight in, and control of the defect generation in MOS devices during their fabrication and their operation is of primary importance for the semiconductor industry. This thesis describes the results of a study on defect structure of metal-oxide-silicon (MOS) systems using positron annihilation spectroscopy. To be able to characterize the defect structure in the MOS system we first developed an improved method for the analysis of positron beam data and we investigated the transport behaviour of positrons in MOS capacitors that were subjected to different bias conditions.

In chapter 3 an improved approach is presented for the analysis of positron beam Doppler broadening data. Instead of analyzing the energy-dependent shape parameter, the so-called $S(E)$ data, we combined the shape $S(E)$ and wing $W(E)$ data by plotting them as a trajectory in the S-W plane, using the implantation energy as a running parameter. It is shown that this plot is of particular interest for the qualitative interpretation of the data. Furthermore, it allows the independent determination of the characteristic shape and wing parameters of the different positron trapping layers without the use of a numerical simulation and fitting program. The method and its advantages and limitations are illustrated for three cases: a silicon sample implanted with helium, a metal-oxide-silicon system subjected to a positive bias voltage and a bare oxide layer on silicon. It appears that this improved data analysis method can be successfully applied to analyze positron beam data from MOS systems.

Chapter 4 describes the results of a study of the effect of an external electric field on the behavior of positrons in metal-oxide-silicon (MOS) systems. Doppler broadening measurements of the annihilation radiation were performed on capacitors with identical thermally grown SiO$_2$ layers and with Al, W and Au layers as a gate. The data

were analyzed by the combined use of the shape- and wing-parameters of the photo peak. The observed effects of the electric field are due to the field-driven transport of positrons through the SiO_2, silicon and the interfaces. By applying a field of the order of 1 MV/cm the positrons can be efficiently transported through the approximately 100 nm thick SiO_2 layer. From the transport behavior of the positrons it is concluded that the positron affinity is higher for SiO_2 than for silicon and for the gate metal. By properly choosing the direction of the field, the positrons implanted into the SiO_2 layer are collected either at the Si/SiO_2 interface or at the SiO_2/gate interface. Using this efficient and external controlled transport behaviour of positrons in the oxide layer one can unambiguously characterize the structure of the interfaces. For negative gate bias the positrons implanted into the substrate, that diffuse back to the SiO_2, are transported through the oxide layer and injected into the gate metal. The concepts developed in this chapter provide a firm basis for the characterization of defects at the Si/SiO_2 and the SiO_2/gate interface using positrons.

To be able to study industrial MOS systems we also investigated the behaviour of positrons in capacitors with polysilicon gate, see chapter 5. It appears that positrons implanted into a 60 nm n-type hydrogen saturated polysilicon layer with large grains, can be pushed out of this layer by an externally induced electric field. In the case of MOS capacitors with such polysilicon gate, polysilicon-implanted positrons can be efficiently transported towards the SiO_2/Si interface where they all are collected. This technique offers new and interesting possibilities to study defects at the SiO_2/Si interface of technologically important MOS systems with polysilicon gate and thin (<10 nm) oxide layers.

Conceivably, an MOS system with a negative gate bias may provide an improved positron moderator that can be used for the generation of positron beams. When applying an electric field, positrons implanted in the Si substrate and the SiO_2 may be sufficiently heated to be re-emitted to the vacuum. To circumvent the problem of trapping in the gate material we have fabricated samples with small Au islands instead of a blanket gate layer. In chapter 6 we showed that it is possible to charge such islands

sufficiently to induce an electric field of 5 MVcm^{-1} in the SiO$_2$ layer. The positron re-emission was investigated using two approaches based on detection with a multiple channel plate (MCP) detector and on recording of the rate of annihilation events in the MOS moderator using the Ge detector, respectively. Our results indicate that field-assisted positron re-emission from the MOS moderator indeed occurs; however, for an efficient moderator, the yield is too low. This yield was in the in the range of 0.1% of the intensity of the primary beam and has to be improved by an order of magnitude at least.

Chapter 7 presents the results of a comparative study on the effect of a post oxidation anneal (POA) at 1000°C in an N$_2$ ambient on defects in thermally grown Si/SiO$_2$ systems using positron annihilation spectroscopy and electrical characterization techniques. For this purpose we applied POA treatments with different duration after which Al gates were deposited. The such fabricated MOS capacitors were investigated using vacuum ultraviolet irradiation for determining the generation of interface traps in combination with positron annihilation spectroscopy to characterize the structure of the oxide network. A correlation was found between the generation of interface traps and the S parameter of the positron trapping sites in the oxide close to the Si. It appears likely that the positrons are trapped in the larger near-interfacial oxide network interstices. These interstices could act as scavengers for the metastable intermediate (atomic hydrogen or excitons) involved in the generation of the interface traps.

To obtain more specific insight in the relation between the structure of defects, the composition of atoms from different elements in their surrounding, and the positron beam data we have studied some well-documented types of defects in the Si/SiO$_2$ system using the coincidence measurement technique. As described in chapter 8, these coincidence measurements yield information on the composition of O- and Si-atoms at the defect site. For charged electron traps in SiO$_2$, most likely related to Si-O$^-$ centers, we observed an increased interaction with oxygen core electrons. At the Si/SiO$_2$ interface our data reveals a decreased signal from valence electrons associated with

dangling silicon bond centers due to a passivation anneal while the ratio between the contributions of core electrons of oxygen and silicon was not affected.

In conclusion, the results presented in this thesis show that positron annihilation spectroscopy is a promising technique for the investigation of the defect structure of the MOS system, providing information that is not obtained by other experimental methods. In principle it can be used to study fundamental aspects of defects and to characterize the defect structure of industrial MOS capacitors with thin oxide layers.

Samenvatting

De aanwezigheid van defecten in een metaal-oxyde-silicium (MOS) systeem veroorzaakt een degradatie van zijn elektrische eigenschappen. Om de dichtheid van defecten in het Si/SiO_2 systeem te reduceren is een goed inzicht in, en controle van de defectgeneratie bij de produktie en het gebruik van MOS componenten van groot belang voor de halfgeleiderindustrie. Dit proefschrift beschrijft de resultaten van een studie naar de defectstruktuur van MOS systemen met behulp van positronannihilatie-spectroscopie. Om de defectstruktuur van het MOS systeem met deze techniek te kunnen bestuderen ontwikkelden we eerst een verbeterde methode voor de analyse van de meetgegevens en onderzochten we het transportgedrag van positronen in MOS condensatoren die waren blootgesteld aan verschillende potentialen op de metallische veldplaat.

In hoofdstuk 3 wordt deze verbeterde methode beschreven voor de analyse van meetgegevens, die we verkregen met positronenbundels. In plaats van de S-parameter, die de algehele Dopplerverbreding van de annihilatiestraling weergeeft, als functie van de implantatiediepte te analyseren, combineerden we de informatie in de S-parameter met die in de W-parameter die gerelateerd is aan annihilatie van binnenschil elektronen. Dit gebeurt door de gemeten S- en W-waarden weer te gegeven als punten in het S-W vlak die te samen een pad in dit vlak vormen (eigenlijk een soort landkaart), waarbij de implantatie-energie de lopende parameter is. Het blijkt dat zo'n S-W diagram goed gebruikt kan worden voor de kwalitatieve interpretatie van meetgegevens. Verder maken S-W diagrammen vaak een eenduidige bepaling mogelijk van de karakteristieke S- en W-parameters van de verschillende defectbevattende lagen zonder gebruik te hoeven maken van computerprogamma's voor nummerieke simulatie en parameterschatting. De mogelijkheden en beperkingen van de nieuwe analysemethode zijn geïllustreerd aan de hand van drie voorbeelden: een silicium preparaat waarin helium is geïmplanteerd, een MOS systeem gemeten terwijl er een positieve potentiaal op de veldplaat was

aangebracht, en een kale oxydelaag op silicium. Het blijkt dat de geïntroduceerde methode de sleutel vormt voor het analyseren van meetgegevens van positronbundels aan MOS systemen.

Hoofdstuk 4 beschrijft de resultaten van een onderzoek van het effect van een extern aangelegd elektrisch veld op het gedrag van positronen in MOS condensatoren. Metingen van de Dopplerverbreding van de annihilatiestraling zijn uitgevoerd aan MOS condensatoren met identieke thermisch gegroeide SiO_2-lagen en met Al-, W-, en Au-lagen als veldplaat. De gegevens zijn geanalyseerd door gecombineerd gebruik van de S- en W-parameters van de fotopiek bij 511 keV. De geobserveerde effecten van het elektrische veld zijn geheel toe te schrijven aan een efficiënt veldgedreven transport van positronen door het SiO_2, silicium en de grensvlakken. Door een elektrisch veld aan te leggen van ongeveer 1 MV/cm kunnen de positronen efficiënt worden getransporteerd door de ongeveer 100 nm dikke oxydelaag. Uit het transportgedrag van positronen is afgeleid dat de positronaffiniteit hoger is voor SiO_2 dan voor silicium en voor het metaal van de veldplaat. Door het juist kiezen van de richting van het veld, kunnen de positronen die zijn geïmplanteerd in de SiO_2-laag verzameld worden bij het Si/SiO_2 dan wel bij het SiO_2/veldplaat grensvlak. Dankzij dit extern controleerbare transportgedrag van positronen kunnen de annihilatiekarakteristieken van de grensvlakken eenduidig worden bepaald. Bij negatieve potentiaal op de veldplaat worden positronen die zijn geïmplanteerd in het substraat, en die terug diffunderen naar het SiO_2, dwars door de oxydelaag getransporteerd en geïnjecteerd in de veldplaat. De concepten, die zijn ontwikkeld in dit hoofdstuk vormen een degelijke basis voor verder onderzoek aan defecten in MOS systemen.

Om industriële MOS systemen te kunnen karakteriseren bestudeerden we het gedrag van positronen in condensatoren met een veldplaat polysilicium, zie hoofdstuk 5. Het blijkt dat positronen in 60 nm dikke, met waterstof verzadigde, n-type polysiliciumlagen met grote korrelafmetingen (>60 nm) uit deze lagen kunnen worden gedreven door een aangelegd elektrisch veld. Bij MOS condensatoren met zo'n polysiliciumlaag als veldplaat kunnen positronen, die zijn geïmplanteerd in de

polysilisium veldplaat, worden getransporteerd naar het Si/SiO_2 grensvlak. Deze techniek biedt interessante mogelijkheden om de defectstruktuur te bestuderen bij het Si/SiO_2 grensvlak van technologisch belangrijke MOS systemen met dunne (<10 nm) oxyde lagen.

MOS strukturen met een negatieve potentiaal op de veldplaat bieden nieuwe perspectieven voor de ontwikkeling van een verbeterde positronmoderator voor de generatie van gethermaliseerde positronen. Door het aanleggen van een elektrisch veld kunnen positronen geïmplanteerd in het Si/SiO_2 systeem wellicht voldoende worden verhit voor reëmissie naar het vacuüm. Om het probleem van vangst in de veldplaat te omzeilen hebben we preparaten gebruikt met kleine Au-eilanden in plaats van een egaal met metaal bedekt oppervlak. In hoofdstuk 6 lieten we zien dat het mogelijk is om de Au eilandjes voldoende op te laden om een elektrisch veld met een sterkte van 5 MVcm-1 in het SiO_2 aan te leggen. De positronreëmissie is onderzocht met twee methoden. Deze methoden zijn repectievelijk gebaseerd op detectie met een multi-kanalen plaat (MCP) detektor en op het meten van de intensiteit van annihilaties in het preparaat met behulp van de Ge detector. Onze resultaten geven aan dat veldgeïnduceerde positronreëmissie van de MOS moderatoren inderdaad optreedt, maar dat de opbrengst onvoldoende is voor een efficiënte positronmoderator. De reëmissie opbrengst was ongeveer 0.1% van de intensiteit van de primaire bundel.

In hoofdstuk 7 worden resultaten gepresenteerd van een vergelijkend onderzoek naar defecten in MOS systemen met positron annihilatie spectroscopie en elektrische karakterisatietechnieken. Hierbij is gekeken naar het effect van een uitgloeibehandeling vlak na het groeien van de oxydelaag (post oxidation anneal, afgekort POA) bij 1000°C in N_2 gas. We pasten POA behandelingen toe met verschillende tijdsduur waarna de Al veldplaat werd aangebracht. De zo geprepareerde MOS systemen zijn onderzocht, gebruik makende van vacuüm-ultraviolet (VUV) straling om de generatie van elektrisch aktieve 'grensvlaktoestanden' bij het Si/SiO_2 grensvlak te bepalen. Parallel hieraan is de positron annihilatie spectroscopie toegepast om de defectstruktuur te karakteriseren. Er is een correlatie gevonden tussen de generatie van grensvlaktoestanden en de S-parameter van het

grensvlak. Het is aannemelijk dat de positronen worden ingevangen in lokaties in het SiO_2 netwerk in de buurt van het grensvlak met meer dan gemiddelde ruimte tussen de omringende atomen. Deze open tussenruimten treden mogelijk als vangstplaatsen op van atomair waterstof of excitonen die verantwoordelijk zijn voor de generatie van grensvlaktoestanden.

Om meer specifiek inzicht te krijgen in de relatie tussen de struktuur van defecten, de atomaire samenstelling van hun direkte omgeving en de met de positronenbundel verkregen resultaten, hebben we aan goed gedocumenteerde soorten defecten in het Si/SiO_2 systeem coïncidentiemetingen uitgevoerd. In hoofdstuk 8 is beschreven welke informatie deze metingen opleveren over de aanwezigheid van O- en Si-atomen bij defecten. Voor geladen elektronenvangstplaatsen in SiO_2 observeerden we een toegenomen interaktie met binnenschil elektronen van zuurstof. Deze waarneming duidt op vangst van positronen aan SiO^- groepen. Bij het Si/SiO_2 grensvlak namen we na het uitvoeren van een uitgloeibehandeling in waterstofgas een afname waar van het signaal gerelateerd aan valentie-elektronen bij onverzadigde Si bindingen. Anderzijds bleef de verhouding tussen de bijdragen van binnenschil elektronen van zuurstof en silicium ongewijzigd.

Concluderend kan gesteld worden dat de resultaten gepresenteerd in dit proefschrift laten zien dat positron annihilate, mits op de juiste manier toegepast, informatie kan opleveren over de struktuur van het MOS systeem die niet kan worden verkregen met andere meettechnieken. Positron annihilatie kan worden gebruikt om aspecten van defectgeneratie te bestuderen en kan worden aangewend om de defect struktuur te karakteriseren van industriële MOS systemen met dunne oxydelagen.

Dankwoord

Op deze plaats wil ik allen die hebben geholpen bij de totstandkoming van dit proefschrift bedanken.

Dit waren de werknemers bij DIMES en bij de afdeling reactorfysica van het IRI die mij op allerlei manieren behulpzaam waren en voor een prettige werksfeer zorgden.

In het bijzonder wil ik Tom van Veen bedanken die het in dit proefschrift beschreven onderzoek mede mogelijk maakte. Zijn kennis van materiaalkunde en positronfysica hebben wezenlijk bijgedragen aan dit proefschrift. Ook mijn 2e promotor, prof. S. Radelaar ben ik erkentelijk voor de mogelijkheid om binnen zijn groep onderzoek te doen en voor het kritisch doorlezen van de tekst van dit proefschrift. Jan de Nijs heeft sterk bijgedragen aan de totstandkoming van dit proefschrift door de vele discussies die ik met hem heb gevoerd over fysica, het onderzoek, en de opzet van publikaties. Verder was ook prof. P. Balk betrokken bij mijn werk door het helpen aanscherpen van de tekst van de publikaties die in dit proefschrift zijn opgenomen als hoofdstuk 3,4 en 7.

Ook allen die betrokken waren bij het voorbereiden of bij het uitvoeren van experimenten wil ik hier bedanken. Dit is allereerst Henk Schut die vaak heeft geholpen bij het opzetten van experimenten met de VEP positronenbundel. Verder heeft hij geholpen bij het modificeren van software voor het aansturen van experimenten en bij het uitvoeren van simulaties voor het positron deflectiesysteem. Jan de Roode heeft bijgedragen aan de reëmissiemetingen beschreven in hoofdstuk 6 door het helpen monteren van het positron deflectiesysteem. Karl Roos vervaardigde voor mij constructietekeningen waaronder de uitgebreide overzichtstekening in figuur 3 van hoofdstuk 2. De coïncidentiemetingen die zijn behandeld in hoofdstuk 8 zijn mede tot stand gekomen door de assistentie van Bram Kruseman. Bij DIMES wil ik Rolf Mallée bedanken voor het vervaardigen van de MOS capaciteiten met een polysilicium veldplaat.

Klaas Druijf en Valery Afanas'ev hebben mij geholpen om thuis te raken in de fysica en fabricage van MOS capaciteiten. De secretaresses Riny Purmer en Nejla Ozkaya komt dank toe voor het helpen uitvoeren van de vele administratieve afhandelingen aan het eind.

In het bijzonder wil ik natuurlijk Inge bedanken. Zij heeft altijd naast mij gestaan en door steeds allerlei dingen voor mij te doen, van brood smeren en eten koken tot nederlandse teksten nakijken en plaatjes plakken, mij steeds met raad en daad bijgestaan.

Maarten

Curriculum Vitae

Maarten Clement is geboren op 3 april 1969 te Voorhout. Na het behalen van het HAVO diploma in juni 1987 volgde hij de propedeuse van de opleiding Technische Natuurkunde aan de Technische Hogeschool Rijswijk. Vanaf 1988 studeerde hij Technische Natuurkunde aan de Technische Universiteit Delft, waar hij in 1993 afstudeerde bij de afdeling reaktorfysica op het gebied van thermische desorptiespectrometrie. In 1994 begon hij zijn promotieonderzoek als assistent in opleiding bij de sectie nanofysica van de vakgroep vaste stof fysica van de faculteit Technische Natuurkunde en de afdeling Reactorfysica van het Interfacultair Reactor Instituut, beide aan de Technische Universiteit Delft. Het onderzoek dat hier is verricht resulteerde in het hier voor u liggende proefschrift. Sinds 1 juli 1998 is de auteur werkzaam bij Hollandse Signaal Apparaten B.V.